

NASA/TP–2018-219033/Vol. 1



**Advances in Above- and In-Water Radiometry, Volume 1:
Enhanced Legacy and State-of-the-Art Instrument Suites**

*Stanford B. Hooker, Randall N. Lind, John H. Morrow, James W. Brown, Koji Suzuki, Henry F. Houskeeper,
Toru Hirawake, Elígio de Ráus Maúre*

National Aeronautics and
Space Administration

**Goddard Space Flight Center
Greenbelt, Maryland 20771**

November 2018

NASA STI Program ... in Profile

Since its founding, NASA has been dedicated to the advancement of aeronautics and space science. The NASA scientific and technical information (STI) program plays a key part in helping NASA maintain this important role.

The NASA STI program operates under the auspices of the Agency Chief Information Officer. It collects, organizes, provides for archiving, and disseminates NASA's STI. The NASA STI program provides access to the NASA Aeronautics and Space Database and its public interface, the NASA Technical Report Server, thus providing one of the largest collections of aeronautical and space science STI in the world. Results are published in both non-NASA channels and by NASA in the NASA STI Report Series, which includes the following report types:

- **TECHNICAL PUBLICATION.** Reports of completed research or a major significant phase of research that present the results of NASA Programs and include extensive data or theoretical analysis. Includes compilations of significant scientific and technical data and information deemed to be of continuing reference value. NASA counterpart of peer-reviewed formal professional papers but has less stringent limitations on manuscript length and extent of graphic presentations.
- **TECHNICAL MEMORANDUM.** Scientific and technical findings that are preliminary or of specialized interest, e.g., quick release reports, working papers, and bibliographies that contain minimal annotation. Does not contain extensive analysis.
- **CONTRACTOR REPORT.** Scientific and technical findings by NASA-sponsored contractors and grantees.
- **CONFERENCE PUBLICATION.** Collected papers from scientific and technical conferences, symposia, seminars, or other meetings sponsored or co-sponsored by NASA.
- **SPECIAL PUBLICATION.** Scientific, technical, or historical information from NASA programs, projects, and missions, often concerned with subjects having substantial public interest.
- **TECHNICAL TRANSLATION.** English-language translations of foreign scientific and technical material pertinent to NASA's mission.

Specialized services also include organizing and publishing research results, distributing specialized research announcements and feeds, providing help desk and personal search support, and enabling data exchange services. For more information about the NASA STI program, see the following:

- Access the NASA STI program home page at <http://www.sti.nasa.gov>
 - E-mail your question via the Internet to help@sti.nasa.gov
 - Phone the NASA STI Information Desk at 757-864-9658
 - Write to:
NASA STI Information Desk
Mail Stop 148
NASA's Langley Research Center
Hampton, VA 23681-2199
-



Advances in Above- and In-Water Radiometry, Volume 1: Enhanced Legacy and State-of-the-Art Instrument Suites

Stanford B. Hooker
NASA Goddard Space Flight Center Greenbelt, Maryland

Randall N. Lind
Biospherical Instruments Inc. San Diego, California

John H. Morrow
Biospherical Instruments Inc. San Diego, California

James W. Brown
RSMAS University of Miami Miami, Florida

Koji Suzuki
Hokkaido University Sapporo, Japan

Henry F. Houskeeper
University of California Santa Cruz Santa Cruz, California

Toru Hirawake
Hokkaido University Hakodate, Japan

Elgio de Ráus Maúre
Nagoya University Nagoya, Japan

National Aeronautics and
Space Administration

Goddard Space Flight Center
Greenbelt, Maryland 20771

Notice for Copyrighted Information

This manuscript has been authored by employees of *Biospherical Instruments Inc.*, *RSMAS University of Miami*, *Hokkaido University*, *University of California Santa Cruz*, *Nagoya University* with the National Aeronautics and Space Administration. The United States Government has a non-exclusive, irrevocable, worldwide license to prepare derivative works, publish, or reproduce this manuscript, and allow others to do so, for United States Government purposes. Any publisher accepting this manuscript for publication acknowledges that the United States Government retains such a license in any published form of this manuscript. All other rights are retained by the copyright owner.

Trade names and trademarks are used in this report for identification only. Their usage does not constitute an official endorsement, either expressed or implied, by the National Aeronautics and Space Administration.

Level of Review: This material has been technically reviewed by technical management.

Available from

NASA STI Program
Mail Stop 148
NASA's Langley Research Center
Hampton, VA 23681-2199

National Technical Information Service
5285 Port Royal Road
Springfield, VA 22161
703-605-6000

ABSTRACT

This publication documents the scientific advances associated with new instrument systems and accessories built to improve above- and in-water observations of the apparent optical properties (AOPs) of aquatic ecosystems. The perspective is to obtain high quality data in offshore, nearshore, and inland waters with equal efficacy. The principal objective is to be prepared for the launch of the next-generation ocean color satellites with the most capable commercial off-the-shelf (COTS) instrumentation in the shortest time possible. The technologies described herein are designed to either improve legacy radiometric systems or to provide entirely new hybrid sampling capabilities, so as to satisfy the requirements established for diverse remote sensing requirements. Both above- and in-water instrument suites are documented with software options for autonomous control of data collection activities. The latter includes an airborne instrument system plus unmanned surface vessel (USV) and buoy concepts.

Prologue

Present ocean color activities date primarily to the start of Earth Observing System (EOS) legacy missions (Asrar and Greenstone 1995). Within the EOS paradigm, AOP observations for vicarious calibration, algorithm validation, and basic research—*hereafter, calibration, validation, and research* (CVR)—are distinct and largely separate activities (Hooker et al. 1992). This hierarchy was codified by the technology and accuracy requirements for each: calibration used strenuous criteria at one site to ensure the highest accuracy; validation relied on numerous investigators and more variable global data; and research involved narrower objectives and sampling for unique hypotheses. New ideas occurred primarily *within* a CVR category, although research was expected to influence validation when a new inversion algorithm needed validation (Hooker et al. 2007).

After integration into routine satellite processing, a new product might trigger more research, e.g., coastal products revealed the importance of absorbing aerosols to atmospheric correction (Ahmad et al. 2010). As legacy missions achieved—and exceeded—their design goals, the interconnections between CVR categories became more apparent. Although inevitable, because the NASA Ocean Optics Protocols (Mueller and Austin 1992 and 1995 plus Mueller 2000, 2002, and 2003), hereafter Protocols, are essentially the same for each category, this was not recognized at the time, because the technologies *matched* the downwards C→V→R accuracy cascade.

Because EOS isolated CVR categories, *achievements with calibration instruments were not typically commercialized*. Although it was demonstrated that both above- and in-water commercial-off-the-shelf (COTS) sensors can provide data to the same efficacy as custom solutions (Zibordi et al. 2006 and Antoine et al. 2008), these accomplishments occurred after the EOS paradigm *defined calibration as an in-water exercise*. Even after COTS community data were used for calibration with comparable uncertainties to one-of-a-kind sensors (Bailey et al. 2008), *the*

mindset persisted that calibration requires a custom solution to satisfy the numerous in-water requirements. Instrument development after EOS reached maturity recognized that the next frontier included optically complex waters (e.g., coastal and ice zones) requiring expanded spectral ranges to derive in-water constituents beyond chlorophyll, faster data rates to improve resolution, and advanced atmospheric correction (Hooker et al. 2007).

To satisfy next-generation CVR requirements, new in-water systems have to be smaller to reduce self-shading effects and resolve thin optically different layers (e.g., fresher over saltier water in estuaries or ice zones), and above-water systems will likely include oceanic-atmospheric measurements (Hooker et al. 2007). One of the first commercial improvements was the *microradiometer* (Booth et al. 2010) codeveloped by NASA and Biospherical Instruments Inc. (BSI), which typically consists of a silicon photodetector (SiP), three-gain preamplifier, 24 bit analog-to-digital converter (ADC), microprocessor, and addressable digital port. A microradiometer is a fully networkable sensor on one small, thin, conformal-coated printed circuit assembly (PCA) sleeved inside a metal cylinder for mechanical support and electromagnetic shielding (Fig. 1). *The assembly is machine made, which significantly improves quality over handmade legacy devices, and has 10 decades of linear dynamic range—i.e., it can view the sea and Sun without saturating and is sensitive enough to view the Moon.*

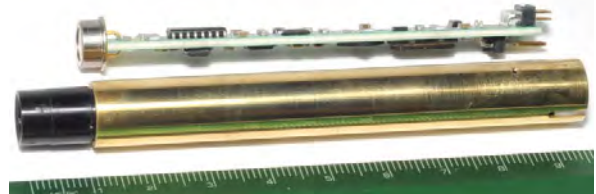


Fig. 1. The two-sided microradiometer PCA with SiP above a brass sleeved unit with black front-end optics (ruler to 9.6 cm).


Figure 1 shows that a limiting size constraint on a microradiometer is the physical dimensions of the photode-

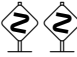
detector. The choice of photodetector also influences the performance obtained during *in situ* observations, particularly as a function of wavelength. For the results presented here, the Hamamatsu Photonics K.K. (Hamamatsu City, Japan) S1226 series was selected. The choice was based on a sensible weighting of the advantages and disadvantages of logical alternatives to fulfill the spectral requirements for the next-generation Compact-Optical Profiling System (C-OPS), wherein the anticipated wavelengths span the ultraviolet (UV), visible (VIS), and near-infrared (NIR) domains.

Both the Hamamatsu S1336 and S1337 series, for example, have a better temperature coefficient, but also have increased infrared (IR) sensitivity relative to the S1226 series, potentially adding out-of-band blocking requirements in certain scenarios. Additionally, the S1336 and S1337 series have a decreased shunt resistance relative to the S1226 series, which can amplify front-end low frequency operational amplifier noise. There are additional intricacies in the decision making to select the photodetector, but these two represent the main tradeoffs that were considered in choosing the S1226 series for C-OPS.


In the microradiometer architecture, an aggregator creates a stand-alone device from a cluster of microradiometers with front-end optics (collector, window, and filter), as well as from one or more ancillary sensors (Lind et al. 2012). The aggregator allows all the individual instruments within an observing system to self-organize based on an initial hierarchy established by a *master* aggregator, which is usually the deck box that provides power plus data and telemetry†. Demonstrated life cycles for instruments built with microradiometers presently exceed 10 yr with no failures.

The material and procedures presented here are applicable to both above- and in-water AOP sampling systems, but the emphasis is primarily on the at-sea collection of in-water data, because it is the most complicated and least forgiving—a ship can decide to not leave port as severe weather approaches, but once at sea, the scientists and crew are obliged to withstand all the conditions presented by the natural environment. Because this means all personnel can be placed in circumstances associated with high risk to the safety of themselves, their equipment, and the quality of the data obtained, the material presented herein includes three levels of warning, where appropriate:

 Cautionary explanations to avoid a needless degradation in performance appear separately with the so-called *dangerous bend* graphic, shown to the left;

 If extra caution is warranted, because there is a significant likelihood of compromising performance, the text appears with double dangerous bends; and

† For the purposes of this document, telemetry is defined to be the command set that is issued by controlling software or firmware, as well as the responses that are generated to ensure the efficacy of the command set.

 If extreme caution is required, because there is an inherent safety risk to personnel (and, secondly, safety of equipment) that must be respected, the text appears with triple dangerous bends.

On marine installations, safety of equipment may also contribute to safety of personnel particularly if loss of vital equipment places the deployment platform in danger.

For instrument systems requiring an expanded spectral domain, e.g., the Compact-Airborne Environmental Radiometers for Oceanography (C-AERO) instrument suite (Chap. 1), the microradiometer interface was enhanced to include alternative detector technologies without altering the basic architecture. Similarly, for observations requiring an increase in flux levels, e.g., the Ocean Color Underwater Low Light Advanced Radiometer (OCULLAR) prototype (Chap. 4), paired detector systems compatible with microradiometer support electronics and size constraints were used.

A prototype in-water (radiance) instrument built with microradiometers is presented in Fig. 2, wherein the internal components are contained within a transparent housing so they are visible. The 19 individual channels can be seen as different colors from the front-end optics (principally the filter stacks) of the hexagonal microradiometer array at the entrance aperture. The microradiometers are sleeved in brass cylinders and appear gold in color. The support electronics include the aggregator and are a combination of circular and rectangular boards, and the end cap contains a six-conductor bulkhead connector for full-duplex communications (two contacts for power and four contacts for data and telemetry).

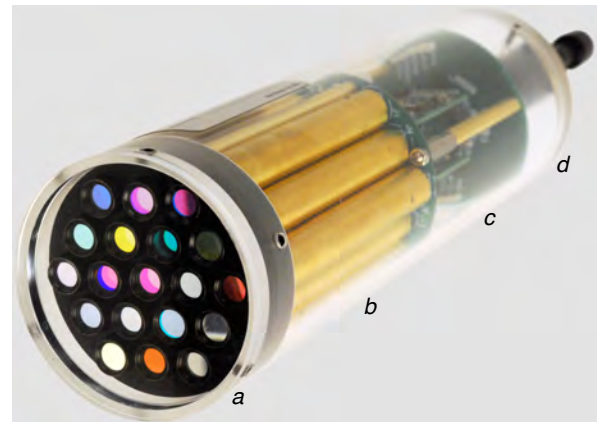


Fig. 2. A radiance instrument built with the modular generalized components as follows: a) entrance aperture, b) microradiometer array, c) support electronics, and d) end cap.

Microradiometers were first exploited by NASA and BSI (San Diego, California) to build the free-fall C-OPS instrument suite, which is a next-generation COTS instrument system (Morrow et al. 2010). Each of the three C-OPS radiometers has 19 fixed-wavelength channels in

a 2.75 in (7 cm) diameter housing, which represents an approximately 86% improvement in packing efficiency compared to legacy instruments. C-OPS uses a kite-shaped backplane, hydrobaric buoyancy, plus adjustable sensor orientation, custom-blended flotation disks, and movable ballast to achieve stable descents as slow as 5 cm s^{-1} with vertical tilts to within 2.5° (Sect. 2.3.4).

Returning up to 15 data frames per second (i.e., 15 Hz), the vertical sampling resolution of a properly trimmed C-OPS is to within 1 cm in near-surface waters (Hooker et al. 2013)—a more than 900% improvement over legacy free-fall devices—and can be close to 1 mm. The unprecedented 1 mm (or less) vertical resolution is because the hydrobaric compressible bladders allow the profiler to loiter close to the surface before reaching terminal velocity (at approximately 3–5 m).

With the Processing of Radiometric Observations of Seawater using Information Technologies (PROSIT) software package (Hooker and Brown 2018), a full suite of CVR data products across all wavelengths (typically 313–875 nm) can be produced from a 1 m vertical excursion in coastal or inland waters and less than 2 m in the open ocean. This is possible because the high vertical resolution minimizes aliasing from both wave focusing and vertical tilting effects (Hooker et al. 2013). Although designed for unprecedented near-surface (airborne or satellite remote sensing) data quality, C-OPS can be ballasted (by adding weight or removing flotation) to sample deeper into the water column for ecological research.

To ensure the required input variables for PROSIT are at the highest quality possible, all data for the systems described herein are collected using the Data Acquisition and Control for Photometric and Radiometric Observations (DACPRO) software. The DACPRO environment computes real-time variables using the same algorithms PROSIT uses with numerous levels of error checking to ensure adherence to the Protocols. Consequently, lessons learned in DACPRO are directly applicable to PROSIT and vice versa.

A schematic of the C-OPS instrument suite is shown in Fig. 3, wherein no alternating current (AC) power cables are shown to emphasize that the deck box and the laptop computer can function on battery power alone, which makes the instrumentation very portable. A complete C-OPS deployment with 19-channel radiometers has the following components:

- The C-OPS profiler is comprised of the backplane plus in-water downward irradiance and upwelling radiance instruments, $E_d(\lambda_{19})$ and $L_u(\lambda_{19})$, respectively, where λ_{19} denotes 19 wavelengths;
- The backplane contains movable weights and flotation to trim the vertical stability and descent rate, plus the radiometers are mounted on movable V-blocks that allow the radiometers to be tilted to offset any vertical bias caused by the sea cable or an ambient current;

- The solar reference, $E_s(\lambda_{19})$ or $E_d(0^+, \lambda_{19})$ depending on the cited literature, with the optional Biospherical Global Positioning System (BioGPS) and Biospherical Shadow band Accessory for Diffuse Irradiance (BioSHADE) accessories (Bernhard et al. 2010);
- The deck box that powers the above- and in-water instruments while providing the data and telemetry for all of the components;
- The (usually laptop) computer hosting the data acquisition software to command the instruments and record the data; and
- The cabling connecting the applicable components.

Both the solar and in-water irradiance radiometers contain tilt sensors to determine the vertical orientation of instrumentation. Additionally, the end cap for the radiance radiometer contains a water temperature sensor and a pressure transducer port.

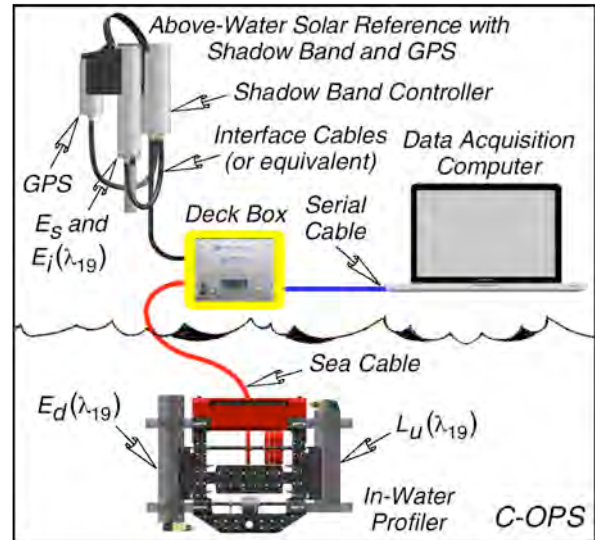


Fig. 3. The C-OPS deployment equipment and architecture. Cable lengths are set by the size of the deployment platform and the desired sampling depth (which is also set by the pressure transducer).


The maximum sampling depth is set by the local bathymetry, pressure transducer rating, and available cable. For coastal research, as presented here, the latter two are usually 125 m. A long cable allows the profiler to be positioned far enough away from the deployment platform to avoid any platform-induced perturbations (e.g., shading and reflections).

⚠️ ⚠️ If the pressure transducer is subjected to a pressure in excess of the rated maximum, *permanent damage and a significant loss in accuracy is likely.*

The bulkhead and in-line connectors used with instrument systems built with microradiometers is described by Hooker (2014), so only a short summary is provided here. The perspective is to make connects and disconnects as

safe and trouble free as possible, while ensuring high quality for long-term ease of use. Consequently, the so-called *wet pluggable* connectors from SubConn Inc.† (Esbjerg, Denmark) are specified to the greatest extent practicable. These connectors are designed to be plugged together underwater, so when the connectors are mated, water is removed by internal O-rings in the female sockets, and a clean dry fitting is achieved.

The connector can have either male pins or female sockets. The choice as to which type is used is based on safety considerations for personnel and the instrumentation.

 Best engineering practices dictate that a *male connector must not provide power*, because if the cable is dropped against a metal surface (e.g., the deck of a ship) or handled by personnel with power applied, the exposed male pins can short, harming the equipment, and potentially the person doing the work.

Because they receive power, the bulkhead connectors on the radiometers in Fig. 3 have male pins, in this case the designation is MCBH6M, i.e., a SubConn micro (MC) circular series bulkhead (BH) with six male pins (6M). A SubConn micro bulkhead connector has a built-in locking sleeve with male ridges (MR) to accept a cable with a locking sleeve with female grooves (FG). Consequently the mating cable for the radiometers is a MCIL6F/FG, i.e., a SubConn MC in-line (IL) series connector with six female sockets and an FG locking sleeve.

The shadow band controller in Fig. 3 receives power on a MCBH6M connector with built-in MR locking sleeve, and distributes it to the GPS and solar reference (irradiance) radiometer on two identical MCBH6F connectors requiring two identical short cables. Each short cable has a MCIL6M/FG connector and a MCIL6F/FG. It does not matter which short cable goes to which device, because microradiometer instruments self-organize.

The advantage of building instruments with microradiometers is they are scalable, which is derived, in part, by the ease in which they can be added to, or removed from, an instrument. Unlike legacy, handmade and hand-wired instruments, microradiometers are built by machine and are plugged together with significantly less labor and risk to create a multi-channel sensor. The ease is also a result of the self-organizing capabilities of the network microradiometers create with their individual onboard (programmable) microprocessor, because each microradiometer is a *smart photodetector*. In terms of next-generation problem sets, one of the principal advantages of microradiometers is their flexibility in providing a multitude of system configurations and upgrade paths for the next horizon of requirements.

† MacArtney Inc. – Northeast is one of the American sales offices for SubConn connectors and cable assemblies. Their contact information is 575 Washington Street, Pembroke, MA 02359, +1-781-829-4440, www.macartney.com.

The flexibility of instruments built with microradiometers is driven, in part, by the presence of a microprocessor in the data acquisition circuitry. The microprocessor provides an inherent ability to facilitate the evolution of an instrument built with microradiometers, i.e., to expand the functionality over time, which has already taken place. For example, a new data collection accessory uses two digital thrusters mounted to the C-OPS backplane, which allow the instrument to be maneuvered like a remotely operated vehicle (ROV). This new accessory is called the Compact-Propulsion Option for Profiling Systems (C-PrOPS) and can include the Compact-Conductivity Accessory for Profiling Systems (C-CAPS), both of which are COTS items (Chap. 2). Other evolutions that have occurred, and are presented herein, include a) a *hybriddynamic* instrument design, wherein the dynamic range expands from 10 decades to 14 (Chap. 4); and b) *hybridspectral* instruments, wherein the spectral responsivity expands from 19 channels to more than 2,048 (Chaps. 3 and 9) and beyond (Chap. 10).

The technologies applied to evolving microradiometer instruments inspire the following: a) airborne instrument enhancements (Chap. 1); b) improvements to legacy systems to maintain their use beyond their design period (Chap. 5); c) remote sample collection to complement remote piloting of the instrument (Chap. 6); and d) autonomous platform applications (Chaps. 7 and 8), with the latter in Vol. 2 of this three-part publication.

When these technologies are viewed as part of a continuum rather than as individual accomplishments, the overarching goal of the technology development exercise emerges. The historical perspective in which calibration, validation, and research were considered separate activities led to the inevitable focus on optically simple case-1 waters for calibration activities, with the assumption that more complex (coastal, estuarine, and inland waters) water masses usually transcended validation and were primarily in the research domain. This led to the development of COTS instrumentation designed primarily for validation and research (i.e., larger markets for commercialization).

The hardware continuum is supported across a commensurate software continuum by using two software environments that link data acquisition and data processing. The DACPRO virtual instrument (VI) environment records data through a unified front panel or graphical user interface (GUI) specifically designed to ensure the scientific efficacy of the data are at the highest quality level. The PROSIT application uses the same computational library as DACPRO to ensure what is learned in one environment can be exactly duplicated and exploited in the other.

The introduction of microradiometers in COTS instruments, and the associated accessories, demonstrates that the same technology can be used across the CVR continuum for above-water, in-water, and laboratory applications. The addition of a single data processing scheme

(PROSIT) that is strongly linked to the data acquisition environment (DACPRO) creates a holistic hardware and software system that provides an ability to deploy instruments and subsequently process the data while strictly adhering to the Protocols across the full range of optical complexity encountered in both marine and lacustrine waters.

Importantly, the hardware and software were developed with a forward-looking viewpoint, meeting or exceeding requirements for both legacy and next-generation instruments. Broad adoption of these sensors would enable a more rapid evolution of CVR activities leading to further refinement and improvement, because COTS instruments are readily accessible to the community.

Chapter 1

The C-AERO Instrument System Concept

STANFORD B. HOOKER
*NASA Goddard Space Flight Center
 Greenbelt, Maryland*

JOHN H. MORROW
*Biospherical Instruments, Inc.
 San Diego, California*

JAMES W. BROWN
*RSMAS University of Miami
 Miami, Florida*

ABSTRACT

The C-AERO instrument suite uses above-water radiometers from the Expandable Technologies for Radiometric Applications (XTRA) class, which typically have 19 different wavelengths (nominally with 10 nm bandwidths). The above-water (airborne) instruments are used to derive normalized data products (which account for the solar illumination during observations) by measuring the total radiance $L_T(\lambda_{19})$ from the sea surface, the indirect (sky) radiance $L_i(\lambda_{19})$, and the global solar irradiance $E_s(\lambda_{19})$. The radiance instruments have a narrow 2.5° full view angle (FVA), which means they can be mounted in a tracker and used as a sun photometer. Two radiance instruments can also be mounted in a frame to make above-water measurements of L_T and L_i , while E_s is measured simultaneously to account for changes in solar illumination. The deck box used for the C-AERO instrumentation suite is the same one used for C-OPS, except flight certification is anticipated to require the removal of the built-in battery and the cable jacketing is replaced with aircraft-grade (Teflon insulated) wiring.

1.1 Introduction

The diversity of the calibration and validation requirements suggests a variety of organizational schemes for executing the tasks involved. The selected formalism for the tasks can be derived from the equation governing the remote sensing measurement, that is, the radiative transfer equation for the satellite observation:

$$L_{\text{sat}}(\lambda) = L_r(\lambda) + L_a(\lambda) + L_{ra}(\lambda) + TL_g(\lambda) + t(L_f(\lambda) + L_W(\lambda)), \quad (1)$$

where $L_{\text{sat}}(\lambda)$ is the total radiance observed by the remote sensor (the top of the atmosphere for a spaceborne instrument), which is composed of the following radiance contributions: a) multiple scattering of air molecules (Rayleigh scattering), $L_r(\lambda)$; b) multiple scattering by aerosols in the absence of air, $L_a(\lambda)$; c) interactions between air molecules and aerosols, $L_{ra}(\lambda)$; d) reflections from glint and foam, $TL_g(\lambda)$ and $tL_f(\lambda)$, respectively (the coefficient T is the direct solar transmittance and t is the diffuse atmospheric transmittance); and e) backscattering out of the water due to subsurface interactions, $tL_W(\lambda)$.

The formulation in (1) can be grouped into simpler interaction terms:

$$L_{\text{sat}} = L_{\text{atm}} + L_{\text{sfc}} + L_{\text{sub}}, \quad (2)$$

wherein

L_{atm} is the contribution from atmospheric interactions, $L_r(\lambda) + L_a(\lambda) + L_{ra}(\lambda)$;

L_{sfc} is the contribution from reflections at the sea surface, $TL_g(\lambda) + tL_f(\lambda)$; and

L_{sub} is the contribution from subsurface interactions, $tL_W(\lambda)$.

The basic equations relating the upwelling radiance field below the water surface with that exiting the surface, the angular bidirectional dependency of these fields, and the transformation of radiance or irradiance values into reflectances are detailed in Morel and Gentili (1996), Mobley (1999), and Mueller (2000), so only the variables needed here are briefly presented. The spectral water-leaving radiance is the principal quantity of interest and is expressed as $L_W(0^+, \lambda, \theta, \phi \in \Omega_{\text{FOV}}, \theta_s)$, which explicitly shows the angular dependencies of L_W on the radiance

direction defined by the zenith angle θ , and the azimuth angle with respect to the Sun direction, ϕ , ($\phi = 0$ for the solar azimuth), and where Ω_{FOV} represents the solid angle of the detector centered on the direction (θ, ϕ) . For a given detector, Ω_{FOV} is constant and L_W is only defined immediately above the surface $z = 0^+$, where z is the vertical (depth) coordinate, so these arguments are not repeated hereafter. The dependence on the illumination conditions above the sea surface is expressed in a simplified way by only introducing the solar zenith angle, θ_s .

The two basic approaches for estimating $L_W(\lambda)$ require either above- or in-water sampling. The above-water approach uses direct observations of the total radiance emanating from the sea surface, L_T , which after correction for glint contamination from skylight, L_i , yields an estimate of $L_W(\lambda)$; the in-water approach uses vertical observations of upwelled radiance to establish a near-surface extrapolation interval from which $L_W(\lambda)$ is estimated after propagation through the sea surface. There are numerous variations in both approaches. In-water methods are distinguished by the vertical resolution of the sampling equipment (profiles versus discrete depths), whereas above-water methods are differentiated primarily by how glint contamination is removed.

There are no *a priori* reasons to select water-leaving radiances from an above-water method, $\hat{L}_W(\lambda)$, over an in-water method, $\tilde{L}_W(\lambda)$, when sampling in the open ocean (which typically has a deep and optically simplistic mixed layer). There are, however, differences between the two methods that are relevant when sampling in the coastal environment or inland waters. The advantages and disadvantages of the two techniques are a function of the data acquisition and processing schemes that can be chosen. What is of interest here are the most significant differences between in-water data collected with a free-fall profiler and an above-water system mounted on an aircraft flying at the lowest safe altitude (LSA) over a featureless water mass:

1. An above-water system is usually mounted on, or close to, the deployment platform, so avoiding platform shading and perturbations is required and can be challenging; an in-water system is easily floated away from the deployment platform, so the negative influences of the deployment platform are avoided.
2. An in-water system is an obstruction to the natural propagation of the ambient light field, so corrections for self-shading effects (which are most significant in turbid waters) must be applied in the data processing scheme; an above-water (or airborne) system does not have this problem.
3. An in-water system provides a large variety of data products describing the physical and bio-optical properties of the water column; an above-water system only provides surface values unless algorithms with necessarily degraded accuracy are used to derive additional products.

4. Fluctuations in the optical measurements from surface effects, which are most significant during clear-sky conditions, are simpler to deal with in above-water data because the problem is one-dimensional (essentially a function of time); for in-water data, there is an aliasing effect because the phenomenon is both a function of time and space (the profiler is sinking).

The surface effects can be substantially reduced for an in-water system if the vertical resolution of the sampling can be significantly increased.

More recently, Hooker et al. (2004) converged the estimation of $L_W(\lambda)$ in coastal waters from above- and in-water techniques to within the uncertainty in the calibration of the sensors by emphasizing accurate metrology in the data acquisition and a more sophisticated technique for removing glint contamination. The above- and in-water methods used in this convergence activity form the basis for documenting the formulations for the two different measurement techniques.

For remote sensing CVR activities, the formulation given in (2) divides the calibration and validation observation requirements into four components (Fig. 4), respectively): the remote sensor (L_{sat}), the two atmospheric contributions ($L_{\text{atm}} + L_{\text{sfc}}$), and the *in situ* term (L_{sub}). The extraterrestrial solar irradiance can be used to express (1) and (2) in terms of reflectances by applying the definition of reflectance. This alternative formulation is not adopted here, because the emphasis within the field program is to make radiance, rather than reflectance, measurements.

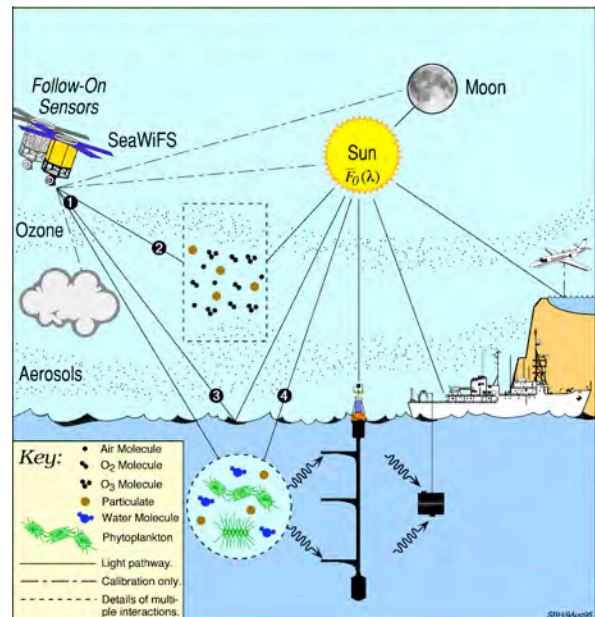


Fig. 4. The legacy calibration and validation paradigm for the Sea-viewing Wide Field-of-view Sensor (SeaWiFS) and Moderate Resolution Imaging Spectroradiometer (MODIS) satellite missions included both airborne and ship-based observations for ground truth (more properly *sea truth*) data, as follows: 1) L_{sat} , 2) L_{atm} , 3) L_{sfc} , and 4) L_{sub} .

1.2 Background


The optical method that is most similar to the satellite observation is the above-water approach, because *the satellite is an above-water radiometer*. The above-water instruments discussed herein are used to derive normalized data products (which account for the solar illumination during observations) by measuring the total radiance L_T at the water surface and the indirect sky radiance L_i in the same viewing plane. The L_W term is derived from the L_T observations by filtering out sun glint in the L_T data and removing the sky reflection based on a reflectance model depending on the viewing geometry (i.e., pointing angle of the radiometers) and wind speed (Hooker et al. 2002 and 2004). The first correction for the solar geometry is to normalize L_W by the global solar irradiance E_s , or $E_d(0^+)$ depending on the literature being referenced, to produce the remote sensing reflectance, $R_{rs} = L_W/E_s$.

The in-water derivation of R_{rs} , which is needed to validate a remote sensor, requires vertical profiles of downward irradiance $E_d(z)$ and upwelling radiance $L_u(z)$. A near-surface extrapolation interval is *objectively* established by converging the extrapolated $E_d(0^-)$ with the contemporaneous above-water E_s observations (Hooker et al. 2013) transmitted through the surface to null depth $z = 0^-$. The extrapolation interval is applied to L_u to estimate $L_u(0^-)$, from which L_W is computed using a constant that accurately accounts for the partial reflection and transmission of L_u through the sea surface (Mobley 1999). As with the above-water approach discussed above, the E_s term is used to normalize L_W to produce R_{rs} .

For remote sensing matchups, a correction to all L_W values for the Earth-Sun geometry as a function of the time of year yields the $[L_W(\lambda)]_N$. Further correction for bidirectional effects from different viewing geometries results in exact $[L_W(\lambda)]_N$ values, which are usually used to intercompare satellite and *in situ* matchups.

1.3 Design

The design of the C-AERO instrument suite is representative of all observational systems built with microradiometers. What is unique about the instruments with respect to C-OPS is their intended platform is an aircraft and the wavelength domain is more expansive.

 *The material presented here is not intended to be a substitute for proper integration leading to subsequent flight certification of the instrumentation on an aircraft—the material is solely to be used to document the radiometers and how the system is intended to function as an airborne remote sensing suite.*

1.3.1 Radiometers

The C-AERO instrument suite uses above-water radiometers from the XTRA class. The radiance (L) and

irradiance (E) instruments are designated XAL and XAE, respectively. If the selected wavelengths include the short-wave infrared (SWIR), the radiance radiometers are fitted with a shroud to reduce long-wavelength scattering at the aperture. For SWIR channels, indium gallium arsenide (InGaAs) detectors are used rather than silicon.

The C-AERO radiance radiometer without a shroud is shown in Fig. 5 and consists of five sections, as follows: a) entrance aperture (with field stops); b) Gershun tubes (which set the field of view); c) array of 19 microradiometers (with individual wavelength filter stack and front-end optics); d) support electronics (for power, ancillary sensors, and aggregator so the ancillary sensors and microradiometers function as a single instrument); and e) end cap with nitrogen fill and purge valve (black) plus six-pin (brass) bulkhead connector. The addition of a shroud to the entrance aperture does not change any of the other components, but it does make the instrument longer.

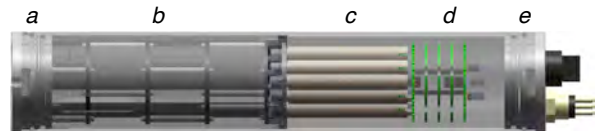


Fig. 5. A radiance instrument built with microradiometers showing the following: a) entrance aperture, b) Gershun tubes, c) array of 19 microradiometers, d) support electronics, and e) end cap.

With respect to an in-water radiance radiometer, an above-water C-AERO instrument is distinguished by a narrower field of view (i.e., the Gershun tubes), which increases the overall length. In the C-AERO instruments, the support electronics reside on circular PCAs to ensure the instrument is as compact as possible.

An irradiance radiometer has the same overall construction as a radiance instrument, wherein the microradiometer array, support electronics, and end caps are identical. The differences are at the entrance aperture end, as shown in Fig. 6. For C-AERO, the anticipated spectral range is 320–1,640 nm, so the cosine collector is an advanced design established for the Optical Sensors for Planetary Radiant Energy (OSPRey) activity (Hooker et al. 2012).

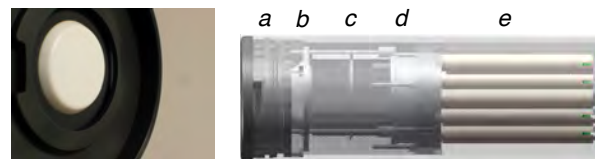


Fig. 6. An irradiance instrument built with microradiometers showing the cosine collector (left) and the components close to the entrance aperture (right), as follows: a) entrance aperture (cosine collector not visible), b) exit of secondary diffuser, c) lens spacing tube with stray light baffles, d) planoconvex lens (lens not visible), and e) *top* of microradiometer array (filter stacks and front-end optics not visible).

A C-AERO radiance instrument is 14.7 in (37.3 cm) long without a shroud, not including the bulkhead connector and nitrogen valve, and weighs 3.6 lb (1.6 kg). The addition of a shroud increases the length to 18.7 in (47.5 cm) and adds 0.5 lb (0.2 kg) to the weight. The C-AERO irradiance instrument is 13.3 in (33.8 cm) long and weighs 3.3 lb (1.5 kg).

1.3.2 Deck Box and Cables

The deck box used for the C-AERO instrument suite is the same one used for C-OPS, except flight certification is anticipated to require the removal of the built-in battery. The C-OPS deck box is thoroughly documented by Hooker (2014), so only a brief summary is presented here. The deck box is housed within a Pelican Products, Inc. (Torrance, California) type 1300 case. When the lid is closed and the latches secured, the deck box is waterproof. From the exterior, the deck box has two MCBH6F/MR bulkhead connectors.

The interior of the deck box contains a master aggregator circuit board with support electronics, plus a sealed 12 VDC battery and charging circuitry. The master aggregator sets the sampling rates and coordinates the polling of all the attached aggregators with their microradiometer assemblies. The deck box support electronics provide microprocessor-controlled power for all the sensors and is designed to avoid instrument damage due to improper power-up sequences over varying cable lengths. The Recommended Standard 485 (RS-485) signals from the two six-pin power-telemetry connectors are combined in the deck box and converted to Recommended Standard 232 (RS-232) or universal serial bus (USB) communications for computer logging.

The deck box control panel provides an on-off switch, 12 VDC power receptacle for the AC adapter, two safety fuses, an RS-232 bulkhead and USB 2.0 connector for computer logging, light-emitting diode (LED) indicators, and a liquid crystal display (LCD). The on-off switch is of the latching type and must be unlatched by pulling up on the switch before changing the switch setting. The two fuses protect each of the power-telemetry ports, respectively, wherein port 1 is the two radiance instruments, and port 2 is the solar irradiance reference. The RS-232 connection is a D-subminiature connector with an E-size (nine-socket) shell (DE-9S) and a pin assignment for communications with a personal computer (PC).

In anticipation of airborne campaigns requiring flight-certified cables, C-AERO uses cabling provided by Vast Manufacturing (Worland, Wyoming). The primary airworthiness requirement is to replace the wire insulation with aircraft-grade Teflon. The applicable standard is for the wiring to be certified commercial grade for avionics with a grounding lead and have jackets that are non-toxic in the event of a fire.

1.4 Results

Deployment of the C-AERO instrument suite does not require an aircraft. The instruments can be mounted in a frame to make above-water measurements of L_T and L_i , while E_s is measured simultaneously to account for changes in solar illumination. The radiance instruments have a narrow 2.5° full-angle field of view, hereafter, full view angle (FVA), and can be mounted in a tracker to be used as a sun photometer. To confirm the functionality of the first C-AERO radiance instrument, a radiance radiometer was mounted in a pan-tilt unit (PTU) model D300 (PTU-D300) manufactured by FLIR Motion Control Systems, Inc.† (Burlingame, California) and successfully made direct solar irradiance, $E(\lambda_{19})$, observations.

Figure 7 provides a schematic of the C-AERO instrument suite in a geometry suitable for above-water measurements of the ocean; the configuration is the same for airborne measurements, which is indicated by the inset aircraft depictions of the instrument pointing axes (orange for E_s , blue for L_i , and magenta for L_T). The deck box is shown with a grounded power cable to emphasize flight certification requires removal of the internal battery. The lighter gray extensions to the darker gray radiance instruments are the aforementioned shrouds to reduce stray light at longer wavelengths.

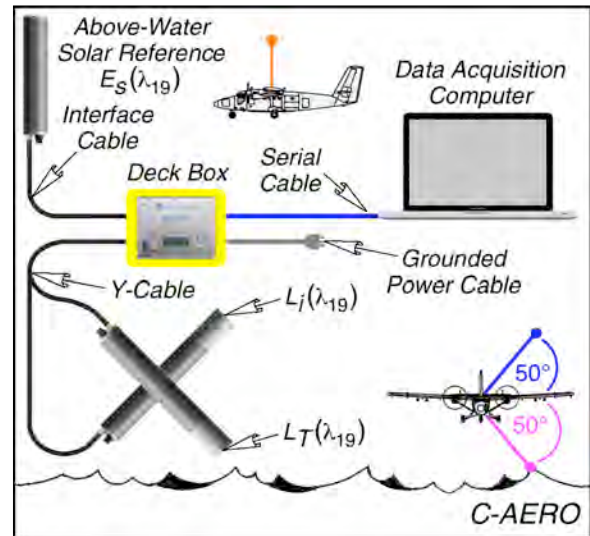


Fig. 7. The C-AERO deployment equipment and architecture, wherein the viewing geometry of the instruments on a Twin Otter aircraft are shown inset (recalling that the solar irradiance instrument makes a hemispherical measurement and can be perturbed by the aircraft tail).

The Twin Otter aircraft from the Center for Interdisciplinary Remotely-Piloted Aircraft Studies (CIRPAS), which is part of the Naval Postgraduate School (Monterey,

† Formerly called Directed Perception.

California), was flown at the LSA, which was typically 100–200 ft (i.e., approximately 30–70 m).

A comparison of microradiometer measurements obtained from an in-water instrument suite deployed from a ship (red) and an above-water instrument suite on an airplane (green) is presented in Fig. 8. The data were obtained within or above a toxic bloom, or red tide, in Monterey Bay using C-OPS and the Coastal Airborne In-situ Radiometers (C-AIR) predecessor instrument suite to C-AERO, respectively. The coincident spectral range of the two observational systems was 320–780 nm. The data compare the nearest in-water station to the nearest airborne observation. The plot shows the in-water data were obtained more substantially inside the red tide, because the highest amplitude peak in the green domain is with the C-OPS data.

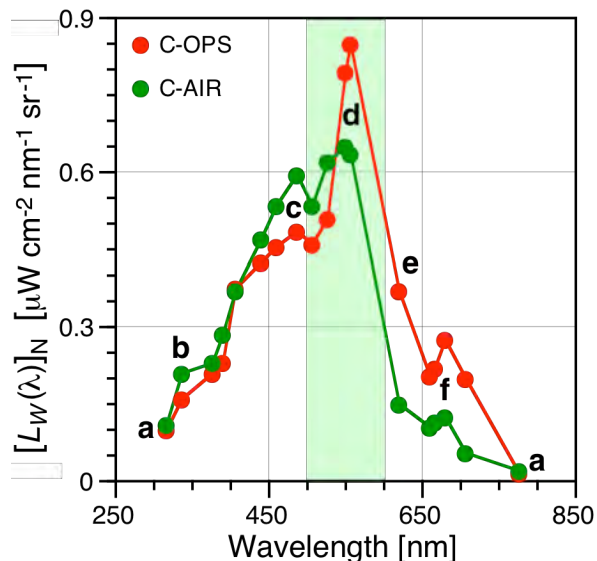


Fig. 8. A comparison of $[L_W(\lambda)]_N$ data obtained from an airborne instrument suite (C-AIR) versus an in-water instrument (C-OPS) within a red tide. The letter designations are explained in the text below, and the green rectangle delimits the green spectral domain.

The degree of validation in Fig. 8 is based on the good agreement between the two sampling systems, as achieved in terms of the following six spectral features spanning the entire spectral domain (UV to NIR): a) the

UV and NIR spectral end members are in agreement; b) the expected UV *shoulder* for the type of coastal water sampled is in both spectra, with the C-OPS data showing the anticipated UV suppression from the more intense bloom conditions; c) the expected blue shoulder for higher productivity coastal water in both spectra, with the in-water data showing greater blue suppression from the more intense bloom conditions; d) the expected peak in the green domain is in both spectra with the higher in-water peak establishing the C-OPS data were obtained more substantially in the red tide; e) the expected higher elevation of the red domain for the in-water spectrum (which was obtained in more intense bloom conditions); and f) the expected fluorescence peak is present in both spectra, with the airborne peak being larger as expected.

1.5 Conclusions

The C-AERO instrument suite was flight certified as the result of the Coastal High-resolution Observations and Remote Sensing of Ecosystems (C-HORSE) and Coastal High Acquisition Rate Radiometers for Innovative Environmental Research (C-HARRIER) projects (Fig. 9). Both activities were done in partnership with the Ames Research Center (ARC).



Fig. 9. The C-AERO instrument suite being flown on the CIRPAS Twin Otter aircraft above Lake Tahoe (Nevada side) during clear-sky conditions.

Chapter 2

The C-PrOPS and C-CAPS Accessories

STANFORD B. HOOKER
*NASA Goddard Space Flight Center
Greenbelt, Maryland*

RANDALL N. LIND, CHARLES R. BOOTH, AND JOHN H. MORROW
*Biospherical Instruments, Inc.
San Diego, California*

JAMES W. BROWN
*RSMAS University of Miami
Miami, Florida*

KOJI SUZUKI
*Hokkaido University
Sapporo, Japan*

TORU HIRAWAKE
*Hokkaido University
Hakodate, Japan*

ABSTRACT

The C-PrOPS accessory consists of two small digital thrusters plus an electronics module mounted on a slightly modified C-OPS backplane. The electronics module can support the addition of a conductivity sensor on the backplane as part of the C-CAPS accessory. Two digital thrusters, one on each side of the backplane, are mounted with both at the same cant angle, which allows the backplane to remain at the water surface while being maneuvered away from the operator holding the sea cable. This allows the avoidance of deployment platform perturbations (e.g., ship shadow), profiling in situations wherein it is not possible to position the profiler by another means (e.g., allowing the wind to move a boat away), and shoreline launches if the water depth and bottom topography are suitable. The thrusters stabilize the orientation of the backplane prior to throwing slack cable into the water and turning off the thrusters, which allows the backplane to free fall. This extra stability reduces the vertical tilting of the backplane and increases the vertical sampling resolution.

2.1 Introduction

Whether obtained with above- or in-water instruments, the most significant problem with making AOP measurements is minimizing the perturbations from the sampling platform the light sensors are deployed on or from. In the case of obtaining AOP measurements from a large platform (e.g., a research vessel), superstructure and submerged *hull* reflections brighten the ambient light field, whereas the platform and its shadow darken it. In all cases, corrections can be produced, but they require significant modeling efforts and involve a large dynamic range in solar illumination, sky conditions, and viewing geometries, which is not practical unless a platform is used repeatedly for extensive time periods.

A simple expedient for avoiding platform perturbations is to sample beyond or outside the perturbation areas. This does not remove the shading effect by the profiler itself, which still requires a correction (Gordon and Ding 1992), but the self-shading effect is inevitably smaller and easier to deal with than the platform perturbation. It is important to recall that the solar reference must be properly sited so it is not subjected to reflections or shading, which usually means it must be mounted well above and far away from any nearby structures.

2.2 Background

Physically positioning a free-falling profiler far enough away to avoid perturbations to the light field created by

the necessarily larger deployment platform is a recurring difficulty with a profiling instrument. In some cases, a fortuitous direction of the ambient current can move the profiler away from the platform with minimal effort, or the ambient wind might blow the platform (e.g., for an unanchored research vessel) away from the profiler.

If fortuitous conditions do not exist when deploying from a boat, short bursts of the propeller or a transversal propulsion device (e.g., on the bow or stern) are frequently used to push the profiler away. Unfortunately, this technique creates a large turbulent wake filled with bubbles and foam (Fig. 10) that usually engulfs the profiler.


 *The turbulent wake from a shipboard propulsion device must be allowed to dissipate before profiling commences*, because the turbulence negatively affects profiler stability, plus the bubbles and foam artificially perturb the *in situ* light field through increased scattering.



Fig. 10. The C-OPS backplane in the dissipating propeller turbulence of a small vessel reveals the large amount of bubbles formed as a result of using the propeller to push the profiler away from the boat.

The ability to maneuver a profiler with small thrusters obviates the need for using the ship's much larger propulsion device(s) and, thereby, also avoids the ensuing bubble- and foam-filled wake. Additional reasons why it is advantageous to maneuver a profiler independent of the deployment platform are as follows:

1. On a research vessel, the free-fall instrument can be launched from amidships or the bow and then moved into undisturbed water free of the mixed environment created by and surrounding the ship;
2. Some vessel operators allow contemporaneous optical sampling with a winched instrument, e.g., a conductivity, temperature, and depth (CTD) package, if the ship does not have to maneuver for the free-fall profiler;
3. The profiler can be launched and maneuvered into position from an immovable platform, e.g., a shoreline, dock, or anchored vessel;

4. Shallow water (e.g., a river, harbor, or near-shore marsh) is easily and turbulently disturbed by a boat propeller but negligibly so by small thrusters;
5. Optically different layers (e.g., a surface-intensified algal bloom) are also disturbed by a boat propeller, but significantly less so by small thrusters;
6. An intervening topographic feature (e.g., a shoal), might be a hazard to a vessel, but poses minimal risk to a profiler maneuvered over the obstacle at the surface using small thrusters;
7. Sampling under an ice floe is not feasible with a ship, but a profiler with thrusters could be deployed from the ship and maneuvered under the ice with the aid of a camera mounted on the backplane, wherein differential thrust is used to execute turns;
8. The thrusters keep the profiler at the surface before a cast commences with the pressure transducer measuring the atmospheric pressure, so each cast can be individually pressure tared;
9. The profiler can be tethered to, but when necessary, maneuvered away from, a slowly moving platform, e.g., a drifting buoy or a USV;
10. The thrusters stabilize the profiler by keeping it vertically oriented before thrust is removed to begin the profile, which significantly improves data quality;
11. After descent begins, low-level thrust can be used to further slow the descent of the profiler in near-surface waters, thereby, further increasing the vertical resolution of the observations;
12. The thrusters can ascend the profiler to the surface faster and automatically reposition the instrumentation away from the operator holding the sea cable, thereby reducing the cycle time between casts; and
13. Ascent thrust levels can be varied to allow for stable measurements, particularly near the sea surface, thereby yielding more profiles than just down casts.

The ability to minimize the disturbance of an optically complex water column—which is defined here as a water mass with one or more (sometimes thin) layers with optically different properties—allows a variety of hydrographic features to be nondestructively sampled. For example, the influence of a thin layer of melt water in the marginal ice zone can be discerned optically, but only if the profiler can be positioned with negligible disturbance. The presence and vertical extent of such a feature can be confirmed with a conductivity probe, because the fresher water overlies saltier water. Consequently, the addition of C-CAPS is considered a logical part of C-PrOPS development.

Thrusters can also be used for autonomous profiling in unmanned sampling systems. The Compact-Submersible Autonomous Winch (C-SAW) concept (Fig. 11), combines a C-OPS equipped with C-PrOPS plus a drifting buoy to produce a fully autonomous AOP sampling system. The

capability to “winch” the profiler up and down is provided by the C-PrOPS thrusters driving the C-OPS profiler to the surface from a stowed position at depth, whereupon the profiler falls freely back to the stowed position. The buoy provides solar panels to recharge batteries housed in the buoy plus a reference instrument to measure the global solar irradiance (E_s).

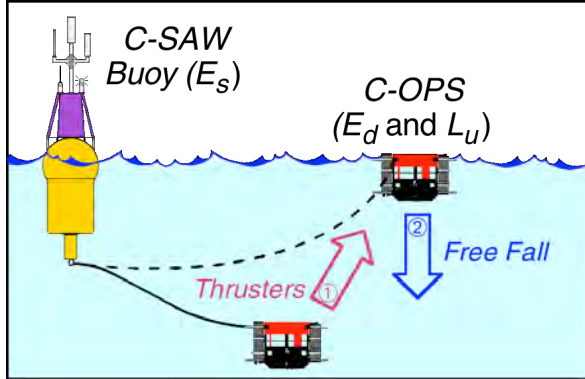


Fig. 11. The C-SAW buoy, wherein a C-OPS instrument with digital thrusters ascends the backplane away from the buoy to the surface, and then the profiler falls freely back to the stowed depth.

A USV can replace the drifting buoy to allow the entire sampling system to be positioned by a shore operator or a pre-determined navigation program, as described in Chap. 7 for the Hybrid System for Environmental AOP Sampling of the Sea Surface Demonstration (HySEAS3D) concept. The first implementation based on the HySEAS3D concept is documented in Chap. 8 for the Hybridspectral Alternative for Remote Profiling of Optical Observations for NASA Satellites (HARPOONS) vicarious calibration project.

2.3 Design

A maneuverable optical profiler allows new sampling opportunities based on a diversity of command and control possibilities using thrusters. Ultimately, capabilities reminiscent of an ROV can be conceptualized, but that is not the focus here. Instead, what is anticipated are simple thruster controls that will significantly improve sampling while minimizing power consumption and complexity of design to ensure reliability. In particular, because the thrusters require more power than the optical instruments and seawater is conductive, *electrical safety for the operator and equipment is a high-priority objective.*

To make the C-PrOPS and C-CAPS accessories as economical as possible, the philosophy of the design effort was to retain as much of the original deployment equipment and architecture as possible. In other words, the new capabilities are anticipated to be an accessory to the standard configuration for a C-OPS instrument suite, which has the following components (Fig. 3): a) the C-OPS profiler comprised of the backplane with in-water instruments

attached; b) the surface reference with above-water instruments (which might include the BioSHADE and BioGPS accessories); c) the deck box that powers all of the instruments while providing the data and telemetry for the above- and in-water components; d) the (laptop) computer for hosting the data acquisition software and recording the data; and e) the cabling that connects the applicable components.

2.3.1 Digital Thrusters

The C-PrOPS accessory digital thrusters are manufactured by SeaBotix (San Diego, California). The model SBT161, which has a brushed direct current (DC) motor and RS-485 communications, is used in tandem, with one mounted on each side of the backplane at a canted vertical angle (Fig. 12). The angle allows the thrust turbulence to be directed below the backplane, but away from the radiance aperture, while propelling the backplane upwards and in the direction of the radiance instrument. The upward component of thrust allows the thrusters to keep the backplane at the surface or return it to the surface from depth (e.g., after a vertical profile is terminated).

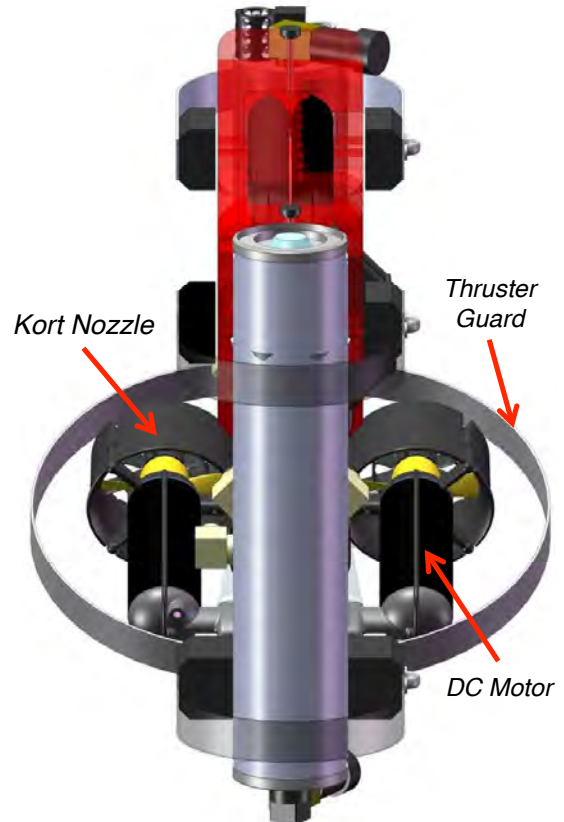


Fig. 12. An edge-on and top-down view of the thruster placement design on the C-OPS backplane with large guards or bumpers to protect against side impacts. The guards allow the instrumentation to be placed on the side while protecting the plastic housing of the Kort nozzle.

The thrusters are 6.9 in (17.6 cm) long, and the Kort nozzle has an outer diameter of 3.7 in (9.5 cm). The nominal voltage to power the thrusters is 28 VDC with a maximum current of 5.0 A. The thrusters are run at 45% of their rated maximum, which ensures the running average current is kept well below the 5.0 A rating to prevent the motor windings from building up excessive heat. Running the thrusters at 45% of maximum thrust yields approximately 3.0 kg of total thrust.

A user-performed service for the SBT161 is recommended for every 50 h of operation or 2 y of life; factory service is recommended every 500 h of operation. Although brushed motors can wear out, they should not do so within the anticipated operation of typical C-PrOPS optical sampling scenarios (i.e., a few campaigns a year with each one lasting a few weeks).

Brushless motors cost twice as much, so the cost benefit of greater longevity is questionable, although brushless motors do have true stall detection and greater power. As shown in Fig. 12, the thrusters are protected with an aluminum bumper similar to the optics bumpers (Fig. 3). The Kort nozzle that surrounds the propeller, as well as the propeller end cap, are field-replaceable (spare parts).

2.3.2 Conductivity Sensor

The conductivity and temperature (CT) sensor used for the C-CAPS accessory is manufactured by Neil Brown Ocean Sensors, Inc. (Falmouth, Massachusetts). The CT mounts within a channel cut into the hydrobaric chamber, which is stabilized using a rigid strut affixed to the backplane in Fig. 13. By positioning the device within the foam used to create the hydrobaric chamber, the probe is protected by the foam. In addition, it is recessed behind one of the harness attachment points, which provides additional protection.

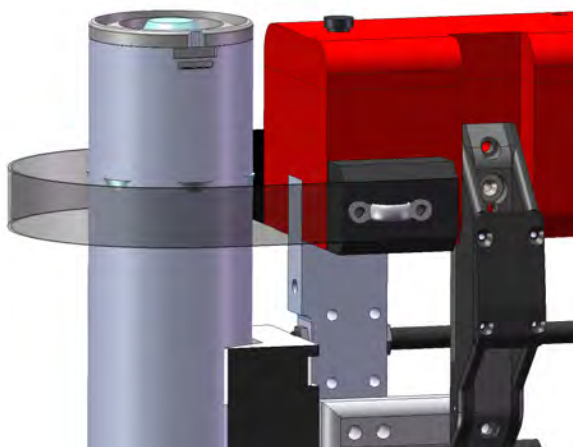


Fig. 13. A side-on view of a portion of the C-PrOPS backplane showing the CT sensor mounted within a channel cut into the hydrobaric chamber (red foam). The sensor is rugged and shaped to be inherently snag proof, to avoid fouling by seaweed and other flotsam.

The CT is a 4-electrode conductivity cell with integral temperature sensor. A fast response thermistor is mounted within the conductivity cell to ensure accurate salinity computations. The CT was designed to meet the needs of a glider and autonomous underwater vehicle (AUV), so it is well suited for C-PrOPS operations. No pump is required and the electronics are self-calibrating with minimal thermal drifts. The CT sensor has superior performance in strong temperature gradients and for studies of thin biological or optical layers in the ocean.

2.3.3 Electronics Module

The C-PrOPS electronics module (Fig. 14) contains the circuitry for controlling the two digital thrusters, as well as the PCA for the CT sensor. The input voltage specification for the electronics module is 36–76 VDC. Because the digital thrusters can use a significant amount of power, which generates heat, the electronics module includes heat sinks to conduct heat to the outer housing of the module. There are five connectors on the module (only four are visible in Fig. 14), as follows: a) two are for the digital thrusters, which use RS-485 telemetry; b) one is for the CT sensor; c) one is for a Y-cable that connects to the two radiometers; and d) the fifth connects to the sea cable. The sea cable can be up to 150 m in length.



Fig. 14. A transparent drawing of the C-PrOPS electronics module that also contains the PCA for the CT sensor.

The CT sensor electronics are contained on a single $1.85 \times 6.0 \text{ in}^2$ PCA (Fig. 15). DC power at $12 \text{ VDC} \pm 10\%$ is supplied to the PCA. A DC-DC converter on the PCA generates the $\pm 5 \text{ VDC}$ required by the board electronics. The PCA draws approximately 35 mA independent of sample rate. The conductivity cell is in electrical contact with seawater but is DC isolated from the system power supply to avoid interfering with ground fault detection circuits.



Fig. 15. The PCA for the CT sensor, which is mounted inside the electronics module.

A microprocessor controlled, transformer-based referencing circuit provides self-calibration of the signal processing electronics on the CT PCA. The sensor output

and reference signals are multiplexed into a single channel where they are amplified and synchronously detected then digitized by the 24 bit ADC. Variations of circuit parameters with temperature and time are substantially removed through digital processing by the microcontroller. The electronics are AC isolated from seawater by transformer-capacitor coupling of the conductivity cell. The drive level of the thermistor circuit is chosen to minimize self-heating effects.

The digital CT data is communicated through an RS-232 serial port in American Standard Code for Information Interchange (ASCII) format. The CT sensor can be configured for sample rate, serial baud rate, and different data output and timing modes. For C-OPS operations, the sample rate is set to 10 Hz.

The CT aggregator is programmed to receive the serial ASCII data stream from the CT sensor asynchronously. Upon completion of the CT sensor data frame, the ASCII encoded, variable-length data stream is parsed and the individual temperature, conductivity, and salinity values are converted from ASCII to floating point short precision format, which matches the format used by microradiometers. In this fashion, each of the three readings are identical in format to readings from microradiometers and can be processed as any other data.

The CT aggregator also transmits diagnostics in a fashion identical to standard C-OPS radiometers. They are in order of transmission, as follows: a) voltage input received by the aggregator, b) current draw of the aggregator, c) temperature (of the aggregator electronics), d) pressure (internal pressure of aggregator housing), e) voltage to the CT sensor, and f) current draw of the CT sensor.

2.3.4 Backplane

The C-OPS backplane is built with synthetic material that is hollowed out to accommodate floats and weights, and then populated with a mostly symmetric grid of 5 mm diameter holes for affixing cables and mounting accessories. The mechanical design to accommodate adding the C-PrOPS and C-CAPS accessories is based on increasing the long axis of the backplane from $12.0 \times 11.7 \text{ in}^2$ ($30.5 \times 29.7 \text{ cm}^2$) to $18.0 \times 11.7 \text{ in}^2$ ($45.7 \times 29.7 \text{ cm}^2$). The C-CAPS sensor requires a companion circuit board and the digital thrusters require additional power and control electronics, so the new backplane also includes a mounting capability for a pressure housing to contain an extra electronics module.

A transparent drawing of the C-OPS in-water instrument components with the C-PrOPS and C-CAPS accessories attached is presented in Fig. 16 (the *roll* axis is the long axis and the *pitch* axis is the short axis into or out of the page). The hydrobaric buoyancy chamber has air holes for flooding, and two screws are used to remove the top to insert up to three compressible bladders. If one or more of the bladders are not used, replacements

made out of the foam flotation material can be inserted instead. The aggregator and support electronics control the 19 microradiometers as a single device. The side bumpers and thruster guards protect the radiometers and digital thrusters from side impacts, respectively. The bumpers and guards are strong enough to be used as *handles* to carry the profiler (although gloves should be worn to ensure safety).

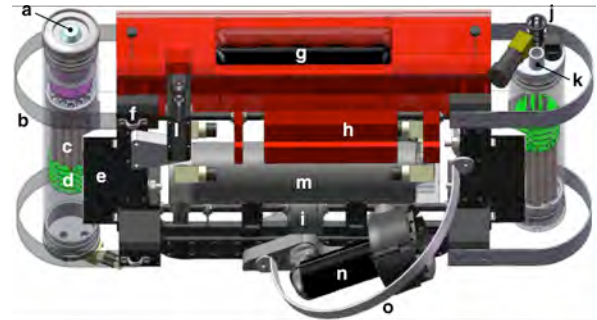


Fig. 16. The C-OPS instrument with C-PrOPS and C-CAPS accessories: **a)** irradiance cosine collector; **b)** bumper; **c)** array of 19 microradiometers; **d)** aggregator and support electronics; **e)** rotating V-block for *pitch* adjustment; **f)** two-point *side-on* harness attachment; **g)** hydrobaric buoyancy chamber; **h)** slotted flotation and **i)** weights for buoyancy and *roll* adjustment; **j)** water temperature probe; **k)** pressure transducer port; **l)** conductivity sensor; **m)** electronics module; **n)** digital thruster (1 of 2); and **o)** thruster guard.

The two digital thrusters are mounted at the same cant angle with respect to the vertical, which directs the turbulence from the thrusters slightly downward and below the irradiance instrument (Fig. 17); the opposite occurs if the thrust is reversed. When thrust is applied to move the profiler forward, the profiler is driven upwards and away from the operator holding the sea cable, which propels the radiance end cap upwards into unperturbed water and the irradiance aperture is pulled downwards.

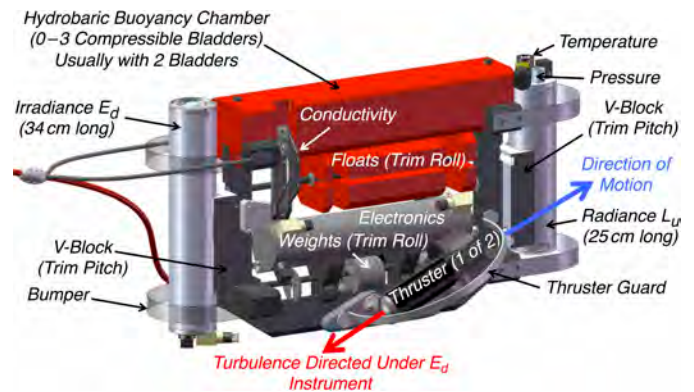




Fig. 17. The C-OPS in-water instrument with C-PrOPS and C-CAPS showing the side harness with original red sea cable attached (strictly for illustrative purposes), *forward* thruster velocity (blue arrow), and the resulting turbulence (red arrow).

When equal thrust levels are applied to both thrusters, the backplane moves in a straight-line direction established by holding onto the sea cable and then slowly letting the cable slip through the hands of the operator.

 *A rough cable can cause injury if it is allowed to rapidly slip over bare skin (e.g., through the hand), consequently gloves are recommended when handling the sea cable.*

This means the radiance radiometer needs to be oriented towards the direction of desired motion, when the profiler is first placed into the water.

 *If the profiler deviates from the desired original course, perhaps by wave or current forces, a sharp pull on the cable usually reorients the direction to line up with the original course.*

Once the profiler reaches the desired position for executing a cast, it can be kept there by maintaining forward thrust and firmly holding onto the sea cable.

To steer the backplane like an ROV, differential thrust is applied to the two thrusters. If forward thrust is decreased to one of the thrusters, the backplane turns toward the side with reduced thrust. If reverse thrust is applied to one of the thrusters, the backplane turns more quickly towards the side with reversed thrust. The ability to steer the profiler allows for real-time positioning adjustments, which is a significant advantage in shallow waters, e.g., a marsh.

The water temperature probe and the pressure transducer port are located in the radiance instrument end cap. During forward thrust, the pressure transducer measures the atmospheric pressure right before a profile is commenced, so each cast can be pressure tared. When the thrust is removed, the momentum of the prior thrust keeps the profiler close to the surface, the roll tilt relaxes, and the profiler starts to descend with stable tilts (the pitch angle is already negligible, because the prior thrust aligns the profiler with almost no pitch angle).

2.3.5 Electric Shock

The design of the needed electrical circuits and equipment includes attention to preventing an electrical shock, as well as trapping fault conditions that can cause a shock. The occurrence and severity of an electric shock is a function of many variables[†] including, but not limited to, the following: the integrity of cables and connectors; the voltage level, type, and frequency (AC or DC); the person's gender (man or woman) and their body mass; and individual resistance factors (e.g., wet or dry conditions).

[†] Because of the individual circumstances of an electric shock there are no absolute parameters regarding occurrence and severity, so what is presented here is a cautious consensus based on numerous sources, e.g., Ferris et al. (2005), Parker (2009), and NEC (2011).

The latter is particularly important during oceanographic fieldwork, because wet skin (from sweat or water) has a reduced resistance compared to dry skin[‡]. Additionally, work surfaces are often wet, providing a reduced resistance from a human body to ground. These factors combine to lower the effective resistance a body presents to an exposed voltage source, allowing greater currents to flow through the body than would normally be expected.




An electric shock will occur when any source of electricity makes contact with a (human) body part such that sufficient current passes through the skin, muscles, or hair. A properly maintained cable of the type used with C-OPS instruments is not a typical hazard. The most likely reason for a hazard to occur is if the integrity of the cable is compromised and it is not noticed or repaired.

As a general guideline, for a man exposed to DC current, the quantitative effects are as follows:

- 1 mA A slight tingling sensation;
- 5 mA The perception threshold, i.e., the accepted maximum harmless current;
- 10 mA A shock with minimal loss of muscular control;
- 60 mA A painful shock with a majority loss of muscular control;
- 75 mA The “let-go threshold” (i.e., the current threshold above which a person is unable to release an electrically energized source because of involuntary muscle contractions); and
- 90 mA A painful and severe shock with difficulty breathing and almost total loss of muscular control.

The quantitative effects of DC current thresholds for a woman are about 70% of a man.

Because wet skin is more conductive than dry skin, a common sense approach to safety when working with electrical equipment is to ensure dry contact with any source of electricity.

   *When handling cable that is wet, it is advisable to wear gloves that keep exposed skin dry, which might require two layers of protection—one for adequate gripping of the cable worn over one that keeps the hands and arms dry.*

2.3.6 Sea Cable

The digital thrusters used with the C-PrOPS accessory require more power than the original six-conductor C-OPS sea cable can accommodate. Simply adding more conductors to the original cable is not an option, because the

[‡] Dry skin has a resistance of about 500–1,000 k Ω , but wet skin has a resistance of approximately 1 k Ω . The resistance of cut or punctured skin can be less than 1 k Ω , because blood contains electrolytes that facilitate the conduction of electricity. If the point of contact is a metal ring worn on a wet hand, the resistance can be on the order of 100 Ω , so removing metal objects while working mitigates the likelihood of a shock.

Table 1. The specifications for the data-telemetry (sea) cables used with C-OPS free-fall optical instruments. The synthetic jacketing materials are polyurethane (PU) and polypropylene (PP). Conductor specifications are given in American Wire Gauge (AWG) sizes.

<i>Cable Characteristic</i>	<i>Pale Red (PU) Cable</i>	<i>Neon Green (Foam PU) Cable</i>
Manufacturer	Storm Products	Outland Technology
Power Conductors	2 × 20 AWG	3 × 18 AWG and 2 × 22 AWG
Telemetry Conductors	2 × 2 × 24 AWG†	2 × 22 AWG‡ and 2 × 24 AWG‡
Video Conductors	None	75 Ω coaxial
Outer Diameter	0.32 in (nominal)	0.55 in (nominal)
Strength Member	Kevlar (500 lb breaking rating)	Kevlar (1,000 lb breaking rating)
Outer Jacket	Red Low-Density PU	Neon Green Low-Density Foam PU
Connectors	SubConn Micro In-Line (MCIL6)	SubConn Micro In-Line (MCIL8)
Weight per 10 m (32.8 ft)	0.8 kg (1.8 lb)	1.5 kg (3.3 lb)
Instruments	SuBOPS and C-OPS	C-OPS with C-PrOPS and C-CAPS

† Twisted shielded pair with PP insulation.

‡ Twisted pair with PP insulation.

cable would no longer be nearly neutrally buoyant. Consequently, a new cable was specified with respect to the original cable used with C-OPS and its prototype (Hooker et al. 2010), which was called the Submersible Biospherical Optical Profiling System (SuBOPS). As shown in Table 1, the new cable has a neon green low-density foam PU outer jacket, 9 conductors with varying wire gauges (two of which are combined to produce an eight-conductor assembly), plus a 75 Ω coaxial cable for future video applications.

The new (neon green) sea cable uses eight conductors, whereas the old (pale red) cable uses six (Table 1). The cable for the solar reference is the same as a regular C-OPS, i.e., six conductors. Both the old and new cables use the same family of SubConn micro circular in-line connectors. The extra two conductors for the new sea cable provide power for the digital thrusters.

In terms of the number of contacts assigned to pins and sockets in the new sea cable, four are used for power, two provide the telemetry for the microradiometers and C-CAPS data, and the remaining two provide the telemetry for data from the thrusters. Although this means the solar reference could operate on a four-conductor cable and bulkhead connector (two for power plus two for data and telemetry), the usual six-contact cabling is retained to minimize changes in cabling inventories and, thus, cost.


For the power conductors, all of the in-water electronics (radiometers, thrusters, etc.) share the same power, with two pins dedicated for power, and two pins dedicated for ground. This is done so as not to exceed the amperage ratings of the SubConn pins. A wiring diagram for the new eight-contact (with nine conductors plus coaxial) sea cable is presented in Fig. 18.

2.3.7 Data and Telemetry



To accommodate the C-PrOPS and C-CAPS data and telemetry, while keeping aspects of the data stream separate within eight contacts, the radiometers use half-duplex

RS-485 communications. The RS-485 communications to the solar reference are not isolated; the RS-485 communications to the in-water radiometers and the two digital thrusters are isolated.

All radiometers and accessories (e.g., BioSHADE, BioGPS, etc.) require a firmware version that is compatible with half-duplex communications. Presently, all radiometers and accessories in the system are physically switched in the aggregator PCA stack to half-duplex for simplicity.

 In theory, a radiometer physically left in the full duplex state would work with half-duplex instruments, but *this has not been rigorously tested.*

Changing to half-duplex communications is reversible, but it requires physical access to the aggregator PCA stack, which means the instrumentation must be opened.

  Consequently, changing a half-duplex system back to full-duplex communications should only be performed by the manufacturer.

The change to half-duplex communications for a radiometer or accessory consists of two required operations, as follows: a) a firmware upgrade, and b) changing the state of a physical switch on a PCA. The change to half-duplex communications for a deck box consists of these two required operations plus a change in the wiring from the deck box MCBH6F bulkheads to the deck box PCA.

To record data and provide telemetry for the radiometers and accessories, the RS-232 communications protocol is used, which is accessed on a DE-9S connector. The pin assignment for communications follows the convention established for a PC. The connector is located on the original C-OPS (yellow) deck box, which also contains a USB 2.0 connector for alternative computer logging. More complete details regarding the use of the C-OPS (yellow) deck box are available in Hooker (2014).

The data and telemetry associated with commanding or controlling the thrusters are provided on a connector

cable that attaches to the side of a new control box using a SubConn three-pin micro in-line cable plus a DE-9S connector, as discussed in the following section. Similar to the original C-OPS (yellow deck box), the communications protocol is RS-232, except it is isolated.

2.3.8 Control Box

The principal purpose of the C-PrOPS control box (Fig. 19) is to provide the power to operate all the in-water instruments, while providing sophisticated shock-mitigation circuitry with LED status indicators. Power conditioning for the thrusters is done in the electronics module mounted on the C-OPS backplane. The control box is designed to return all the data and telemetry from the in-water instruments, with the data and telemetry for the thrusters available as a separate connector on the side of the control box.

The perspective adopted here is that all cable connects and disconnects should be done with the power off, because fieldwork—most notably an oceanographic expedition—involves the high probability of working with wet components, as well as wet hands or feet, which can result in unintended and potentially hazardous electrical pathways that might go unnoticed.

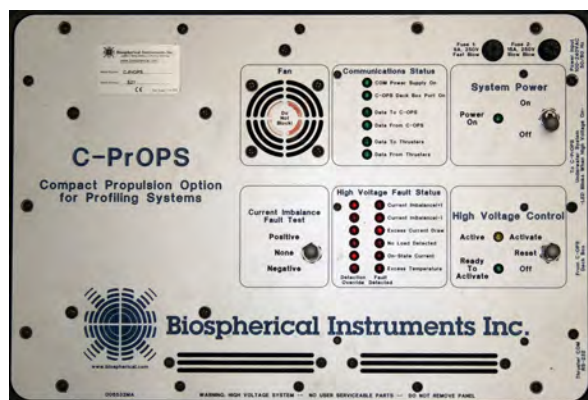


Fig. 19. The C-PrOPS control box front panel showing from the right edge to the left middle the following: a) the labels for the four bulkhead connectors; b) the system power above the high voltage control, both with status lights and switches; c) the communications status above the high voltage fault status; and d) the cooling fan above the current imbalance fault test switch.

The data and telemetry for the thrusters are made separately available, so the control box can be positioned close to where the in-water profiling is occurring, if desirable. The control box is built inside a Pelican 1500 case with latching cover and waterproof gasket. All connections are SubConn wet pluggable, so the control box can be used outside, and if the lid is latched shut, there is no risk of water ingress.

The control box contains a fan for internal air circulation and cooling. Consequently, it can be operated with the lid latched for short periods, e.g., the time needed to conduct three vertical profiles, especially if it is kept out of direct sunlight.

The internal temperature of the control box is monitored. If the control box PCA temperature sensor reaches 100°C, the power is automatically turned off for safety (Sect. 2.3.9). The control box consists of the following functional elements:

1. System Power On-Off latching switch and Power On indicator;
2. High Voltage Control with Activate-Reset-Off latching switch plus Active and Ready To Activate indicators;
3. Communications Status circuitry with indicators;
4. High Voltage Fault Status with detection and override capabilities; and
5. Four SubConn bulkhead connectors.

The four SubConn bulkhead connectors have the following specifications and purposes (all MCBH connectors have built-in MR locking sleeves):

- a) BH3M (with MR locking sleeve) to connect the three-conductor 120 VAC power cable,
- b) MCBH8F to connect the eight-conductor sea cable (MCIL8M),
- c) MCBH6M to connect the six-conductor in-water cable from the deck box.
- d) MCBH3F to connect the three-conductor serial cable for the thruster, and

There are two LED indicators on the control box front panel to show the high voltage is active, one on the top panel and one on the side where the bulkhead connectors are located. The indicators are yellow and blink when the high voltage is on; the one on the side is rather large, so it can be seen from a distance. If the control box lid is closed for a short period of time while operating, the side indicator is visible.

The control box is a high voltage system nominally providing 60–64 VDC at a maximum of 8 A with no user-serviceable parts except fault overrides; it should not be opened except by the manufacturer or after consultation with the manufacturer.

For a C-OPS backplane equipped with the C-PrOPS and C-CAPS accessories, the above-water components are connected to the (yellow) deck box as usual (Fig. 3). A DE-9S serial cable is used to connect the data acquisition computer to the deck box, and an AC adapter is used to power the (yellow) deck box (as appropriate). For most modern computers, a USB serial adapter is also required to connect the DE-9S to the computer recording the data. The in-water circuitry requires four connections to the control box, as shown in Fig. 20.

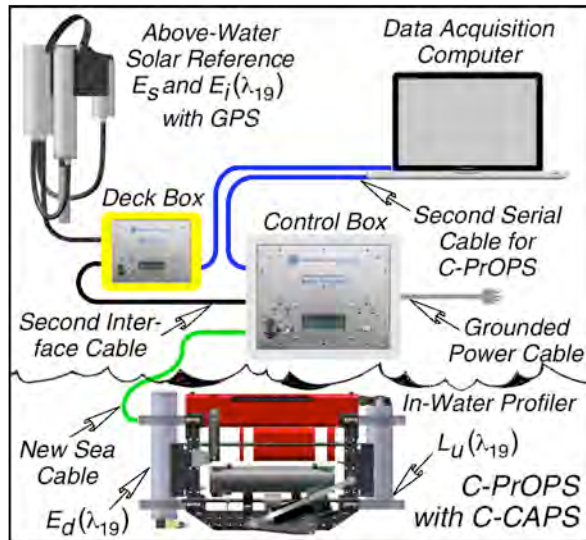


Fig. 20. The C-OPS deployment equipment and architecture redesigned to include C-PrOPS and C-CAPS accessories (compare to Fig. 3).

The thruster serial cable need not be connected to the same computer used for the above- and in-water optical data and telemetry; a second computer can be used if desirable (perhaps located with a good view of the profiling operations). In general, however, good radio communications will allow a data acquisition operator to control the thrusters from a remote location, and this is the usual deployment scenario.

On larger platforms (e.g., an ocean-class research vessel), an additional eight-conductor cable with a neoprene jacket (and appropriate locking sleeves) is run from the control box to the basket or bucket holding the profiler sea cable. This so-called interface cable (Hooker 2014) permits almost all the sea cable to be deployed into the water and it allows the sea cable basket or bucket to be disconnected and easily moved inside as a protection against severe weather (recalling that dummy plugs are needed to protect the exposed connector pins and sockets).

⚠ ⚠ ⚠ *Under no circumstance should the sea cable be completely deployed into the water, because the mated locking sleeves for the interface and sea cables, as well as the strength of the neoprene cable (which does not have an aramid internal strength member), are not sufficient to ensure recovery of the profiler.*

The four connections to the control box are identified on the front panel, as follows:

- The Power Input 100-240 VAC 50/60 Hz bulkhead connector mates to an IL3F/FG cable connected to a three-prong 120 VAC power outlet.

⚠ ⚠ ⚠ *To ensure the proper functioning of the fault detection circuitry, the control box must always be connected to a properly grounded three-contact power outlet.*

- The To C-PrOPS Underwater System bulkhead connector mates to an MCIL8M/FG connector for the sea cable with the other end connected to the backplane Y-cable.
- The From C-OPS Deck Box bulkhead is the usual six-pin connector and mates to an MCIL6F/FG connector with the other end connected to the C-OPS (yellow) deck box in-water (profiler) port.
- The Thruster COM RS-232 bulkhead connector mates to an MCIL3M/FG cable with the other end connected to the data acquisition computer via a DE-9S connector (and, usually, a USB serial adapter).

All the connecting cables have FG locking sleeves, which means some cables (e.g., the sea cable) might need adapter cables (Hooker 2014) to convert from MR to FG. In addition to changing the sex of the locking sleeve, the adapter cables absorb the stresses associated with connections and bending radius limitations without damaging the higher cost and difficult to replace sea cable.

Powering the system on requires both the C-OPS original (yellow) deck box and the (silver) control box. The deck box provides power to the solar reference; the control box provides power to the in-water instruments and the thrusters. The deck box contains the master aggregator, and constructs each complete data and telemetry frame for the solar reference and the profiler, but not for the thrusters. The solar reference is connected to the master aggregator with a six-conductor interface cable. The profiler is connected to the master aggregator through the eight-conductor sea cable plus an eight-conductor adapter (or interface cable, depending on the size of the ship). A second six-conductor interface cable connects the deck box to the control box.

The interconnection for the thruster is inside the electronics module (Sect. 2.3.3) mounted on the backplane (Fig. 16m). The data and telemetry connection between the thrusters and the data acquisition computer is through a serial connection on the control box.

⚠ ⚠ *Before attempting to apply power to any one component, confirm all cables are properly connected, as shown in Fig. 20.*

To power on a C-OPS equipped with the C-PrOPS and C-CAPS accessories, the following Control Box steps, in the order specified, are required:

1. Set the System Power latching switch to the Off position and set the High Voltage Control latching switch to the Reset position;
2. Confirm the connection of all four system cables as indicated on the side of the control box, as well as the cable connections for the above-water instruments to the C-OPS deck box (Fig. 20);
3. Set the System Power latching switch to On (the green Power On indicator should illuminate);

4. Wait for the green Ready To Activate indicator to illuminate;
5. Set the High Voltage Control latching switch to Activate (the yellow Active indicator should start blinking on the control box panel and the side where the bulkhead connectors are); and
6. Power on the C-OPS deck box and wait for it to inventory all instruments.

If any indicators do not illuminate as anticipated, set the system power latching switch to the Off position and the high voltage control latching switch to the Reset position and try the power-on sequence again. Only start up the C-OPS and thruster data acquisition software (recalling there are two serial ports to be used) if the power-on sequence is successful.

The control box Communications Status function includes the following (green) indicators:

- COM Power Supply On;
- C-OPS Deck Box Port On;
- Data To C-OPS;
- Data From C-OPS;
- Data To Thrusters; and
- Data From Thrusters.

During operations wherein all components are being used, the above indicators will all illuminate green and the data to and from illuminators will flash. In the event of one or more system faults, the communications status indicators should be investigated to determine if the fault is immediately identifiable.

To turn off the power to the system, the following steps, in the order specified, are required:

- Stop or shut down all data acquisition software;
- Set the High Voltage Control latching switch to Off (the yellow indicator should stop blinking);
- Set the System Power latching switch to Off (the green power indicator should turn off); and
- If the system is not to be used again in the configured state, disconnect all four cables from the control box.
- If demobilizing, reinstall the four dummy plugs.

2.3.9 Fault Detection and Overrides


In addition to providing the power needed to operate all the in-water system components, the control box has built-in circuitry to identify power fault conditions and if present, shut the power off to protect the operator(s). There are six High Voltage Fault Status indicators, which illuminate as fault warnings based on when the following triggering thresholds are exceeded:

1. Current Imbalance (+) triggers when the current measured on the high voltage supply line is more than 40 mA greater than that measured on the return conductor;

2. Current Imbalance (–) triggers when the current measured on the return conductor is more than 40 mA greater than that measured on the high voltage supply line;
3. Excess Current Draw triggers when current sourced by the high voltage supply to the underwater components exceeds 8 A;
4. No Load Detected triggers when the High Voltage Control latching switch is set to On and the current drawn by the underwater components is less than 40 mA;
5. On-State Current triggers when the High Voltage Control latching switch is set to Off and the current drawn from the high voltage supply is more than 40 mA; and
6. Excess Temperature triggers when the control box PCA temperature sensor reaches 100°C (the fault automatically resets when the temperature subsequently drops to 60°C).

The thresholds cited above are approximate, and can vary as a function of circuit variables and physical conditions. Consequently, they may drift to a point wherein a fault is spuriously triggered.

If a fault is determined to be spurious and if consultation with the manufacturer produces agreement, the fault may be overridden in the field. The control box will have to be disconnected from the four cables attached to it and taken to a clean, dry area.

 *The override procedure involves applying a jumper on a PCA, so the work should be done with a grounding strap.*

If it is not possible to work with a grounding strap, excess static electricity may be removed by plugging in the AC power cord for the control box, but without turning on or activating any of the latching switches. Once the power cable is connected to grounded AC power, the control box panel will be tied to AC ground. Excess static electricity is removed by touching the screw above the fan vent, which is the ground connection for the panel, with each bare hand. Unplug the power cable before proceeding.

To access the fault control jumpers, remove the 16 perimeter screws and set them aside. Assuming the edge of the panel that is nearest the handle for the control box case is the front, and the back is along the hinge side, lift the panel starting at the right side near the High Voltage Control latching switch. Then lift from the front (handle) edge, tilting the panel up on its back (hinge) edge. To avoid stressing any of the cable connections, work slowly and patiently.

While tilting the panel upward from the front edge and downwards along the back edge, unplug the three-pin connector with white wires. Lift the panel the rest of the way up, carefully resting it vertically on the back

edge. The override jumpers are located near the upper right corner of the PCA and are labeled JP1–JP6 (Fig. 21), inclusive, as follows:

- JP1 Current Imbalance (+);
- JP2 Current Imbalance (-);
- JP3 Excess Current Draw;
- JP4 No Load Detected;
- JP5 On-State Current; and
- JP6 Excess Temperature.

Fault detection is enabled for three-pin jumpers (JP1–JP4) when the lower two pins are shorted, and fault detection is disabled when the upper two pins are shorted. For two-pin jumpers (JP5 and JP6), fault detection is enabled when the pins are open, and fault detection is disabled when the pins are shorted. The amount of space on the PCA is limited, so it may be helpful to use a tool to move the jumpers. A pair of needle nose pliers with the metallic jaws wrapped in vinyl electrical tape can be used safely with little chance to scratch or damage the PCA.

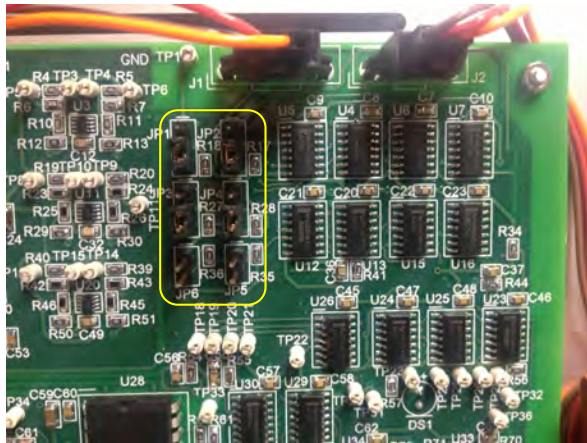


Fig. 21. The control box PCA showing the fault override jumpers (yellow rectangle) with all of the jumpers set to enable fault protection. The “upper” orientation is set by the letters on the PCA being normally oriented (i.e., vertical).

To reassemble the control box, connect the three-pin connector with white wires, lower the panel into its horizontal position, align the 16 screw holes, and tighten (but do not over tighten) the screws in place. To confirm the detection override is as anticipated, follow the power-on sequence in Sect. 2.3.8. After a successful power-on sequence, Detection Override red indicator for the selected fault should be illuminated and there should be no corresponding Fault Detected red indicator illuminated. If this is not the case, the most likely problem is an incorrect placement of the jumper.


Before repeating the procedure, verify an unanticipated Detection Override indicator is not illuminated. If the incorrect jumper was installed, this jumper will have to be returned to its original position, and the one that was

originally intended to be put into place will need to be moved.

2.4 Results

The protocol for executing a vertical profile or *cast* with a C-OPS equipped with C-PrOPS involves the following steps (when working in shallow water from a boat, the boat is usually anchored):

1. The operator lowers the profiler into the water with the long axis between the irradiance aperture and radiance end cap pointed in the direction of where the casts will be collected.
2. The thrusters are turned on, usually with a 45% thrust rating (the thrusters should not be operated above a 50% thrust rating and the software used prevents that from occurring).

 With the exception of very short duration and very low thrust levels for functionality testing, *the thrusters should not be used in air.*

3. Sea cable is fed into the water as the profiler moves to the desired location and distance from the deployment platform (usually the distance is marked on the cable with vinyl electrical tape and is 20–30 m for a small deployment platform and 40–50 m for a large platform).
4. Once the profiler is in position data recording is started, and then about two coils of slack are thrown into the water, and the thrusters are turned off after about 5 s to ensure the collection of data while the radiance end cap is out of the water (for a pressure tare, if needed, during subsequent data processing).
5. At the bottom of the cast, the thrusters are turned on (usually at a 45% thrust rating), the sea cable is hauled in quickly until the resistance from the thrusters are felt; and if the mark for cable distance has not been reached, more cable is slowly hauled in until the desired distance is reached.
6. The profiler continues to ascend and move away from the operator until it surfaces for the next cast; if cable has been hauled in past the distance marked on the cable to execute a cast, cable is slowly released until that mark is reached.

The steps above are repeated until all repetitive casts (usually a minimum of three) are collected under stable illumination conditions.

A comparison of C-OPS deployed with and without the C-PrOPS accessory in the shallow waters of Elkhorn Slough (Monterey, California) aboard the inflatable R/V *Recon 18* verified an improved ability to collect high quality data using C-PrOPS in shallow waters. A direct and tangible expression of the improvement is how long it takes to collect the replicate casts at each station and whether

or not the extrapolation interval used to derive the water-leaving radiance had to be substantively changed from one cast to the next at a particular station.

Without the C-PrOPS accessory, 17.6 min were needed (on average) to collect 4 replicate casts; whereas with C-PrOPS, 5 replicate casts were obtained in 8.8 min (on average)—an improvement of approximately a factor of 2.5. Equally important, either no or minor adjustments to the extrapolation intervals for each station of replicates were needed, because C-PrOPS minimized the influence of heterogeneity on the sampling across all wavelengths.

In the open ocean, the ocean-class R/V *Hakuho Maru* was used as the deployment platform and deeper casts were executed. Once again, the improvements in execution time were similar, i.e., about a factor of 2.5. In all water masses the thrusters were used to position the profiler before casts were executed. The thrusters were subsequently turned on at the bottom of the cast, which reduces the chance of a bottom impact in shallow waters; in deep and shallow waters, this reduces the amount of time needed to bring the profiler back to the surface and position it for the next cast.

The cycle time to perform repetitive casts are reduced with the C-PrOPS accessory due to the following: a) not having to maneuver the deployment platform or wait for the turbulence from maneuvers to dissipate (if a boat or ship is used); and b) the thrusters assist in bringing the profiler to the surface faster while also moving it away from the deployment platform to avoid perturbations. Reduced cycle time improves the coherency between casts and shortens the time between the *in situ* water sample and the casts, which lowers the uncertainty between data products.

Other advantages from C-PrOPS that improves data quality are as follows:

- Differential (or unequal) thrust levels can be used to navigate around small topographic features or overcome current and surface wave effects to position the profiler more exactly at the desired profiling location.
- The thrusters stabilize the orientation of the backplane, so when a cast commences, the backplane is closer to a near-vertical position than a C-OPS without C-PrOPS.
- If the profiler experiences a tilt bias along the long axis of the backplane during descent, e.g., if the irradiance instrument end is raised upwards due to excessive cable tension at the harness, the thrusters can be turned on at a low thrust level (e.g., 15%) to raise the radiance end.
- If the profiler is falling too quickly or slowly, the thrusters can be turned on at a low thrust level (e.g., 15%) to alter the descent rate (which might require reverse thrust). The vertical tilts must be observed to ensure the vertical stability is to within 5° .

- At the start of a cast, when slack cable is thrown into the water, the thrusters propel the profiler at the surface with the radiance end cap out of the water (Fig. 22). These data can be used for a pressure tare (because the pressure transducer port is in the radiance end cap), which significantly improves the quality of the derived data products as shown by Hooker et al. (2013).



Fig. 22. C-OPS deployed in Mono Lake (California) and being maneuvered with C-PrOPS, wherein the radiance end cap is propelled above the surface and the irradiance aperture is pulled below (the irradiance diffuser is visible as the white disc immediately between the green sea cable and the red hydrobaric flotation chamber).

- Once slack cable is thrown into the water and thrust is subsequently removed, the momentum from the thrusters continues to propel the profiler *forward*, and the surface loitering from the hydrobaric bladders provides the time for the profiler to further stabilize and descend with vertical tilts of 5° or less.
- The data collected when the thrusters are on after the slack is thrown into the water provide the shallowest L_u observations, which are important for improving data quality in the VIS spectral domain and frequently critical for the deriving high quality data products for the UV and NIR wavelengths.

The ability of C-PrOPS to improve data quality was evaluated during the KH-15-1 campaign aboard the R/V *Hakuho Maru*. Two C-OPS systems with 16 identical channels (to within 1 nm) were deployed in open-ocean (case-1) waters, i.e., in waters with significant wave focusing. System 21 had the C-PrOPS and C-CAPS accessories and system 34 did not. Both systems obtained data at 11 different stations comprised of 38 casts from system 21 and 36 casts from system 34. With the exception of one station for system 34, wherein no data products for the 875 nm channel could be derived, all casts resulted in data products for all 19 channels in each system.

The two C-OPS systems had different sampling objectives, so the buoyancy configuration for the profilers

was not the same. System 21 was ballasted to sink slowly (about 10 cm s^{-1}) and collect three shallow casts (e.g., 10–25 m), whereas system 34 was ballasted to descend more quickly (about 20 cm s^{-1}) and collect at least one deep cast (e.g., 75 m). The average vertical stability of the two profilers was nearly identical in the selected extrapolation intervals and to within 2.5° , but that does mean the near-surface sampling capabilities were the same. A summary of the extrapolation parameters for the two systems is provided in Table 2.

Table 2. A comparison of C-OPS systems 21 and 34 in terms of parameters associated principally with the selected extrapolation intervals to derive optical data products.

Extrapolation Parameter	C-OPS	
	21	34
Descent Velocity [cm/s]	11.3	18.2
Vertical Tilt [°]	2.5	2.5
Red–NIR Interval [m]	0.41	0.70
UV–Blue–Green Interval [m]	0.84	1.24
E_d Points in Interval	76	61
L_u Points in Interval	63	52

An intercomparison of the spectral normalized water-leaving radiances, $[L_W(\lambda)]_N$ or $L_{WN}(\lambda)$, depending on the citation, derived from the C-OPS systems 21 and 34 data are presented in Fig. 23. The data from each station are averaged and the average for each system is intercompared. The data show agreement for the UV, blue, and green wavelengths are excellent and unbiased (follow the 1:1 line). The red wavelengths show a small bias (departure from the 1:1 line), which increases for the NIR wavelengths.

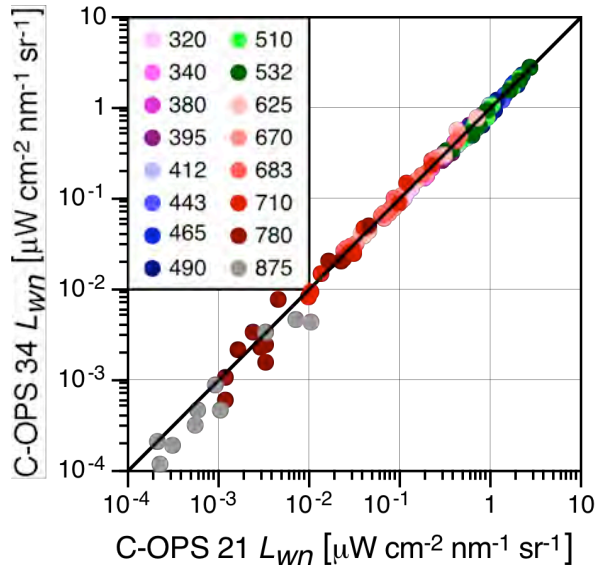


Fig. 23. The intercomparison of C-OPS systems 21 (with C-PrOPS) and 34 (hand held) span five decades of dynamic range.

To investigate the bias in the longer wavelengths, system 21 is chosen as the reference in the relative percent difference (RPD) calculations, ψ , as follows for an arbitrary variable X : $\psi = 100(X^{34} - X^{21})/X^{21}$, wherein the superscript denotes the system number. The absolute percent difference (APD) is the absolute value of the RPD, i.e., $|\psi|$. The intercomparison is based on the average ψ values across all 11 stations, wherein $\bar{\psi}$ denotes the average.

The results of the intercomparison as a function of the spectral domain are presented in Table 3. For the RPD, the stochastic effects of natural variability can cancel during the averaging process, so agreement is expected to be to within the calibration uncertainty, i.e., 2–3%. For the APD, the stochastic effects of natural variability *cannot* cancel during the averaging process, so agreement is expected to be to within 5–6% for case-1 waters.

Table 3. A statistical comparison of C-OPS systems 21 and 34 based on percent differences with system 21 as the reference in the calculations. The averages are for the 11 stations occupied during the KH-15-1 campaign.

Spectral Domain		Statistic	
Name	Range [nm]	$\bar{\psi}$	$ \bar{\psi} $
UV	300–399	1.6	5.6
Blue	400–499	0.4	6.1
Green	500–599	0.9	6.6
Red	600–699	7.4	8.6
NIR	700–899	–6.1	25.1

The data in Table 3 show the two C-OPS systems were performing as expected in the UV, blue, and green domains, i.e., $\bar{\psi}$ agreement is unbiased to within 3% and $|\bar{\psi}|$ is less than or close to 6%. In the red and NIR domains, however, there is a bias with the largest bias exhibited in the NIR. The bias in the longer wavelengths is probably due to the fewer number of near-surface data obtained with system 34 (Table 2), which descended 65% faster, so the profiler could reach the deep chlorophyll maximum (DCM). These results provide a tangible quantification of how the C-PrOPS accessory can improve the quality of data products derived from optical profiles.

2.5 Conclusions

As new features are added to an instrument system to solve problems that were not previously addressed or that were solved incompletely, portability frequently suffers. In the case of the original C-OPS instrumentation, as well as legacy profilers, a recurring difficulty is the inability to independently maneuver the profiler away from the deployment platform. The solution for this problem was to add two small digital thrusters to the C-OPS backplane, so the profiling package behaves somewhat like an ROV.

The thrusters require an increase in the power that must be delivered to the backplane. The increased power requirements necessitate additional electronics for power conditioning and user protection, as well as increased wire gauges to support anticipated cable length options. Consequently, it might be anticipated that the addition of the thrusters sufficiently decreases portability such that shallow water or remote location sampling is curtailed.

Although a C-OPS with C-PrOPS and C-CAPS is larger and a little bulkier than C-OPS alone, it is still quite portable as shown in Fig. 24, wherein the entire system was mobilized at a wharf near the Golden Gate Bridge in San Francisco (California). One of the reasons the system is so portable is that high quality small generators exhibiting light weight and long endurance are readily available and may be carried by hand to remote sites. This provides a simple solution for the extra power the system requires.



Fig. 24. The deployment of a C-OPS using the C-PrOPS and C-CAPS accessories from Torpedo Wharf near the Golden Gate Bridge in San Francisco Bay, wherein the reference and support equipment (left) are shown with the profiler (right).

Chapter 3

The C-HyR and C-TRAC Accessories

STANFORD B. HOOKER
*NASA Goddard Space Flight Center
Greenbelt, Maryland*

RANDALL N. LIND, CHARLES R. BOOTH, AND JOHN H. MORROW
*Biospherical Instruments, Inc.
San Diego, California*

KOJI SUZUKI
*Hokkaido University
Sapporo, Japan*

HENRY F. HOUSKEEPER
*University of California Santa Cruz
Santa Cruz, California*

ABSTRACT

The Compact-Hybridspectral Radiometer (C-HyR) profiler is a technology testbed combining a hyperspectral spectrograph, C-OPS 19-channel radiometers mounted on a modified C-OPS backplane with a C-PrOPS accessory, plus new ancillary sensors, e.g., an altimeter and gyro. The spectrograph measures upwelled radiance at a similar depth as downward irradiance to allow L_u observations close to the sea surface. A hybridspectral power (HyPower) box provides power and telemetry for the spectrograph, and can operate the thrusters integral to the backplane. An active user-protection module monitors the power supply for faults. A single USB cable connects the HyPower box to the data acquisition computer and carries all of the independent data streams for the C-HyR system. The data from ancillary sensors are integrated into the microradiometer data stream. These advancements resulted in new thruster-assisted technologies, i.e., the propulsion power (ProPower) box and the Compact-Thruster Remote Accessory (C-TRAC) accessory.

3.1 Introduction

Next-generation satellite designs emphasize near-shore, as well as open-ocean, processes. Consequently, obtaining high quality light measurements in the coastal environment is an inevitable requirement for CVR fieldwork to support these missions. The anticipated benefits of this new sampling capability are an improved ability to accurately separate the living and abiotic components of seawater, an improved calibration and validation capability in optically complex waters, and better atmospheric correction of ocean color remote sensing data.

The C-HyR instrument addresses a variety of these requirements with particular emphasis on two priorities, as follows: a) in-water instruments for oceanic, coastal, and freshwater measurements of AOPs; and b) hyperspectral (350–900 nm) observations for use in near-surface profiling. The anticipated range in water depth for the sampling capability is 1.5 m to more than 4 km, i.e., rivers to ocean

gyres. To advance CVR field activities, UV measurements are desirable at the shortest wavelengths possible.

A desire for improved radiometric accuracy, decreased costs, and more extensive multidisciplinary research are all technology-forcing challenges to be addressed by the next generation of ocean color satellites. An immediate concern is ensuring the science teams have access to the requisite field instruments for successful CVR activities. For global participation, this requires the development of COTS aquatic radiometers that appeal to a majority of investigators working in the field. Issues that confront these investigators include, but are not limited to, the following:

- Radiometers with full characterization of dynamic range, stray light, linearity, and bandwidth across the thermal environment encountered in the field;
- High measurement accuracy across the entire sampling spectrum including domains exhibiting significantly different attenuations that can cause large

spectral imbalances (e.g., the NIR in clear ocean waters and the UV in turbid coastal waters);

- Comprehensive uncertainty budgets and quality control of data products;
- Innovations to address the difficulties of deploying sensors in optically complex shallow water bodies;
- Reduced cycle times to obtain sequential profiles;
- Improved instrument operator and equipment safety;
- Avoidance of platform- and sensor-induced perturbations to the *in situ* light field; and
- Sensor miniaturization to improve near-surface and NIR observations.

The C-HyR accessory uses a C-OPS backplane with C-PrOPS digital thrusters (Chap. 2) plus a hyperspectral spectrograph and (rigid) radiance collector assembly (RCA) optics, a gyro, an altimeter, a new sea cable supporting greater data transmission, and a HyPower box that works in parallel with the original C-OPS deck box. The digital thrusters allow the new profiling package to be maneuvered beyond deployment platform perturbations and to return the profiler to the surface after a profile is executed, which provides the needed surface loitering and reduces the cycle time between profiles.

The data acquisition software can be programmed to turn on the thrusters automatically (e.g., at a set depth), thereby minimizing bottom collisions. Free-fall profilers, however, are at risk for collisions with the deployment platform when wind and currents are unfavorable. Making compass information available to the operator coupled with small thrusters for accurate positioning significantly reduces the risk of platform collisions, and allows safer shoreline deployments in lakes or slowly flowing rivers.

3.2 Background

The self-shading of AOP instruments degrades the accuracy of data products (typically associated with the L_u measurements, because the aperture is pointed downwards and is the primary variable for deriving data products). The degradation increases as the wavelength of the measurement increases, which is important for next-generation problem sets emphasizing an expansion of the spectral domain with hyperspectral resolution, including the NIR.

To ensure negligible NIR shading perturbations, it was desirable to produce a profiler wherein a hyperspectral L_u aperture was at the end of a long arm. The RCA immobilized the optical fiber to prevent motion-induced perturbations to light transmission. The ultimate objective was to collect uncontaminated hyperspectral L_u measurements, but the vulnerability of the arm suggested trials with a single-channel L_u instrument would be less risky (spectrographs are much more expensive than a single-channel radiometer).

The purpose of the C-HyR prototype was to demonstrate that valid L_u measurements in the NIR (at 875 nm)

could be made using the proposed RCA approach. Consequently, a very small single-channel submersible sensor called the Monochromatic Microradiometer Radiance model 100 (MML-100) was developed. The MML-100 has a 1.8 cm outside diameter that is mated to a 50 cm long RCA to minimize instrument self-shading. This sensor was equipped with a 875 nm filter assembly, and oriented so that it could measure $L_u(z, 875)$ where depth was very close to zero just below the water surface. High density (more than 1,000 data frames) sampling in the top 50 cm of the water column was necessary because of the very large attenuation coefficients observed during field deployments in near coastal and inland waters.

Observations of $L_u(875)$ with the MML-100 mounted at the end of the RCA on the C-HyR prototype (Fig. 25) presented unexpected challenges in measuring the depth of the radiance sensor at the end of the RCA in real time. At 875 nm, the inverse of the diffuse attenuation coefficient, $K_d(875)$, can be less than 20 cm. This constraint requires data be acquired with millimeter depth resolution. Trials with the C-HyR prototype revealed that the measurement must be made in close proximity to the radiance entrance optic for a variety of reasons, such as the effect of motion-induced changes in water momentum and positional changes in the pressure sensor.



Fig. 25. The C-HyR prototype being propelled by C-PrOPS thrusters, wherein the white disk of the E_d aperture (left) is pushed down below the water surface, and the single-channel MML-100 L_u aperture at the end of the RCA (right) is raised above the water surface.


Spectrograph selection to replace the single 875 nm channel in the prototype received significant attention, which included surveying a large number of COTS devices. Two candidate devices were selected for intensive testing, and then one was selected. During testing, a flaw was detected that would have significantly compromised operation for the intended application. Persistent effort was made to resolve the flaw by working with the two companies producing the spectrograph, as follows:

1. Carl Zeiss Spectroscopy GmbH (Jena, Germany) is the manufacturer of the Compact Grating Spectrometer (CGS) with 2,048 pixels spanning the UV-VIS-NIR (190–1,000 nm); and
2. tec5USA, Inc. (Plainview, New York) supplies the electronics interface for the CGS.

Additionally, the performance of the spectrograph in clear and turbid waters was modeled, and used to identify optical filters to extend the working spectral range of the spectrograph depending on the environment and goals.

The innovative integration of a pair of thrusters significantly enhances deployment protocols compared to legacy approaches which often involved counteracting water currents, accommodating ship windage, and ultimately using shipboard propulsion devices (e.g., a transversal propulsion device on the bow or stern) to push the instrument away from the vessel. During testing, C-HyR was easily placed overboard and the thrusters used to drive the profiler away from the boat or dock, adjust orientation to minimize self-shading using the integrated compass, and profile vertically with positive control.

Thruster-controlled profiler motions included hovering, repeated near-surface profiles in the top meter of the water column, and collecting thousands of data frames without significant manual cable handling or ship repositioning. The C-HyR prototype was also successfully deployed from shore and a dock.

 Profiles with over 1,000 data frames in the top meter shows how far the technology documented here has advanced, and how *data quality can be avoidably compromised if the 4–8 samples per meter called for in the SeaWiFS Ocean Optics Protocols (Mueller and Austin 1992 and 1995)—which are still in use today—are relied upon.*

3.3 Design

The C-HyR instrument concept has multiple components acting together to ensure optimal ocean color data acquisition in shallow aquatic systems from a small boat or deeper waters from a large vessel, as follows:

- Spectrally identical 19-channel (fixed wavelength) in-water downward irradiance and upwelling radiance profiling instruments, $E_d(z, \lambda_{19})$ and $L_u(z, \lambda_{19})$, respectively;
- A matching above-water global solar irradiance reference instrument, $E_s(\lambda_{19})$, equipped with a shadow band and GPS;
- Two digital thrusters (C-PrOPS), which can be controlled separately with differential thrust, to position the profiler away from the deployment platform;
- A 2,048 pixel spectrograph to collect upwelling radiance very near the surface of the water column, $L_u(z, \lambda_{2,048})$; and
- A hybridspectral power (HyPower) box to integrate the spectrograph data with the fixed-wavelength radiometers.

The spectrograph includes an RCA that places the entrance aperture far away from the main body of the profiler with a separate altimeter (i.e., a high precision pressure transducer), and the solar reference is powered by a standard C-OPS deck box (Fig. 26).

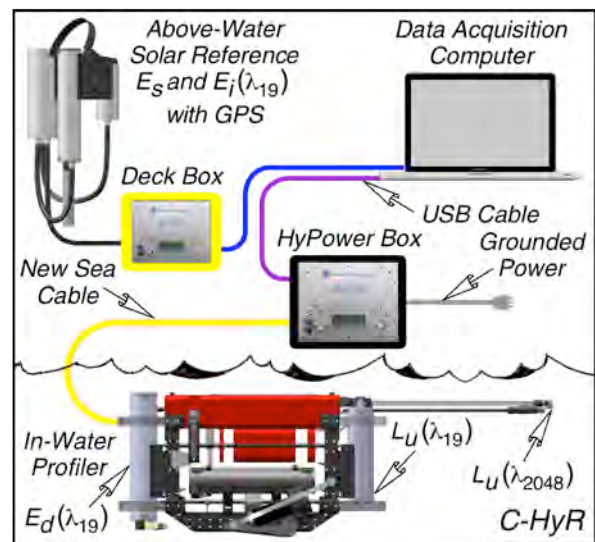


Fig. 26. The C-HyR profiling concept showing the above- and in-water instruments, support electronics, wiring required for data acquisition, standard (λ_{19}) radiometers, plus a new hyperspectral ($\lambda_{2,048}$) aperture at the end of the RCA.

3.3.1 Sea Cable

The large number of discrete wavelengths in hyperspectral sampling (e.g., 2,048) makes data rates associated with RS-232 or RS-485 protocols inadequate for data telemetry and acquisition (even at 115.2 kbaud). Increasingly, a common capability built into many instruments and computers is the USB interface. As shown in Sect. 3.3.6, the spectrograph selected for C-HyR has a USB 2.0 interface. Consequently, all telemetry to and from the profiler is transmitted using USB communications.

The nominal cable length limitation for USB communications (approximately 5 m) does not support the long distances normally used in vertical profiling, which is typically 100–300 m. Consequently, a USB extender is used to send the data from the spectrograph over a much longer distance, whereupon, another converter establishes a USB interface for data acquisition on a computer.

SubConn Ethernet connectors provided the first underwater communications with gigabit performance. The series includes different types of Ethernet and combined power with connector options in the following configurations: a) circular, b) metal shell, and c) low profile configurations. All three provide gigabit performance and a high depth rating based on the proven SubConn contact and socket design with a power rating of 600 V at 4 A.

In the C-HyR development activity, circular and low profile connectors were used, denoted DIL and DLPIL, respectively (Fig. 27). Two connector types were used because of availability and expediency of construction considerations. For the subsequent HARPOONS project and the development of the C-PHIRE and C-OSPREY instrument systems (Chaps. 9–11), only the circular series of connectors are used.

Table 4. The specifications for the C-HyR accessory data-telemetry (sea) cable versus the standard cable used with the C-OPS backplane (compare to Table 1). Both cables are used in handheld applications without termination of the strength members, but the former use with HARPOONS requires termination (Sect. 8.3.1).

Cable Characteristic	Neon Green (Foam PU) Cable	Yellow (Foam PU) Cable
Manufacturer	Outland Technology	Storm Products
Power Conductors	3×18 AWG and 2×22 AWG	4×20 AWG
Telemetry Conductors	2×22 AWG [†] and 2×24 AWG [‡]	8×26 AWG [‡] Cat 6 [§]
Video Conductors	75 Ω coaxial	Cat 6
Outer Diameter	0.55 in (nominal)	0.55 in (nominal)
Strength Member	Kevlar (1,000 lb breaking rating)	Kevlar (500 lb breaking rating)
Outer Jacket	Neon green Low-Density Foam PU	Yellow Foam PU
Connectors	SubConn Micro In-Line (MCIL8)	SubConn Power Ethernet (DLPIL)
Weight per 10 m (32.8 ft)	1.5 kg (3.3 lb)	1.5 kg (3.3 lb)
Instruments	C-OPS with C-PrOPS and C-CAPS	C-HyR and HARPOONS

[†] Twisted shielded pair with PP insulation.

[‡] Twisted pair with PP insulation.

[§] Shielded bundle.



Fig. 27. A SubConn DIL13F (left) circular connector next to a DLPBH13M bulkhead (right) with mating DLPIL13F connector (left of right). The strap that holds the mated DLP connectors together is not shown, but the DIL red locking sleeve is shown.

Once the connector design was selected and successfully tested, a new sea cable containing the necessary number of conductors plus the requisite wire gauges and buoyancy had to be obtained as a custom cable. Unfortunately, the manufacturer used for C-OPS with the C-PrOPS and the C-CAPS accessories (Table 1), Outland Technology (Slidell, Louisiana), could not provide the C-HyR cable with the necessary buoyancy characteristics.

A difficult part of the newest sea cable design was achieving near-neutral buoyancy, which is a weight per 10 m of about 1.5 kg, while maintaining an outer diameter of approximately 0.5 in (13 mm) with the needed American wire gauge (AWG) sizes. The only manufacturer that could supply the cable was Storm Products Co., which is owned by Teledyne Cable Solutions (Dallas, Texas).

The specifications for the newest (yellow) sea cable are provided in Table 4 and are compared to the existing C-OPS sea cable. A stripped-back end of the cable is presented in Fig. 28 to reveal the following layout (approximately following an outer to inner radius):

- a) A polyurethane (foam) yellow jacket;
- b) An overall foil shield with 20 AWG drain wire;
- c) An aramid fiber (Kevlar) strength member with a 500 lb breaking rating;

d) Three 20 AWG conductors for power (plus the drain wire); and

e) A shielded Category 6 (Cat 6) Ethernet sub-cable.

The Ethernet sub-cable, which is used to extend USB communications over longer wire lengths, is made up of the following:

f) An overall polyvinyl chloride (PVC) jacket with foil shield;

g) A 26 AWG drain wire; and


h) Four 26 AWG twisted pairs (i.e., 8 conductors).




Fig. 28. The C-HyR cable with outer foam jacket (bright yellow) stripped back to reveal the strength members (pale yellow Kevlar fibers), shields (e.g., blue foil folded back over the foam jacket), drain wires (bare silver), and power conductors (white, red, and black), plus the twisted-pair conductors.

The outer jacket of the newest sea cable has a 0.55 in (14 mm) diameter and a slightly rough texture, which were

selected to facilitate handheld deployments, because the cable is easy to grip and hold onto when wet.

 A rough cable can cause injury if allowed to rapidly slip over bare skin (e.g., through the hand), consequently gloves are recommended when handling cable.

 A small diameter cable attached to a heavy load (e.g., C-HyR) can cause injury if a bight in the cable closes over a hand or finger, which is one reason why the C-HyR cable has a larger diameter.

Specifying and testing cable can be a time consuming and expensive exercise. This is particularly true for complicated cable configurations wherein multiple conductors and wire gauges are used, e.g., the C-HyR cable, because the cost of terminating a connector onto the cable can be significant. For handheld deployment scenarios, the aramid strength member is not terminated, but for HARPOONS (Sect. 8.3.8), the strength member is terminated to ensure a transfer of the towing forces to an appropriate fixture on the tow vehicle.

3.3.2 USB Extended

The large number of discrete wavelengths in hyperspectral sampling (e.g., 2,048 are used in the spectrographs selected for C-HyR, as well as for the C-PHIRE and C-OSPReY instruments) makes data rates from the serial communications (RS-232 or RS-485) inadequate for data telemetry and acquisition (even at 115.2 kbaud, which is what is used for C-OPS). The spectrograph selected for C-HyR (plus C-PHIRE and C-OSPReY) has a built-in USB 2.0 interface, which means all telemetry to and from the backplane used to deploy the new hyperspectral instruments must be transmitted using USB communications.

The nominal cable length limitation for USB communications is less than approximately 5 m, which cannot support the long distances normally used in vertical profiling (typically 100–300 m) nor the sensitivity to losses at connectors and internal wiring associated with complex instruments. In fact, the maximum achievable distance between the C-HyR spectrograph and the data acquisition computer using USB alone is approximately 2–3 m. Consequently, a USB extension capability was designed and implemented into the C-HyR profiler to send the data from the spectrograph over a much longer distance, whereupon, another converter establishes a USB interface for data acquisition on a computer.

The conversion required the specification of a new cable and connectors that have not been used in the past, as well as an integration of the normal RS-485 telemetry from the two radiometers (L_u and E_d), the altimeter, the gyro, and the two digital thrusters. The additional electronics were housed with a 60 VDC step-down power converter, which is needed to operate the thrusters over the wire gauges and extended cable lengths required for this application. The new RS-485 to USB communications

capability (Fig. 29) is also used with the new C-PHIRE and C-OSPReY instruments for the HARPOONS activity (Chap. 8).

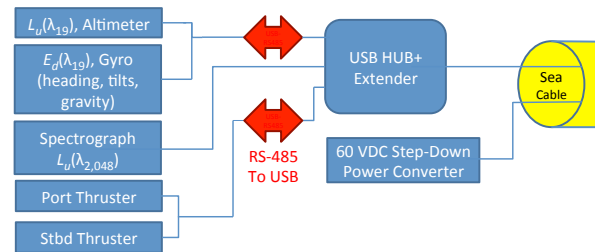


Fig. 29. The RS-485 to USB conversion (red double arrows) and subsequent USB extension allows the use of a 100 m sea cable. This capability is housed with the 60 VDC step-down power converter implemented in the C-HyR profiler.

3.3.3 HyPower Box

The HyPower box (Fig. 30) provides power and communications for the C-HyR accessory, which is mounted on a slightly modified C-OPS backplane with a C-PrOPS accessory. In addition to powering the hybridspectral instrument, the power supply in the HyPower box is capable of operating the thruster-assisted backplane the C-HyR accessory is integrated to. As part of this functionality, an active user-protection module monitors the power supply for faults.

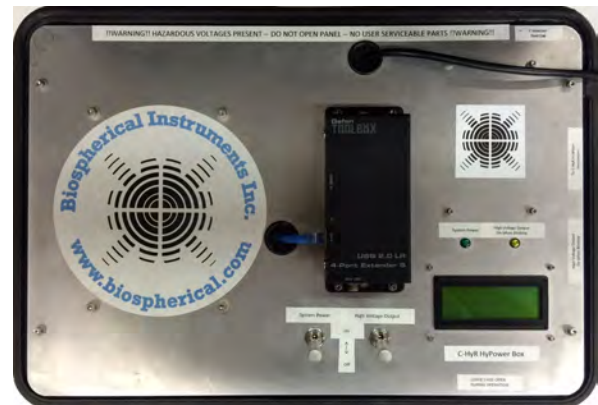


Fig. 30. The prototype HyPower box developed for the C-HyR profiling accessory, wherein the USB extender is the black rectangular box in the middle is the USB-to-Ethernet extender and the cable exiting above is the 120 VAC power cable used to supply power to the box.

The HyPower box uses 120 VAC power, and connects to a single instrument assembly via a sea cable. Additionally, the HyPower box connects via a single USB cable to the data acquisition computer. The USB connection carries all of the independent data streams for the C-HyR system, i.e., the microradiometers, CGS spectrograph, and thrusters. The data from the ancillary sensors (e.g., the altimeter and gyro) are integrated into the microradiometer data stream (Fig. 29).

The HyPower box uses a USB extender technology developed by Gefen, LLC (Petaluma, California) to transmit USB data streams at the native data rate over the necessarily long cable lengths encountered in profiling. Because of the common architecture employed in hybridspectral Enhanced Performance Instrument Class (EPIC) sensors, the HyPower box may also be used to operate any single instrument assembly from the C-PHIRE and C-OSPREy instrument inventory (Sects. 9.3.4 and 10.3.6).

The USB extenders allow the transmission of USB data streams over distances of up to 100 m using a single Category 5 (Cat 5) Ethernet cable, supporting USB 2.0 with data rates up to 480 Mbps. The USB extender sender module (at the acquisition computer) is powered by the computer USB port. The USB extender receiver module (integrated into the C-HyR in-water instrument housing) requires a separate power source, which is provided by the C-HyR instrument. The extenders chosen also have an integral 4-port USB hub at the receiver module to facilitate the interconnection of the multiple data streams a C-HyR system requires.

3.3.4 Altimeter

A “traditional” pressure transducer, like the 30 psia strain gauge transducer presently mounted on the end cap of an in-water C-OPS optical instrument, is inadequate (confirmed by engineering analyses) to return the low-exursion pressure changes that the near-surface optical data need to resolve for C-HyR. Fortunately, the recreation community has inspired the production of the MEAS (Switzerland) MS5806-02BA altimeter, wherein the gel protection and an antimagnetic stainless steel cap used in high-end dive and flight (chronograph-type) watches allows the use of the altimeter (Fig. 31).



Fig. 31. The MS5806-02BA miniature altimeter from Measurement Specialties (Fremont, California) is a very small ($6.4 \times 4 \times 2.8 \text{ mm}^3$) lightweight (0.14 g) device with very low power consumption (1.4 mA at 3 VDC, peak) spanning a wide operating temperature (-40 to 85°C).

The MS5806-02BA miniature altimeter has a Serial Peripheral Interface (SPI) interface and can provide 2,048 (averaged) samples during 8.3 ms. An aggregator averages these output cycles with a stated accuracy to within 1.5 mbar and a resolution of 0.024 mbar, i.e., a precision less than 1 mm. The linear range, is 10–2,000 mbar and the maximum pressure is 10 bar (i.e., 100 m), with an operational range of 0–10 m). The latter provides the opportunity to provide high-resolution depth data close to the surface where it is needed most, and the former allows deeper casts without damaging the sensitivity of the device. The temperature responsivity of the MS5806-02BA is more than a factor of 10 better than legacy pressure transducers, e.g., the devices presently being used with C-OPS.

3.3.5 Gyro

In the present generation of C-OPS instruments, two-axis accelerometers are used to determine the orientation of the profiling package. The two axes are arbitrarily referred to as pitch and roll. The orientation data are needed to satisfy the sampling protocols, which require the in-water radiance and irradiance apertures to be planar to within 5° during profiling; all in-water data collected beyond that threshold are ignored during processing of the light observations to derive data products, e.g., L_W and its normalized forms.

For next-generation sampling systems, like C-HyR, the orientation of the sensor package relative to the sun is an advantage, because it can aid in orienting the package to minimize self-shading. A second concern centers around the fact that the instrument suspended in the near-surface wave field will experience an orbital motion that will add a variable bias to the traditional pitch and roll measurements from two-axis accelerometers.

To improve the traditional two-axis approach, while providing the heading of the profiling package (relative to the axis set by the velocity vector from the C-PrOPS thrusters), a COTS ultra-miniature (UM) orientation sensor was selected. The UM7 is a third-generation Attitude and Heading Reference System (AHRS) with an onboard processor to integrate nine sensors into pitch, roll, and yaw measurements corrected for platform motion at binary data output rates up to 255 Hz.

The UM7 (Fig. 32) can be operated in either a streaming mode or polled mode. The latter was adopted, because the microradiometer architecture uses polling to obtain data from all instruments. The polled data set reported by the UM7 includes measurements of the three accelerometers, as follows: a) the traditional pitch and roll orientations, plus vertical acceleration or gravity; b) pitch and roll measurements corrected by the rate gyros to remove the effects of wave-driven acceleration; and c) yaw, which provides the compass heading calculated from the magnetic field sensors.



Fig. 32. The UM7 orientation sensor from CH Robotics (Payson, Utah) is a comparatively very small ($27 \times 26 \times 6.5 \text{ mm}^3$) lightweight (11 g) device with low power consumption (50 mA at 5 VDC) and a wide operating temperature (-40 to 85°C).

The UM7 sensor was combined with a dedicated processor and integrated into a standard aggregator that is present in all instruments that are built using the microradiometer architecture. Changes to the aggregator firmware interfacing with the UM7 sensor include the ability to provide three different levels of data for acquisition, as follows:

- Level-1 data are provided for the purpose of calibrating the magnetometer. This must be done in the fully assembled system where any static magnetic influence is present and away from external magnetic fields or large iron structures (e.g., the deck of a ship).
- The suite of 13 level-2 data products includes the processed three-axis gyro components, magnetometer, and acceleration sensors; the derived pitch, roll, and yaw angles; and the sensor temperature.
- The level-3 data consist of a subset of essential data as follows: vertical acceleration (to indicate wave height), pitch, roll, and yaw.

3.3.6 Spectrograph

The original spectrograph to be installed in the C-HyR profiler was to be a duplicate of the Zeiss spectrograph used in the OSPREy instruments (Hooker et al. 2012). To support the HARPOONS activity, the spectrograph was upgraded to match the ones selected for C-PHIRE instruments.

The selected spectrograph for C-HyR is a COTS device from Zeiss having 2,048 pixels spanning 190–1,000 nm.

The anticipated spectral range for validated data products is 305–900 nm, although the future applications discussed in subsequent chapters for supporting the PACE mission anticipates a validated range of 320–900 nm. The CGS UV-NIR spectrograph (Fig. 33) as implemented herein is the result of collaborations between the authors and the manufacturer’s representative, tec5USA, and supplements OSPREy modules (Hooker et al. 2012).

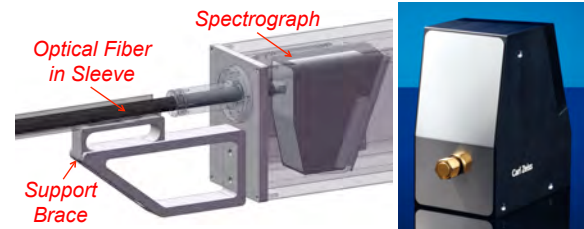


Fig. 33. The CGS spectrograph module without support electronics (right) and mounted (inverted) as part of the RCA (left).

The CGS comprises an imaging grating, optical port, and a charge-coupled device (CCD) detector with electric shutter to minimize integration times. The CGS is compact ($74 \times 30 \times 76 \text{ mm}^3$) and thermally stable with a spectral resolution less than 3 nm (in keeping with PACE mission requirements for vicarious calibration exercises). The spectrometer core is a blazed, flat-field grating for light dispersion and imaging. The CGS has excellent stability coupled with very low stray light and high reliability in rough environments. The CGS was selected based on exhaustive market surveys during OSPREy (2009–2012) with trade study refinements during C-HyR (2013–2014) development.

The new CGS spectrograph with tec5 support electronics fit within a 4 in (10 cm) housing compatible with established Sun and Moon tracker (PTU-D300) capabilities (Hooker et al. 2012); an existing 305–1,640 nm cosine collector design (Hooker et al. 2012); and the C-OPS backplane with C-PrOPS and C-CAPS accessories.

3.3.7 RCA Optics

For the CGS fiber to be adapted for the hyperspectral radiance collector, a fiber with subminiature version A (SMA) connectors was chosen to permit a common fiber architecture to allow continuity and predictability between the various phases of testing and validation. It also provides positive location, centering, and retention of the fiber in the assembly. A cap-retained bore seal was designed to accomplish the task of providing environmental sealing at both ends of the RCA. The location of the spectrograph within its housing has a slight range of adjustment to allow precise alignment and mating of the fiber SMA connector.

At the aperture end, an O-ring sealed cap was designed containing the FOV optics and optical components for bending the light path and an exit window. A 5 mm sapphire prism was chosen and the design was based around

it. Sapphire was selected because of its highly elevated index of refraction relative to other available materials, its spectral properties are very flat over a wide band, and it is a very rugged material for windows in environmental applications. A coupling providing positive mating of the SMA fiber fitting and a FOV limiting aperture were designed along with an optics cap to house all the components. The cap also holds a sapphire exit window to the underwater light field along with provisions for field or laboratory mounting of up to 3mm thickness of light balancing filters (Fig. 34).

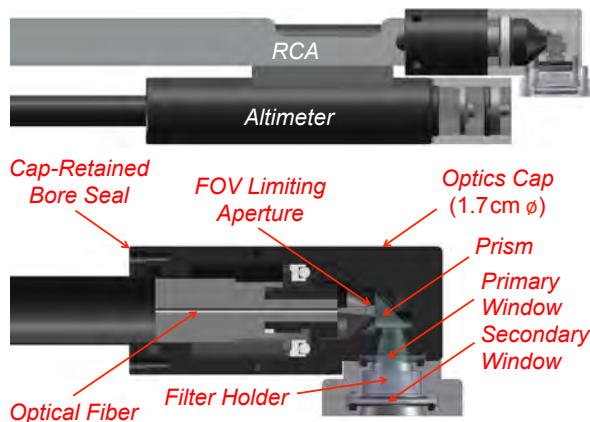


Fig. 34. The RCA configuration with respect to the altimeter (top) with internal details for the former (below) showing the entrance optics for the RCA, including optical fiber path, FOV limiting aperture, the prism, entrance windows, and light-balancing filter holder.

The mechanical mounting of the pressure transducer for use in C-HyR proved to be a much greater challenge than anticipated, because the miniature O-ring size and corresponding machining requirements were demanding. Additionally, the sensors proved to be very fragile. The combination of miniature size, fragility, and lack of visibility of assembled components made getting a reliable seal with the original bore seal O-ring design an impractical endeavor from a production standpoint. This design was revised in multiple phases to determine a solution that provided reliable and repeatable results.

The final design uses a urethane potting compound to carefully pot the sensor in two stages, first from the front, then from the back. The sensor retaining piece was made shallow enough that visual inspection of both sides of the assembly was possible to verify correct alignment and potting compound fill level. The retaining pieces were fitted to a 3 in (7.62 cm) long lens tube that afforded splicing to a SubConn underwater sea cable, providing connectivity back to the host instrument housing. For C-HyR, the host instrument was a C-OPS in-water radiance instrument that also contained a legacy 30 psia strain gauge pressure transducer, allowing comparison between the two sensors.

A picture of the assembled C-HyR instrument system oriented from the distal end of the RCA and viewing the rest of the profiler is shown in Fig. 35. The upper right corner of the image shows the altimeter affixed below the RCA and pointing at the FVA volume of the hyperspectral L_u aperture, which is pointed downwards per Fig. 34. The perspective establishes the narrow dimension of the RCA, which has an outer diameter (OD) of 3/8 in (1.0 cm) and the small size of the L_u aperture.



Fig. 35. The optical and altimeter apertures as viewed from the distal end of the C-HyR RCA.

3.3.8 The C-TRAC and ProPower Box

The Compact-Thruster Remote Accessory (C-TRAC) is a wireless unit designed to control the C-PrOPS accessory during data acquisition instead of using a computer program (Fig. 36). The range of the controller depends on environmental conditions, but the expected range is 30 m. The handheld unit allows setting the thrust levels for the thrusters, starting and stopping data collection, and constant updates of C-PrOPS.



Fig. 36. The handheld C-TRAC developed for the C-HyR profiler (left) and a close up of the display and controls (right).

Wireless control of the backplane thrusters improves data quality by allowing the person who is operating the thrusters to maneuver the backplane as required for improved line-of-sight observations in regards to the location and attitude of the backplane when it is at or near the surface of the water. Additionally, data recording for casts may be started and stopped using the C-TRAC unit, thereby maximizing the opportunity for high quality profiles to be recorded at each station with reduced time and effort. This capability provides the possibility that optical casts may be obtained with a single operator rather than the normal case, wherein the person managing the sea cable communicates with the computer and thruster operator as to when thrust is applied or removed as part of profiling operations.

The TRAC display area on the ProPower box (Fig. 37) and C-TRAC unit have identical configuration and thruster response. C-TRAC must be charged prior to going into the field using the provided micro USB to USB cord, and the charge must be maintained periodically while in the field. The LCD provides updated thruster status, which consists of the following: requested and delivered thrust, temperature in Celsius, and the input amperage. Displayed beneath the thruster status are pitch, roll, depth of the C-PrOPS backplane, and record count for the cast being executed.



Fig. 37. The ProPower box panel showing the TRAC components (lower middle), and the LCD display for instrument power status (lower right) above the system and instrument power switches.

3.4 Results

Field commissioning of the C-HyR profiler involved the collection of data within a coastal water mass (Tokyo Bay) as part of a joint campaign with Hokkaido University (Sapporo, Japan) aboard the R/V *Hakuho Maru* (campaign KH-15-1) in March 2015 (Sect. 8.4.1). For this activity, the C-HyR instrumentation was shipped approximately half way around the world, assembled, mobilized on the ship, and then deployed to collect validation data in a coastal water mass. Consequently, the deployment was a comprehensive test of the robustness of the C-HyR accessory design.

A picture of the C-HyR accessory being maneuvered by the thrusters in the eutrophic waters of Tokyo Harbor is presented in Fig. 38. The C-HyR accessory (black rectangle with black Velcro straps affixing it to the C-OPS backplane with C-PrOPS) has the narrow RCA extending well beyond the body of the backplane, so the $L_u(\lambda_{2,048})$ aperture, which is very small in cross-sectional area, experiences a negligible self-shading perturbation from the backplane and the RCA.

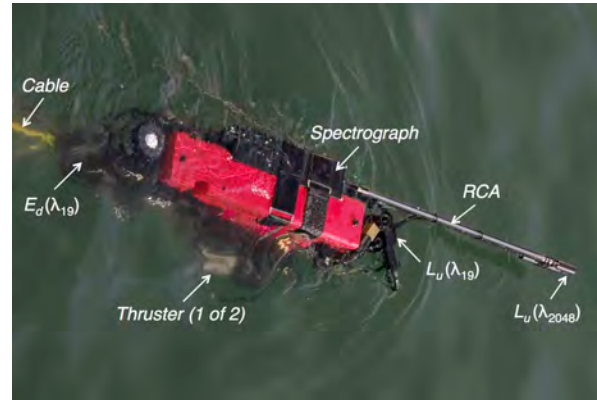


Fig. 38. The C-HyR instrument system being maneuvered by thrusters prior to the start of the KH-15-1 field campaign aboard the R/V *Hakuho Maru* (Tokyo, Japan).

When the C-OPS backplane with the C-HyR profiling accessory is maneuvered using the thrusters, the backplane is raised upwards at the radiance end, so the $L_u(\lambda_{19})$ end cap and the RCA is elevated above the sea surface, while the irradiance diffuser (white circular disk in Fig. 38) is pulled down below the surface. This means the L_u observations begin above the water surface, so the subsequent in-water data are obtained as close to the sea surface as possible. When the backplane is at the surface prior to the start of obtaining a profile, the thrusters align the backplane in both horizontal axes (Fig. 38), so a significant amount of data is acquired with minimal vertical tilts.

Because the radiance end of the C-HyR profiler is elevated above the sea surface at the start of a profile, pressure tares can be obtained before profiling commences for both the traditional strain gauge transducer in the $L_u(\lambda_{19})$ end cap and the altimeter affixed to the RCA at the $L_u(\lambda_{2,048})$ aperture. This represents a significant opportunity to improve the quality of the data products derived from the subsequent vertical profile of the light field (Hooker et al. 2013).

Figure 39 presents $L_u(\lambda)$ spectra from both the 19 fixed-wavelength microradiometers and the hyperspectral CGS spectrograph (2,048 pixels) for a C-OPS instrument suite equipped with the C-HyR accessory. The data below the lower end of the PACE domain of 350–900 nm distinguish this technology as exceeding PACE requirements. The data were obtained in eutrophic conditions (Tokyo Harbor) as evidenced, in part, by the green peak

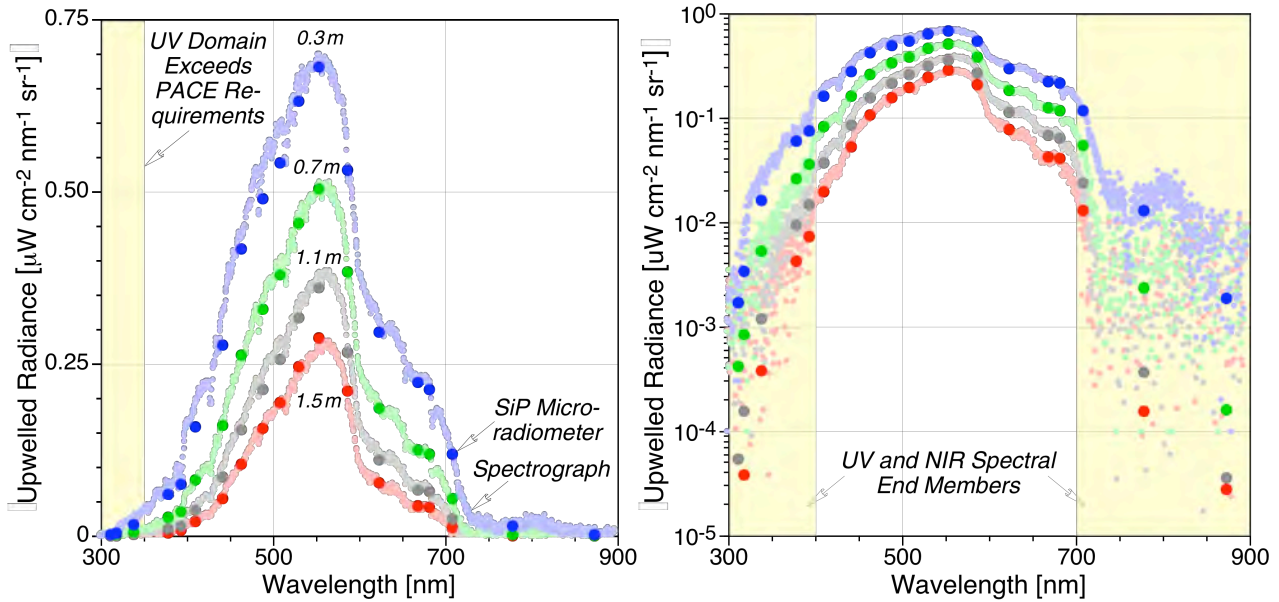


Fig. 39. Spectra from the C-HyR instrument system showing both the microradiometers (large darker circles) and the CGS spectrograph (small lighter circles) spanning a depth range of 0.3–1.5 m. Linear (left) and logarithmic (right) scales provide two perspectives of the two detector systems. The extended spectral capabilities with respect to PACE requirements are highlighted in yellow (left) as are the UV and NIR spectral end members (right).

in the spectra. The spectra are from a water depth of 0.3–1.5 m and establish an ability to collect data at near-surface depths and obtain high quality results.

The platform orientation for the spectra are pitch to within 0.6° and roll to within 2.3° , i.e., to within a vertical tilt of 2.5° . The spectrograph integration time was 100–200 ms. As long as profiling extends down to approximately 1 m (this profile goes to a bit more than 3 m), all the usual ocean color data products can be derived, e.g., L_W , R_{rs} , etc.

The two (linear and logarithmic) scales in Fig. 39 expose the usual noise sensitivity of spectrograph data as a function of wavelength. The VIS domain is characterized by low hyperspectral noise, whereas the UV and NIR are the opposite. The advantage of the hybridspectral approach is the highly accurate microradiometer data can be used to facilitate the processing of the noisier hyperspectral data.

3.5 Conclusions

The C-HyR accessory was used to affirm or improve the design of the follow-on C-PHIRE instruments, as follows:

1. The Zeiss CGS spectrograph with tec5 electronics and distinct slit width was successfully characterized for linearity and spectral response;
2. The spectral peak seen around 820 nm in Fig. 39 resulted in a reappraisal of the original C-PHIRE

microradiometer wavelength assignments, so that a channel at 820 nm could be added;

3. The sea cable, which has a single conductor bundle for all required communications streams, supported USB data rates and thruster-assisted deployments with a cable length of 100 m (the cable is slightly positively buoyant, which means it is excellent for shallow-water deployments);
4. The magnetometer and gyro sensors provided instrument vertical tilt and heading for the profiler;
5. The digital circuitry and high resolution residual current measurements in the HyPower box supported enhanced intelligent safety decision matrixes with increased reliability over the C-PROPS control box;
6. A handheld controller (C-TRAC) provides untethered operation of the thrusters from the deck of a ship or platform; and
7. The right-angle prism allows a perpendicular FOV to the fiber optic cable without bending the cable. This accomplishment has application to unusual payload geometries (e.g., in an AUV), wherein one dimension is constrained, but the other is not.

For the development of the in-water C-PHIRE instrument system within the HARPOONS project (Chap. 8), the UM7 was found to be incompatible with the inclusion of additional sensors sharing the same digital communications bus (e.g., the high resolution temperature sensor). In addition, the UM7 manufacturer was anticipating that

production and support for the UM7 would be discontinued in the near future, thereby necessitating a candidate replacement device.

A BNO055 nine-axis absolute orientation sensor produced by Bosch Sensortech (Reutlingen, Germany) was selected as the UM7 substitute. This sensor was integrated into the existing aggregator architecture such that the new subassembly may be deployed across the full suite of instrumentation as a standalone accessory called the BioGyro (Fig. 40), allowing science teams greater flexibility when platform attitude or heading information may add value to an activity, e.g., knowing the orientation with respect to the Sun. When installed in a C-PHIRE irradiance instrument, the BioGyro accessory is mounted such that the integrated circuit comprising the gyro sensor is aligned with the pitch axis of the radiometer.

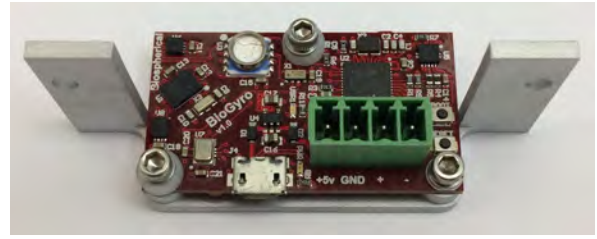


Fig. 40. The BioGyro PCA shown mounted to a purpose-built bracket for installation in EPIC class instruments. U1 on the left edge of the PCA is the BNO055, which is purposefully rotated to establish the alignment of its sensor axes with established external features of the EPIC instrument class. The integrated circuit (U2) above the green connector is a microprocessor that implements the aggregator architecture.

Chapter 4

The OCULLAR Hybridnamic Multitector

STANFORD B. HOOKER
*NASA Goddard Space Flight Center
 Greenbelt, Maryland*

RANDALL N. LIND, CHARLES R. BOOTH, AND JOHN H. MORROW
*Biospherical Instruments, Inc.
 San Diego, California*

ABSTRACT

The development of the OCULLAR sensor paired a new miniature photomultiplier tube (PMT) microradiometer with an existing SiP microradiometer in order to extend the linear dynamic range of instruments used to measure AOPs. The pairing produced the first hybridnamic microradiometer *multitector* and successfully demonstrated that high-accuracy, high sensitivity light measurements can be made in normal and very low-light regimes, thereby creating the opportunity of measuring ocean color at night. This demonstration project constructed, characterized, and deployed an irradiance sensor with PMT and SiP microradiometers centered at 490 nm. The miniature and ruggedized PMT that was selected had a form factor compatible with existing instruments built with microradiometers and an expected survivability typical of the thermal and handling environment of oceanic and atmospheric radiometers. The successful pairing of the PMT and SiP microradiometers permitted using the latter to determine when light levels were below a safety threshold before applying high voltage (HV) to the PMT, thereby *protecting* it from potentially harmful incident light levels. The large overlap in responsivities between the two detectors (about two decades) and the near-linear response of both, allowed the linear 10 decades of useful dynamic range for a SiP microradiometer to be extended to approximately 14 linear decades for the operationally-paired multitector.

4.1 Introduction

Presently, the plans for next-generation NASA satellites emphasize coupled ocean-atmosphere missions. The Aerosol, Clouds, and ocean Ecosystem (ACE) mission, as well as the Plankton, Aerosol, Cloud, ocean Ecosystem (PACE) mission, are both expected to provide high quality ocean color and atmospheric measurements in the coastal environment where turbid atmospheres overlay, and thus confound, the remote sensing of shallow optically complex water masses.

Measurement sensitivity as a function of wavelength and turbidity becomes a concern as the number of measurement channels for next-generation missions extend beyond the VIS domain of legacy missions to include shorter wavelengths in the UV plus longer wavelengths in the NIR and SWIR domains. The spectral domain for next-generation satellites that field instruments will have to support is anticipated to be approximately 340–1,640 nm, with the SWIR observations designed to improve the atmospheric correction process. Consequently, simultaneous

oceanic and atmospheric observations are needed to support CVR activities.

AOP measurements of the ocean or atmosphere, by definition, require a light source. Typically, the Sun is used because it provides sufficient flux across a wide spectral range and supports a diversity of detectors. Nonetheless, the continuing requirement to collect sea-truth observations for the vicarious calibration of ocean color satellite sensors and to validate the algorithms for which the remotely sensed observations are used as input parameters—including atmospheric correction—necessitates improved sensitivity for both air and sea measurements in the coastal zone.

Although some AOP measurements have been made using the Moon as a light source, in general, the diurnal cycle of oceanic and atmospheric optical parameters are not well understood because of the paucity of instruments that can make high quality observations in low-light conditions during nighttime. Similarly, observations in highly turbid conditions are sparse compared to the open ocean, because signal levels quickly reach the noise level of many existing detector systems.

In addition, the inability to make accurate measurements at low-light levels has constrained the understanding of other important light-based phenomena. For example, research opportunities benefitting from OCULLAR sensors include the following (to name a few examples): characterization of the environment experienced by pelagic visual predators, such as tuna and squid; onset of the spring bloom under polar ice sheets; the response of the atmosphere and ocean to twilight illumination levels, particularly at high latitudes; and the use of very narrow bandwidths to exploit specific spectral signatures of oceanic and atmospheric phenomena.

4.2 Background

PMTs are one of the most sensitive optical devices, but their use has a number of vulnerabilities including the inevitability of irreversible damage if exposed to full sunlight while powered, and the possibility of damage occurring when exposed even if not powered. Other drawbacks such as shock and vibration sensitivity, magnetic field susceptibility, and non-linearity under very high light levels are also potential issues.

At the start of the OCULLAR development activity, Hamamatsu was consulted to select a PMT that had a form factor compatible with standard microradiometer dimensions, and also could survive the thermal and handling environment typical of marine radiometers. A semi-custom packaged PMT based on the Hamamatsu Model R9880 (Fig. 41) was selected, featuring a multi-alkali photocathode, 10-stage, metal channel PMT in a 16 mm diameter package.

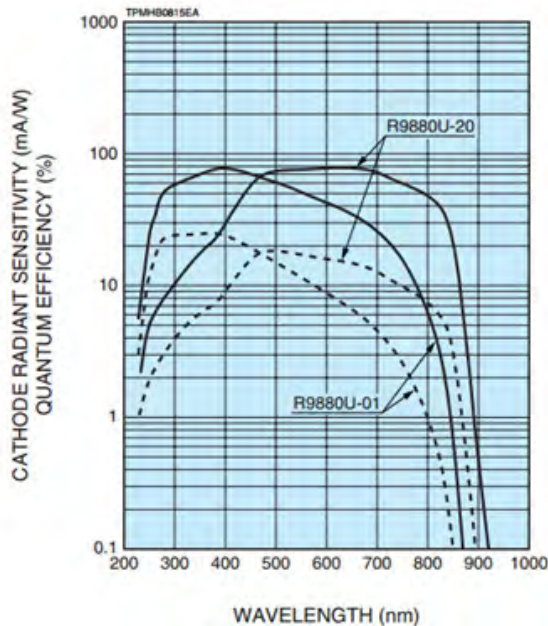


Fig. 41. The spectral sensitivity (solid) and noise (dashed) response of the R9880U-01 PMT chosen for the OCULLAR prototype as compared to the model R9880U-20 (from Hamamatsu).

The PMT chosen for the initial OCULLAR instrument uses the photocathode identified as R9880U-01, has decreasing sensitivity at wavelengths greater than 400 nm in contrast to SiPs which have increasing sensitivity with wavelength up to about 1,000 nm. This means that the overall dynamic range combination of a combined SiP and PMT hybrid dynamic detector will decline with increasing wavelength and at 800 nm the effect will be significant. This issue may warrant switching to the R9880U-20, an extended multi-alkali PMT with a response that has approximately tenfold higher noise levels. A complete evaluation would be required to determine its suitability and was not performed for the prototype.

The objective of the demonstration project presented here was to construct, characterize, and deploy an irradiance instrument with a hybrid dynamic pairing of two types of microradiometers. The first was a standard SiP microradiometer. For the second type, the signals from a miniature and ruggedized PMT were digitized using a microradiometer modified specifically for the task, and the resulting paired assembly—called a PMT microradiometer—was controlled using a modified aggregator.

The measured capabilities of the two microradiometer types are presented in Table 5. Based on the measured sensitivity of the two devices, the PMT is a factor of 8.7×10^4 more sensitive than the SiP, i.e., almost five orders of magnitude more sensitive. The low saturation of the PMT microradiometer, however, makes it problematic to use during normal solar illumination flux levels.

Table 5. The comparison of the two OCULLAR detector types configured for irradiance in units of $\mu\text{W cm}^{-2} \text{nm}^{-1}$, including the noise equivalent irradiance (NEI).

Type	NEI 20°C	NEI 5°C	Satur- ation	Dynamic Range
SiP	1.2×10^{-5}	1.2×10^{-5}	2.9×10^5	2.5×10^{10}
PMT	5.1×10^{-9}	2.2×10^{-9}	0.2	8.7×10^7

4.3 Design

In the hybrid dynamic design of paired PMT-SiP microradiometers, the high 10 decades of responsivity from the SiP microradiometer (which does not saturate if pointed at the sun) protect the lower and more sensitive 6 decades from the PMT microradiometer (two decades overlap), thereby providing unprecedented low-light oceanic, atmospheric, and terrestrial measurements. The SiPs are sampled and compared to a maximum irradiance exposure limit to determine if the HV can be applied without damaging the PMT. Sensitivity comparisons of the PMT and SiP, which are useful in detecting changes in PMT calibration caused by over-exposure to light, can also be made using the region of overlap between PMT and SiP sensitivities. Dark current stability is maintained through look-up tables based on detector temperature characterizations spanning an operational range of -13 to 40.6°C .

To minimize cost, the mechanical design anticipated the PMT-SiP pairing to fit within the existing architecture of building 19-channel SiP microradiometer instruments, e.g., the C-AERO and C-OPS instruments. The basic philosophy was to remove enough SiP microradiometers to make room for two of the new PMT microradiometers, wherein a PMT microradiometer is one miniature PMT plus a companion microradiometer that has been modified to accept the current output of the PMT. The modifications to the paired microradiometer do not change its size or shape.

A schematic of the physical layout for the prototype OCULLAR radiometer is depicted in Fig. 42, which shows seven microradiometers and two PMTs. Of the seven microradiometers, the two end ones in the row containing four microradiometers were modified to be the companions, providing acquisition and digitization for the two miniature PMTs situated in the row below. The remaining five microradiometers were standard SiP microradiometers. Although the five *extra* microradiometers could have had different filter assignments, they were made identical for simplicity. Nonetheless, the prototype is a seven-channel radiometer, wherein two channels have 14 decades of dynamic range and five have 10 decades.

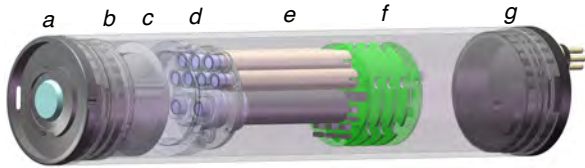


Fig. 42. An OCULLAR irradiance instrument built with microradiometers showing components, as follows: a) entrance aperture (cosine collector), b) exit of secondary diffuser, c) lens spacing tube with stray light baffles, d) plano-convex lens (lens not visible), and e) SiP and PMT microradiometer array (purple filter stacks and front-end optics), f) support electronics (green), and g) end cap.

A customized retainer was designed and fabricated to hold each PMT securely and establish alignment with its companion microradiometer to create the new PMT microradiometer. A filter-retaining cap was also designed and fabricated to mount interference filters for wavelength selection. In the prototype, five standard SiP microradiometers, with all detectors having matching interference filters centered at 490 nm, accompanied two PMT microradiometers. Given that a PMT microradiometer includes a modified microradiometer, this means a total of seven microradiometers and two miniature PMTs were accommodated in a standard 2.75 in (7.0 cm) housing.

The task of physically integrating the PMT involved establishing mechanical clearances for both the increased diameter of the PMT housings relative to the microradiometers, and for routing the signal and control wires exiting from the PMT to be connected to a companion microradiometer and aggregator, respectively. An effort was

made to place a single PMT at the same radial distance from the central axis of the instrument's cosine collector to facilitate direct comparison between the two detector types. An important constraint was that the location of microradiometers could not be changed without significant engineering effort because the microradiometer bus positions on the aggregator are fixed by their PCA. Consequently, microradiometers could be omitted to provide clearance, but not arbitrarily located.

Upon determination of a feasible radial distance from the center of the detector, it was noted that a patterned 120° rotation of the PMT location would allow two PMT and two microradiometers to co-locate on a 0.438 in radius from the detector's center. By locating the PMT close to a hole in the backplane PCA, the signal cables back to the companion microradiometers could be routed cleanly.

The final configuration of the new array of microradiometers is presented in Fig. 43, wherein two miniature PMTs paired with two modified SiP microradiometers (as identified by the coaxial signal wires) create two PMT microradiometers, along with five *standard* SiP microradiometers. The apparently “wasted” space for the HV wire is only an expedient to produce a prototype quickly and cost effectively. A future seven-channel device would not require a modified microradiometer for acquisition and digitization. This function would be provided by a new support electronics PCA, i.e., it would be added to the boards shown in Fig. 42f.

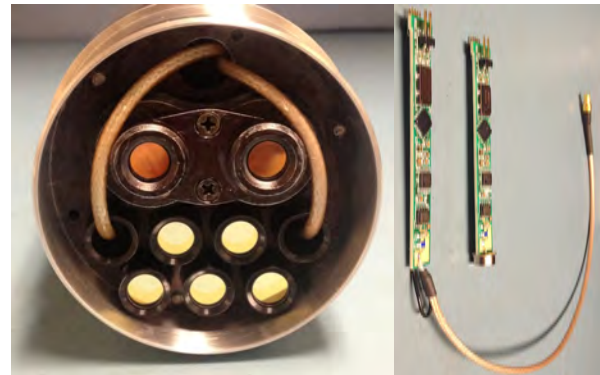


Fig. 43. The array of microradiometers for the OCULLAR prototype (left) and the regular SiP microradiometer above a modified microradiometer with coaxial signal cable attached (right).

Based on microradiometer software, a new computer program was created to control the prototype OCULLAR instrument. This software controls the digital-to-analog converter (DAC) that generates the programming signals controlling the HV to the PMTs. In the prototype instrument, one DAC channel controls both PMTs, because they are identical in design and filtered to the same wavelength. In future multichannel OCULLAR instruments, it may be necessary to have one DAC control each PMT, because they will be operating at different wavelengths and, thus, exposed to different light intensities.

The software has both manual and automatic modes. In the automatic mode, to protect the PMTs, the SiPs are sampled and compared to a maximum irradiance exposure limit. If the irradiance is below the threshold, the PMT HV is set to 500 V. If the resulting PMT current is above the desired maximum (e.g., 10 μ A), the PMT is shut down and automatic mode is terminated.

In normal operation for collecting a time series (e.g., sometime after sunset), the HV is automatically applied as light levels decrease. Subsequently, after nighttime operations, the HV is shut down shortly before sunrise as light levels increase. Sensitivity comparisons in the field of the PMTs and SiPs, which are useful to detect any change in PMT calibration due to overexposure to light, can be made by ensuring that there is a region of overlap between PMT and SiP sensors.

Although the region of overlap reduces the total dynamic range that can be achieved with the two detector systems, it provides the benefit that the simultaneous data collected by both detector systems during overlapping observations allows calibration monitoring of the PMTs by the companion SiP microradiometers, i.e., the two decades of overlap was anticipated to produce a total of 14 linear and calibrated decades of dynamic range.

4.4 Results

A functioning prototype was created by joining the PMT and SiP microradiometer array, with support electronics and front-end optics (Figs. 42d–f), to the assembled components comprising the entrance aperture, secondary diffuser, spacing tube with baffles, and the plano-convex lens (Figs. 42a–c). The assembled prototype is presented in Fig. 44. Much of the laboratory testing of the new instrument took place in this configuration, because it provided easy access to a wide variety of internal components and signaling.



Fig. 44. The OCULLAR prototype irradiance instrument without the external housing (right) next to a SiP microradiometer (left). The two PMTs (black with silver and blue labels) are above the microradiometers, which are in aluminum (silver) sleeves.

Demonstrating that the PMT-SiP hybrid dynamic multi-detector responded in a predictable and linear fashion involved assessing the stability of the PMT HV supply and linearity of the combined detector system. These tests were run in a custom-built linearity test apparatus, or *lineator* (Fig. 45). The lineator is composed of an integration sphere with reference detector, and multiple LED sources under computer control, wherein flux levels across a wide dynamic range can be produced. All data were taken with the data acquisition systems in the SiP microradiometers running at 125 Hz, and with averaging to output data at 1 Hz, which was deemed a sufficient temporal resolution given the stable light source (microradiometer instruments operated in the field typically acquire data at 15 Hz).

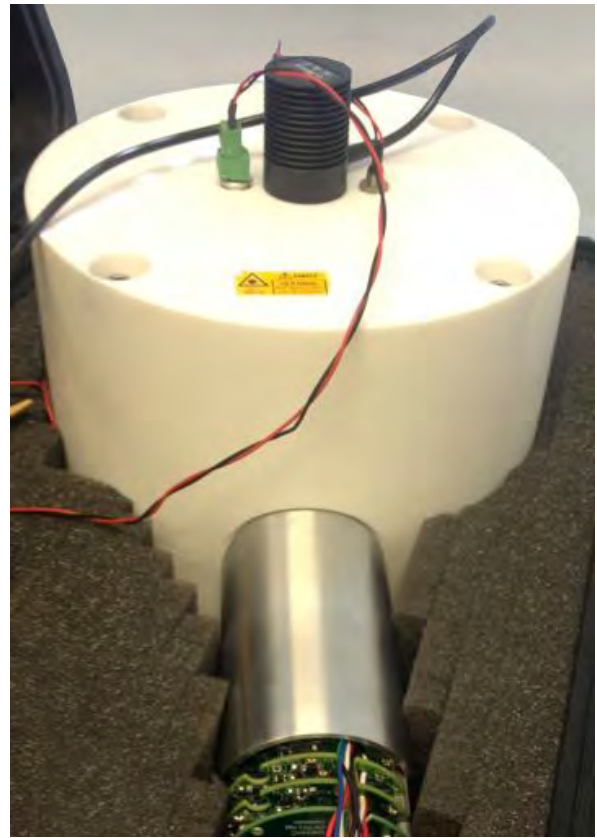


Fig. 45. An early version of the OCULLAR prototype radiometer (contained principally within the silver cylinder) with exposed support electronics boards (green) and mounted in the lineator (white). The foam (gray) provides insulation for temperature stability and support for the prototype.

Testing in the lineator showed the PMT and SiP microradiometers agreed with respect to linearity for over five decades (Fig. 46). A least-squares regression of the data indicates almost linear correspondence to within 0.1%, with more than 99.9% of the variance explained, and a root mean square error (RMSE) of 0.1%. To allow direct comparison with the PMT and SiP microradiometers, the former had its sensitivity reduced approximately 107

times with neutral density filters. Both microradiometers reported raw units expressed as photodetector current in units of nanoamps.

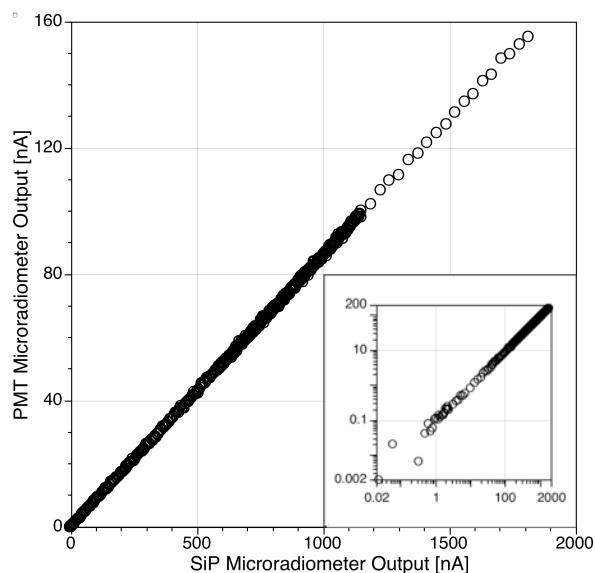


Fig. 46. Linearity results for the PMT and SiP microradiometers. Both units report raw values expressed as photodetector current in nanoamps with a log-scale rendition shown in the inset panel.

After the stability and linearity of the PMT components integrated with the SiP microradiometers were determined to be operating properly, the system was re-assembled using 490 nm interference filters attached to the two PMT and five SiP microradiometers. The calibration of the PMTs proceeded using the same principals associated with calibrating SiP microradiometers, i.e., a stable light source and geometry is an unequivocal requirement. Consequently, the lineator was modified to attenuate the LED sources for data collection with the PMTs alone. The prototype instrument was then mounted in the lineator so the PMT components could be characterized and calibrated.

The OCULLAR prototype was deployed for a series of nights in late September and October 2013 near the Pacific Ocean under time periods encompassing the full Moon (Fig. 47). The prototype instrument had an almost unobstructed view of the western horizon, which was ideal for observing sunset, moonrise to moonset, and then sunrise. The system was deployed shortly before sunset and operated continuously until the next morning under a variety of atmospheric conditions. During the September and October deployments, the PMT microradiometers were programmed to automatically turn on when the SiP microradiometer incident irradiance (at 490 nm) decreased during sunset to below $0.12 \mu\text{W cm}^{-2} \text{nm}^{-1}$, with the HV set to 500 V; when the PMT microradiometer current subsequently exceeded $9 \mu\text{A}$, the HV was turned off to protect the PMT from the potentially harmful high flux from the rising Sun.

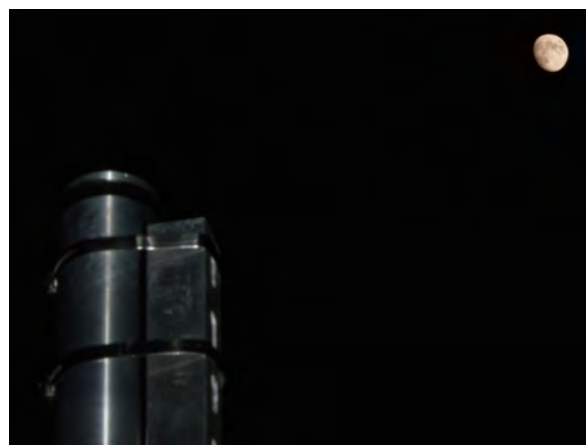


Fig. 47. The OCULLAR prototype deployed to measure low-light levels during full Moon illumination.

Field tests spanning sunset to sunrise under a full Moon were conducted (Fig. 48). These trials showed increased noise in the PMT dark data at the beginning of the time series (collected the prior day at the same time under nearly identical conditions) due to the warmer temperature associated with sunset, which raised the PMT noise levels due to thermionic emission. The excellent agreement between the PMT and SiP microradiometers under the full Moon convincingly showed the OCULLAR system is capable of measuring approximately five orders of magnitude below full moonlight (at 490 nanometers).

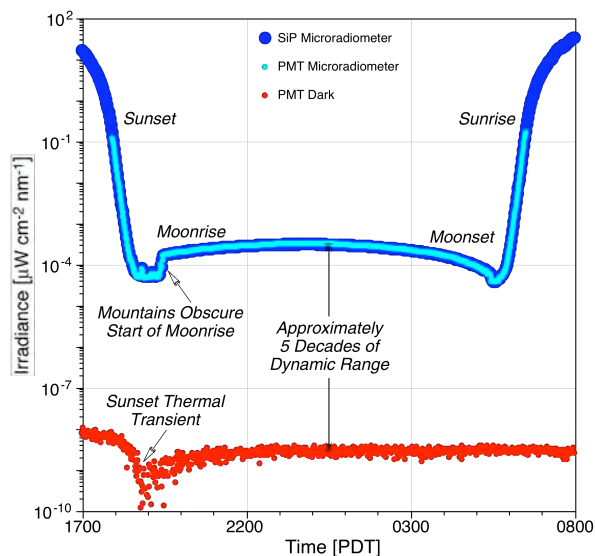


Fig. 48. A time series of SiP (dark blue) and PMT (light blue) data acquired at 1 Hz, with the PMT dark noise (red) collected the night before. The increased noise values at the beginning of the trace are due to the warmer temperatures before sunset, which raises the PMT noise levels due to thermionic emission. Offsets were subtracted by using temperature-based lookup tables generated in an environmental chamber.

Data obtained during twilight periods, wherein the SiP and PMT detectors overlap in responsivity, provided ongoing verification of PMT calibration. In fact, the reverse is also possible wherein PMT microradiometer responsivity can be used to detect anomalous responses in the companion SiP microradiometer. The ability for one detector system to verify the performance of the other, in this case twice per day, is one of the unique strengths of the hybrid architecture, especially for long-term deployments in isolated regions.

The OCULLAR irradiance prototype equipped with a BioSHADE accessory (Bernhard et al. 2010) was deployed under a partly cloudy full Moon. During the test, the shadow band angle was moved from below the OCULLAR field of view (FOV) at 0° , across the entire hemisphere, to 180° (below the FOV). The OCULLAR irradiance collector is cosine weighted, and the effect of shading the sky by the band increases as it moves from the horizon toward the zenith. At about 78° of shadow band angle (Fig. 49), the band starts to block the direct component of the lunar illumination, and the irradiance rapidly decreases until the entire cosine collector is shaded (starting at about 88°). Between 91° and 101° , the band is no longer occluding the entire diffuser and direct moonlight again begins to reach the collector, increasing the measured irradiance.

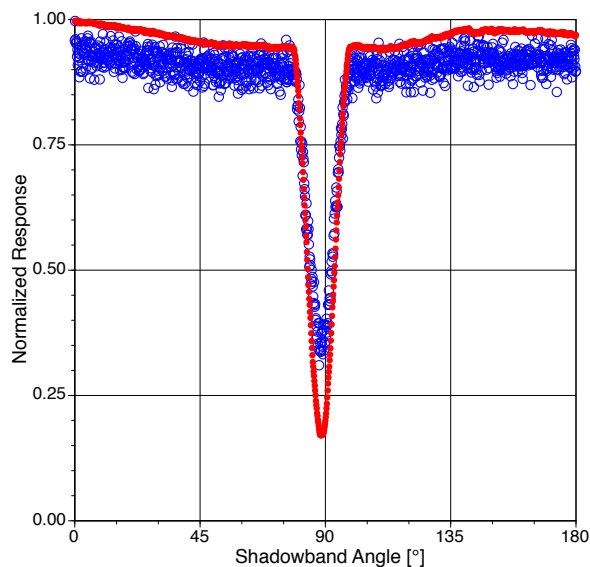


Fig. 49. Shadow band SiP (blue) and PMT (red) microradiometer measurements that were collected under moonlight.

The BioSHADE data show that a standard SiP microradiometer occulted to full moonlight under a cloudy sky has a measured signal-to-noise ratio (SNR) of about 60 at 490 nm; for PMT microradiometers, the corresponding SNR exceeds 600, which is sufficiently sensitive that accurate aerosol optical depth (AOD) measurements at night are possible. The number of samples recorded while the shadow band is blocking moonlight allows the direct-horizontal and direct-normal irradiance to be calculated.

For the most accurate results, the system needs to be calibrated using the Langley technique wherein the calibration is determined from measurements of the Moon at different lunar elevations and the simultaneous lunar extraterrestrial irradiance can be obtained (U.S. Geological Survey Robotic Lunar Observatory).

4.5 Conclusions

To exploit the results achieved with developing the OCULLAR prototype, the primary follow-on objective is to increase the technology readiness level (TRL) of a hybrid dynamic multitector, while advancing the state of the art for AOP instruments by developing COTS radiance and irradiance instruments compatible with existing protocols (Hooker 2014) and new low-light data processing for diurnal and polar studies (Hooker and Brown 2018).

The prototype was built with existing components to keep the costs down and to allow the work to be done quickly. Consequently, the PMT-SiP microradiometer pair involved four components: a) a miniature PMT for low-flux measurements; b) a modified SiP microradiometer to acquire and digitize the signal from the PMT; c) a modified aggregator to control the HV to the PMT; and d) a second SiP microradiometer to make high-flux measurements. For the follow-on instrument system, the second two will be combined into a single subsystem, so the SiP-PMT pairing will involve only three components as shown in Fig. 50. A task for realizing the combined functionality described above in a COTS instrument is the design of a new aggregator board, so the needed electronics for the PMT microradiometer architecture are accessed by plugging a PMT onto the new board, rather than mating it with a modified SiP microradiometer as was done (for expedience) with the prototype.



Fig. 50. A drawing of the new PMT microradiometer (dark gray) paired to a standard SiP microradiometer (light green). The PCA with integral HV control and digitization (dark green) for mounting the PMT-SiP microradiometers is redesigned both for added functionality and packing efficiency.

As part of the aggregator redesign, the offset between the length of a PMT and SiP microradiometer, which are slightly different, will be removed so the PMT and SiP detectors are planar. The anticipated housing for the COTS

instrument will be 3.5 in (9 cm), which provides more space for the hybriddynamic pairing and for securing the PMTs with front-end optics in place. This form factor is compatible with existing irradiance cosine collector designs, although a new lens design for the microradiometers will be created.

The new instruments will have seven paired PMT-SiP microradiometers, plus an eighth SiP microradiometer to measure a wavelength useful to ocean color that is not compatible with existing PMTs, e.g., a SWIR channel for atmospheric correction (Fig. 51). In terms of legacy instrument configurations, seven channels has proved effective, because they can be used in dyads to create 14-channel instruments.

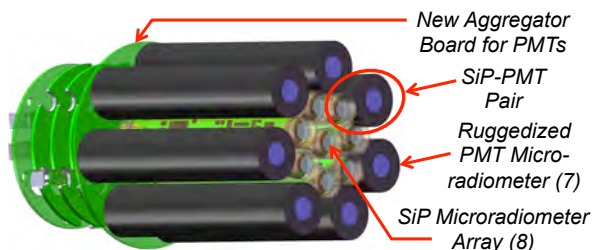


Fig. 51. A drawing of the proposed COTS hybriddynamic multitector concept.

Large-scale above-water mappings of $L_W(\lambda)$ in coastal waters were demonstrated in 2011 and 2013 using the C-AIR instrument suite, which are built with SiP microradiometers. Consequently, the proposed COTS development activity includes thermal and vibrational testing of the prototype instrument to evaluate if design changes are necessary for the proposed instrumentation to be used in airborne campaigns, including UAVs. Presently, airborne

microradiometer instruments are distinguished from in-water radiometers solely by a different FOV to provide the needed ground resolution—*no other design changes are required to collect high quality airborne data*. The proposed instrument development is for ground- or (more properly) sea-truth instruments that do not require thermal or vibrational enhancements.

For PMTs, other factors besides temperature influence dark offsets, e.g., dynode change, amount of time since application (or change) of HV, and light exposure history. Anticipated COTS designs include in-water profiling wherein the instruments will be subjected to a wide change in illumination in a short time, so PMT stability based on these other factors are important. Some of these can be mitigated with revised deployment protocols, but others might require design studies to establish appropriate engineering solutions. Another area of anticipated design study is the response of the selected PMTs to excessive illumination, which might require an internal shutter capability. The OCULLAR prototype was not tested under full (noon) sunlight, but no damage was noted to levels of approximately 25% of full sunlight ($60 \mu\text{W cm}^{-2} \text{nm}^{-1}$ at 490 nm). Fortunately, any adverse overexposure-related changes should be readily detected using the field calibration methods described above. Also, the prototype did not utilize the full active surface area of the PMT. In order to integrate the PMT within existing microradiometer architecture while using stock interference filter sizes, the effective aperture of the PMT was decreased. A flux increase of approximately 50–100% is anticipated for the COTS instrument if larger interference filters are used. A design study will be conducted to determine if the use of larger filters warrants the added cost and integration issues.

Chapter 5

The C-SLOWS Accessory for Legacy Profilers

STANFORD B. HOOKER
*NASA Goddard Space Flight Center
Greenbelt, Maryland*

JOHN H. MORROW
*Biospherical Instruments, Inc.
San Diego, California*

TORU HIRAWAKE
*Hokkaido University
Hakodate, Japan*

ELÍGIO DE RAÚS MAÚRE
*Nagoya University
Nagoya, Japan*

ABSTRACT

A new set of buoyant clamshells with hydrobaric bladders were designed for the legacy Biospherical Profiler (BioPRO), built with profiling reflectance radiometer (PRR) series 800 (PRR-800) sensors. Two advantages the new Compact-Surface Loitering Option for Water Samplers (C-SLOWS) accessory provides are as follows: a) the BioPRO is now able to obtain a significant amount of near-surface data, and the increase in descent speed when the hydrobaric bladders compress allows the entire euphotic zone to be sampled; and b) the extrapolation of the near-surface light field to $z = 0^-$ at UV and NIR wavelengths was almost infeasible with a PRR-800 deployed without the C-SLOWS accessory in coastal waters, because of the high attenuation of these data close to the sea surface. These two advantages mean the PRR-800 with the C-SLOWS accessory is useful not only for remote sensing, but also for primary production studies. Also, any residual vertical resolution problems, perhaps caused by a high sea state, can be overcome with repeated data sampling using the C-SLOWS accessory.

5.1 Introduction

A reliable procedure to obtain a vertical light profile devoid of ship perturbations is to use a free-fall instrument that is floated away from the vessel before measurements begin. This technique has been used extensively based on a common instrument design developed for open-ocean waters (Hooker and Maritorena 2000), i.e., deep water and extensive mixed layers). The light sensors are connected in line with power and telemetry modules to form a long cylinder. A radiance sensor is positioned on the *nose* to measure $L_u(z, \lambda)$ and an irradiance sensor on the *tail* to measure $E_d(z, \lambda)$. The addition of weight to the nose and buoyancy to the tail, sometimes in the form of buoyant fins, produces a rocket-shaped package that falls through the water column with minimal tilts (usually less than 5° over much of the profile except at the start).

Adjustments to the amount of weight and buoyancy are used to fine tune the stability of the package during

descent, but fundamentally, the most stable configuration occurs at the highest descent velocities. The power and telemetry cable extends through the field of view of the irradiance sensor, but the small diameter of the cable minimizes any negative effects on the measured light field. The addition of a temperature (and, if possible, a conductivity) probe, provides a good description of basic water column properties. To ensure the data are acquired during stable illumination conditions, a separate irradiance sensor is mounted as high on the ship's superstructure as possible (so the data are not degraded by shadows or reflections) to measure the global solar irradiance, $E_d(0^+, \lambda)$.

One advantage of a hand-held profiler, in terms of sampling capabilities, is it can be deployed by only two people (and with caution and experience, by one person), so data collection can commence quickly when light conditions are optimal. Hand-held profilers are usually deployed from the stern of the vessel, and whenever possible, the ship maintains a small or impulsive headway speed of approximately

0.5 kt or less (depending on surface currents, winds, and waves). The profiling instrument is carefully lowered into the water and repeatedly dropped and recovered within the near-surface layer until it has drifted clear of any possible perturbation effects from the vessel. When the profiler reaches the desired distance from the stern (usually 30–50 m), it is ready for deployment and can be *dropped* by releasing the cable and providing slack cable overboard.

5.2 Background

BioPRO is a 19-channel legacy device based on the PRR-800 (Hooker et al. 2010). Rather than dividing the downward irradiance and upwelling radiance capabilities into two cylinders, in the BioPRO design the light apertures are connected in line with power and telemetry modules to form a single long cylinder. A buoyant collar provides flotation at the irradiance (*top*) end of the instrument and accommodates two hard-plastic fins (Fig. 52), which stabilize the rocket-shaped design. The addition of an adjustable weighted collar to the radiance (*bottom* or nose) end, produces a rocket-shaped package that falls through the water column with minimal tilt angles (typically less than 5° after the near-surface righting has occurred). The adjustable weighted collar, which can rotate around the nose to remove tilt biases, has small *wings* to hold the weights. The weights have holes and are attached to the wings using a bolt and nut.

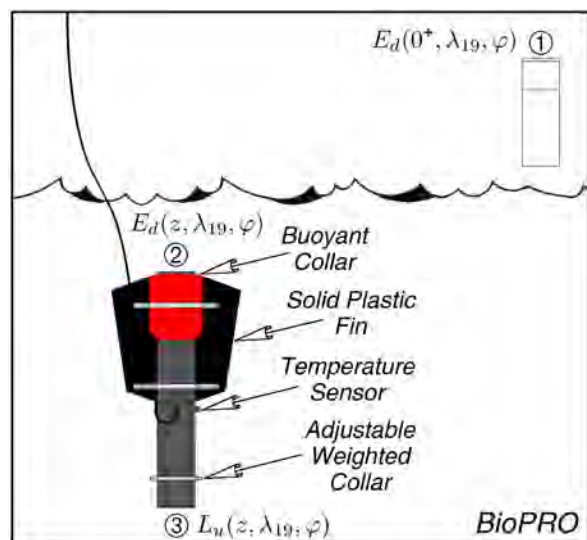


Fig. 52. A schematic of a (PRR-800) BioPRO free-fall system with 19 channels (λ_{19}) showing the three light measurements. The two solid plastic fins provide some protection for the buoyant collar during deployment and recovery, and allow the instrument to be brought to the surface like a kite. (The gray colors provide contrast to facilitate interpretation and are not indicative of the actual coloring.)

The overall length of the BioPRO instrument is approximately 59.7 cm, so it is a comparatively compact design (typical legacy free-fall profilers in use for open-ocean

sampling at the time BioPRO was designed were about 1.24–1.78 m in length). Using only the collar weight and adding no additional weights, the descent speed is about 30 cm s^{-1} . To achieve greater stability, weight is added resulting in a typical descent speed of $40\text{--}60 \text{ cm s}^{-1}$.

Once a BioPRO is properly positioned outside the perturbation of the deployment platform and the cable is released by the operator, the nose weight orients (or *rights*) the profiler into a vertical alignment, and the entire package starts to descend. The top-most data frequently have large tilts and are ignored. The greater the nose weight, the shorter the righting time, but there is also an increased chance of large back-and-forth oscillations, because the weighted nose and buoyant fins establish a natural pendulum. The cable is almost neutrally buoyant and has a low coefficient of drag, so the profiler falls freely through the water column. The desired depth is usually the 1% light level, but deeper casts to completely sample some other aspect of the water column are frequently made, e.g., to the depth of the DCM.

5.3 Design

To improve the vertical resolution of rocket-shaped profilers, like the BioPRO, the original free-fall buoyant collar was redesigned to add compressible air bladders, similar to what SuBOPS and C-OPS use (Hooker et al. 2010). This hydrobaric feature supports slow, near-surface descent rates that are unprecedented in rocket-shaped profilers, and significantly improves the deployment of a BioPRO in optically complex shallow coastal waters by increasing the near-surface vertical resolution obtained during profiling. The increase in vertical resolution, which is in addition to setting the PRR-800 sampling rate to 12 Hz, is provided by the air bladders.

The air bladders cause the profiler to *loiter* near the surface (Hooker et al. 2013) as they slowly compress, and push the terminal velocity deeper into the water column where surface effects (e.g., wave focusing) are less significant. In other words, the profiler sinks slowly when surface effects are greatest and high vertical-resolution data are needed, and more quickly when coarser resolution is not a detriment.

By design, the buoyancy system of a profiler used in aquatic research must be adaptable to allow deployments in both fresh and salt waters, as well as warm and cold temperatures, which represents a wide range in water density and, thus, buoyancy. For the C-SLOWS accessory, the wide range of this adjustment is controlled by the combined use of air bladders, buoyant collars, and weights. Assuming there are adequate air bladders (these would not normally be changed except if one failed, for instance), other gross adjustments of the buoyancy of the system to achieve a near-neutral condition are normally performed by adding a strip of lead sheeting to the bottom of the instrument, covered with multiple layers of black plastic tape (e.g., Scotch Super 88 vinyl electrical tape).

The tape secures the lead without interfering with capping the radiance aperture for dark measurements, and provides a smooth surface for laminar flow. The circular position of the adjustable weighted collar, as well as the amount of weight added, are used to *trim*† the profiler vertical orientation and descent rate. With no weight added to the adjustable collar, but with the nose lead weight affixed, the profiler should be slightly positively buoyant in freshwater. With respect to Fig. 52, the new buoyant collars are longer, and the air bladders are enclosed within the collar (i.e., not visible). The prototype had stainless steel (SS) screens covering the air bladders, as shown in Fig. 53, which provides a frontal view of the prototype buoyancy collars (made out of spare custom foam used with SuBOPS and C-OPS) fitted to a PRR-800.

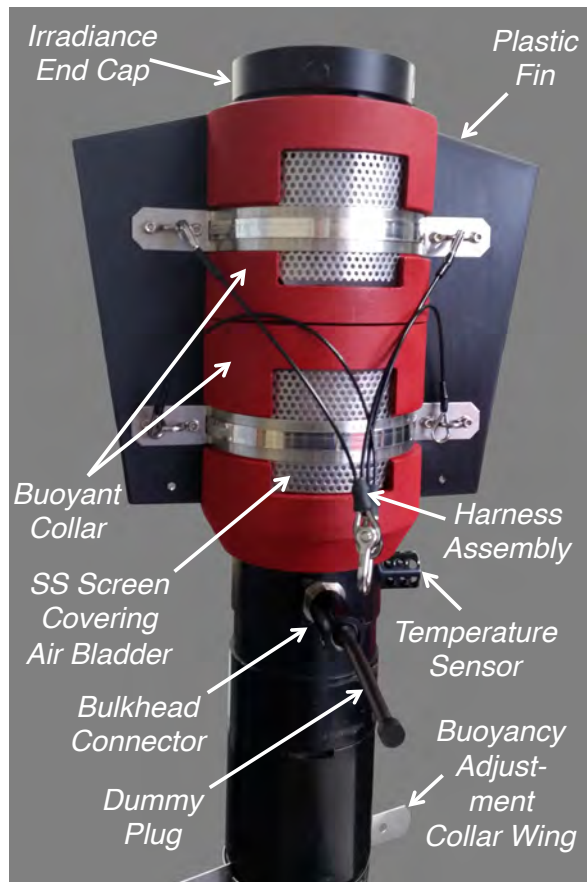


Fig. 53. A frontal view of the new prototype collar with air bladders behind stainless steel screens and the cable harness attached to the wing hardware on the fins. The fasteners for the hose clamps are on the back of the instrument and not visible.

The NASA data processing protocols require the optical data to be restricted to a vertical tilt angle less than 5° . When deployed, it may be observed that the profiler

† **Trim (nautical):** To adjust the port-starboard list, or fore-aft draft of a vessel by changing the distribution of weight on board, especially the ballast.

has a bias in either of the two-axis tilts, usually referred to as the pitch and roll angles, that subsequently combines to exceed this threshold.

⚠ *Older calibrations and older versions of the manufacturer’s data acquisition software and accompanying documentation mistakenly referred to “tilt” and “roll” rather than the more common “pitch” and “roll.”* If “tilt” is used in the BSI software display, the user is advised to contact support@biospherical.com for corrections.

Unlike some instruments, a BioPRO does not have an obvious front-back or left-right symmetry. Consequently, the orientation is somewhat arbitrary and is assigned by the manufacturer as follows: a) the pitch plane is parallel with the bulkhead connector for the sea cable, and b) the roll plane is orthogonal to the pitch plane. In regards to Figs. 52 and 53, pitch is into or out of the page, and roll is clockwise or counterclockwise within the page. The *front* of the instrument is defined by the presence of the cable connector, and the right *side* of the instrument is defined by the presence of the temperature sensor.

With this orientation in mind, the process for trimming the profiler can be conveniently divided into three steps. The first step is to attach the fins and buoyancy collars (with air bladders); the second step is to adjust the buoyancy for the desired descent rate; and the third step is to adjust the vertical tilt angle to remove any pitch and roll biases observed during the descent.

5.3.1 Fins and Collars Attachment

The two fins and two buoyant collars are all held together in a clamshell configuration secured to the PRR-800 instrument cylinder with SS hose clamps (Fig. 53). The SS hardware clamp at the nose or bottom end of the instrument is where additional trimming weights are attached to the wings. To affix the buoyant collars to the PRR-800, the clamping hardware is first loosely assembled with the air bladders in place, and the assembly is subsequently lowered on to the PRR-800 from the top, gently pushing the air bladders into position individually. The ring on the inside of the buoyancy collar rests at the bottom of a groove in the housing of the PRR-800, providing clearance for the dark cap over the irradiance collector. Next, the fins are positioned between the collar halves, and the hardware is tightened while paying attention to maintain the correct front-back orientation. The harness is attached as shown in Fig. 53, and all remaining hardware tightened.

The next step confirms the pitch and roll angular relationships, as well as their sign (positive or negative). To accomplish this, the instrument is placed upright on the radiance end cap (with the protective dark cap installed) on a stable surface. The software is turned on and the pitch and roll values observed (they should both show approximately 0°). Next, facing the instrument on the connector side (i.e., the front of the instrument, as in

Fig. 53), the irradiance (top) of the instrument is moved so it tilts toward the operator. The pitch value should increase and roll should be relatively stable. This is normally defined as positive pitch, but the actual behavior should be noted and the subsequent procedures adjusted accordingly to suite the particular instrument. The instrument is then returned to a vertical orientation and the irradiance end tilted to the right. This is normally defined as positive roll, but once again, a note should be made of the result for future reference. Establishing these relationships is important when adjusting the trim of the instrument using the procedures outlined below.

⚠ The DACPRO and PROSIT software calculate the vertical tilt (φ) as a signed value from pitch and roll (φ_1 and φ_2 , respectively). The calculation uses the equation $\varphi = \tan^{-1} \sqrt{\tan^2 \varphi_1 + \tan^2 \varphi_2}$, wherein the sign is arbitrarily set using the sign of φ_2 (roll), so biases can be detected. BSI is adding this feature to their data acquisition software.

5.3.2 Buoyancy Adjustment

Buoyancy adjustment for C-SLOWS is a straightforward exercise. The goal is to add just enough weight so the profiler loiters at the surface, slowly breaks the surface tension, and then begins to sink. As the water pressure increases with depth, the air bladders in the buoyancy collars are compressed, resulting in a loss of buoyancy. This cycle continues until the bottom of the profile is reached or until the bladders are completely collapsed and the profiler reaches *terminal velocity*, wherein the retarding forces of drag and buoyancy equal the downward force of gravity. To aid in trimming the instrument, BSI supplies three sets of standard SS weights: small, medium, and large. For additional small adjustments to the trim (i.e., fine tuning), SS washers are recommended. Based on prior experience, type 316 SS flat washers with M12 screw size, e.g., 13.0 mm inner diameter (ID) and 24.0 mm OD, are useful for this purpose (in comparison to alternative SS metals, 316 SS has superior corrosion resistance and stability in salt water).

5.3.3 Angular Adjustment

After adjusting the buoyancy to the desired initial descent rate and terminal velocity, the tilt angle of the instrument is trimmed using the weighted collar at the bottom (nose) of the instrument. The goal is for the instrument to be plumb (vertical) as it descends. Various asymmetries contribute to the final behavior of the instrument, but the largest is the drag and subsequent tension from the cable. During deployment, it is important for the operator to place slack cable in the water ahead of the demands of the instrument descent to avoid any effect from tension by the cable. Nevertheless, there is some inherent tension or pull from the cable, and this tends to tilt the instrument with

a small amount of positive pitch. Similarly, near-surface currents and waves, asymmetric internal buoyancy distribution, and other factors may cause tilts.

To counteract the influences from tilt forces, without changing the amount of weight from the second step, the weight-bearing collar is rotated so the external weights offset the tilt forces. If the cable is the main source of tilt, the weights are rotated to the back of the instrument, opposite the cable. Also, the weights need not be placed on the collar symmetrically—the majority of the weight is frequently placed on one side and this is usually opposite the cable harness. Once released, the first few meters of data may have somewhat larger tilts, but adjustment of the weights should ensure that any induced oscillations go through zero degrees without a tilt bias. It is important to achieve a weight distribution so there is a minimum tilt bias, because during data processing, all tilts exceeding 5° will be ignored. Consequently, as long as the profiler oscillates through 0° , only the extreme data will be lost, and a majority will be retained.

5.4 Results

The results presented herein were obtained with two legacy PRR-800 instruments. One was a BioPRO system, although it had larger fins and a larger buoyant collar, than a production unit (Fig. 54). The increased fin area improved the stability of the profiler during descent. The other was one of the first PRR-800 systems, and it was deployed with the C-SLOWS accessory.

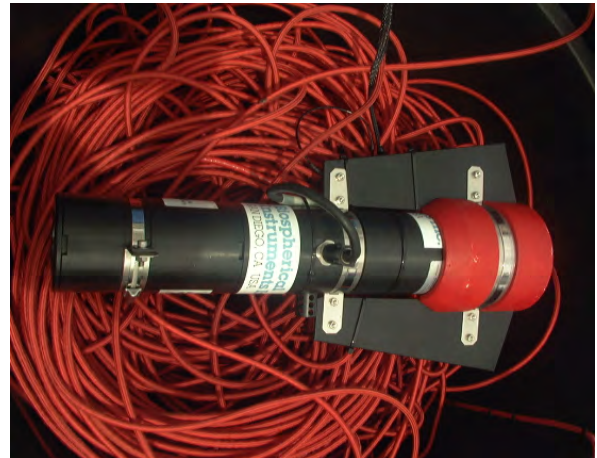


Fig. 54. A legacy BioPRO profiler on top of the sea cable coiled into a large black bucket.

Figure 55 shows pitch and roll values in the upper 15 m of the water column for the BioPRO instrument in Fig. 54. The data were collected in the South Pacific Ocean during strong swell conditions. This profile was selected to establish the limitations of legacy systems under adverse conditions. The shallowest data are characterized by large tilts and the deepest data by smaller tilts, which is typical; the former is associated with the righting of the instrument shortly after it is released by the operator.

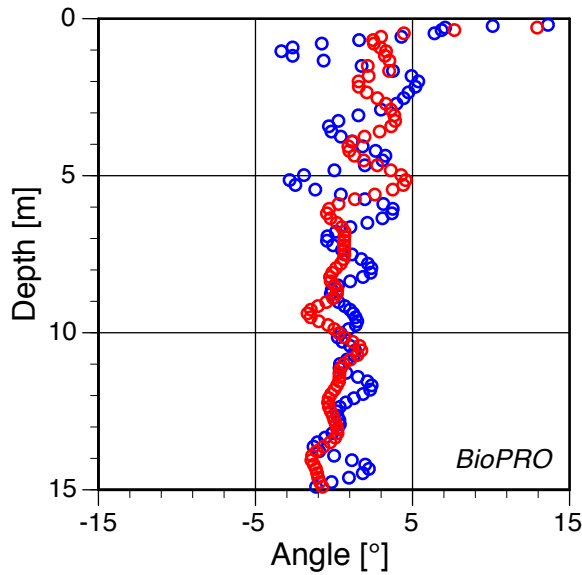


Fig. 55. The pitch (blue) and roll (red) values obtained in the upper 15 m of the water column for the legacy BioPRO instrument.

Figure 56 shows typical pitch and roll values in the upper 15 m of the water column for a PRR-800 instrument with the C-SLOWS accessory. Like Fig. 55, this profile was obtained in the open ocean in a developed sea state, but at a different time and place. The level of wave activity is well established by the large tilt excursions when the profiler was loitering close to the surface as the hydrobaric bladders slowly compressed. Once the profiler sinks out of the influence of the surface wave field, the tilts quickly converge to small values around zero, with little evidence of bias, although the pitch axis is the most variable.

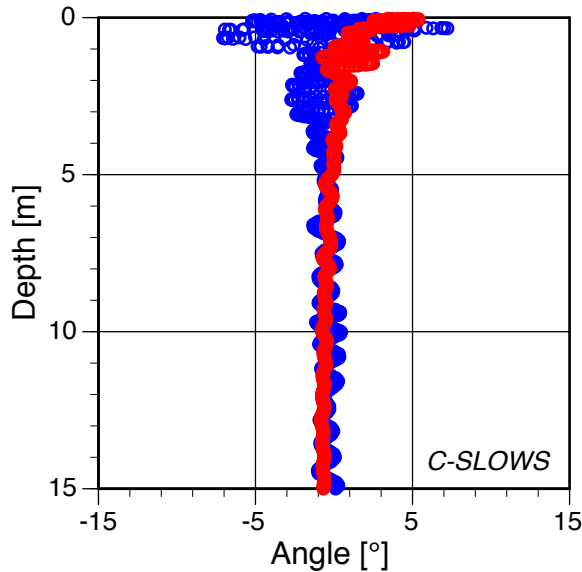


Fig. 56. The pitch (blue) and roll (red) values obtained in the upper 15 m of the water column for a legacy PRR-800 instrument equipped with C-SLOWS.


The principal differences between a PRR-800 deployed as BioPRO or as C-SLOWS are the number of samples, $N_s(z)$, which establish the vertical resolution, V_r , obtained within the water column above depth z . Table 6 provides a summary of the sampling information for the two profiles shown in Figs. 55 (BioPRO) and 56 (C-SLOWS) using the following near-surface depths: $z = 1$, $z = 5$, $z = 10$, and $z = 15$ m.

Table 6. The N_s obtained at four depth levels for a BioPRO and C-SLOWS deployment. The V_r in centimeters (i.e., z/N_z) for the water column above the four depths is given as $V_r(1)$, $V_r(5)$, $V_r(10)$, and $V_r(15)$, respectively.

Profiler	$N_s(1)$	$N_s(5)$	$N_s(10)$	$N_s(15)$
BioPRO	8	34	69	105
C-SLOWS	204	440	666	840
Profiler	$V_r(1)$	$V_r(5)$	$V_r(10)$	$V_r(15)$
BioPRO	12.5	14.7	14.5	14.3
C-SLOWS	0.5	1.1	1.5	1.8

The data in Table 6 show the use of C-SLOWS significantly increases the number of samples obtained in the water column. With respect to BioPRO, the increases range from factors of 8–23, with the largest increase in the shallowest near-surface waters. The nominal V_r values in Table 6 show C-SLOWS can result in near-surface sampling to within 1 cm, and this changes slightly (to less than 2 cm) as the profiler descends deeper into the water column.

From the perspective of satellite or airborne remote sensing applications, the near-surface data are arguably the most important. For C-SLOWS, $N_s(1) = 204$, which equates to a nominal $V_r(1)$ value of 0.5 cm, i.e., sampling that starts to approach the 1 mm level. A nominal vertical resolution less than 1 cm is a state-of-the-art accomplishment (Hooker et al. 2013). In comparison, the BioPRO V_r values are all larger than 10 cm, which was typical for instruments designed when BioPRO was built. The PRR-800 Proteus electronics, however, are not typical of legacy instruments. The PRR-800 has a dynamic range and responsivity that is still state of the art and almost identical to C-OPS. *Consequently, the use of the C-SLOWS accessory will allow a BioPRO instrument to produce data products at a quality level in keeping with C-OPS, but there is a cautionary aspect that must be respected.*

 The nominal vocabulary used with V_r above and in Table 6 is to emphasize that all data with $\varphi > 5^\circ$ will be filtered out during data processing, so the actual vertical resolution achieved for deriving data products will be degraded.

Although both Figs. 55 and 56 show evidence of large near-surface tilt excursions, an order of magnitude or more

increase in data sampling will ensure significantly more data will be retained using C-SLOWS once all data with $\varphi > 5^\circ$ are removed for data processing.

Even for carefully deployed instruments, the amount of data lost close to the sea surface due to tilt filtering can be worrisome for rocket-shaped profilers, because the righting of the profiler can cause substantial data loss close to the surface. *Ultimately, this is why the C-PrOPS approach yields significantly higher-quality shallow observations—there is no righting of the profiler, because it is already stably oriented in the wave field.*

For example, if tilt filtering is applied to the Table 6 data, $N_s(15) = 89$ for BioPRO and $N_s(15) = 780$ for C-SLOWS (versus 105 and 840 without filtering, respectively). The corresponding $V_r(15)$ BioPRO and C-SLOWS values are 16.9 cm and 1.9 cm (versus 14.3 cm and 1.8 cm without filtering), respectively. Most of the data removed by tilt filtering, however, are close to the surface. The corresponding BioPRO and C-SLOWS $N_s(5)$ values are 21 and 400 (versus 34 and 440 without filtering), yielding $V_r(5)$ values of 23.8 cm and 1.3 cm (versus 14.7 cm and 1.1 cm without filtering), respectively.

Consequently, the changes in BioPRO V_r values as a result of filtering are an increase of 2.6 cm at 15 m and 9.1 cm at 5 m; whereas, the corresponding changes in C-SLOWS V_r values as a result of filtering are approximately an increase of 0.1 cm for both depths. It is anticipated that the most dramatic changes in N_s (and, thus, V_r) are seen for tilt filtering at the shallowest depths. Tilt filtering yields $N_s(1) = 3$ for BioPRO and $N_s(1) = 144$ for C-SLOWS; the corresponding changes in $V_r(1)$ values are an increase of 20.8 cm and 0.2 cm, respectively. The estimates require consideration, however, because both filtered data sets are not evenly distributed throughout the top 1 m of the water column; they are clustered in groups or periodically, because the wave field is periodic.

In the case of BioPRO the clustering is significant, because, the righting of the profiler prevents observations within a depth interval corresponding approximately to the length of the instrument (which is 59.7 cm). The first observation with a vertical tilt of 5° or less is at 0.68 m for BioPRO, whereas for C-SLOWS the first tilt-compliant measurement is at 0.04 m. The difference is caused by the different behavior of the instruments near the surface.

When BioPRO is at the surface, it is negatively buoyant and starts sinking immediately if the cable is released. Consequently, to start a cast at the surface once the profiler is at a shallow depth, the operator must haul in cable, and to keep the profiler at the surface, cable must continuously be hauled in unless a strong enough forward progress of the ship is present (e.g., if the ship is slowly underway or if there is a favorable current or wind). This means BioPRO will almost always be oriented horizontally (large vertical tilts) when it is released, and the profiler must acquire a righted vertical orientation (small vertical tilts)

after it is released and is already sinking at near-terminal velocity.

When C-SLOWS is at the surface, the anticipated deployment scenario is that it is only slightly negatively buoyant and will slowly start sinking if the cable is released. Consequently, to start a cast at the surface once the profiler is at a shallow depth, the operator pulls on the cable, and to keep the profiler at the surface, small tugs produce a bobbing motion wherein the profiler is oriented vertically for release. Consequently, tilt-compliant data can be recorded earlier with C-SLOWS than BioPRO (recalling that the first good L_u data cannot be shallower than the length of the profiler for both BioPRO and C-SLOWS, but E_d data can).

All free-fall profilers close to the surface can be negatively influenced by surface waves, which can produce large tilt excursions. Rocket-shaped devices suffer additional challenges, because the form factor resembles a pendulum. This means oscillations persist for longer time periods unless the descent speed is high, which will dampen the oscillations as a function of depth. One of the reasons C-OPS with C-PrOPS is not as negatively influenced by surface waves is the pendulum form factor is minimized, and the entire kite-shaped backplane provides a more uniform restorative surface area.

5.5 Conclusions

The results displayed in Table 6 plus Figs. 55 and 56 should not be construed as typical, because both profiles could be easily improved with added care in deploying the instruments. The two casts were purposely selected to show data with some challenging aspects, so the tangible benefits of C-SLOWS is not targeted to ideal circumstances that might be hard for some practitioners to achieve. Usually, the weather for a particular campaign cannot be selected beforehand, so there will always be time periods wherein challenging data are all that can be acquired. What the results in Figs. 55 and 56 show is that the C-SLOWS accessory will improve data quality, even under challenging conditions.

The production C-SLOWS accessory used the same design concept as the prototype, but it was more compact and had fewer parts (Fig. 57). Despite being more compact (compare to Fig. 53), the hydrobaric chamber contained a greater volume of space for compressible bladders than the prototype. This allows up to six (three in each half of the clamshell buoyant collar) compressible bladders to be installed. At the top and bottom of each clamshell, openings allow water to enter the hydrobaric chamber and for air to escape. The openings are in line with the stainless steel hose clamps used to hold the buoyant collar to the profiler body, which ensures retention of the bladders even when they are fully compressed. The accessory also comes with six foam inserts made from the same material as the buoyant collar that are approximately the same size as a compressible bladder, and can be used in place of the bladders.

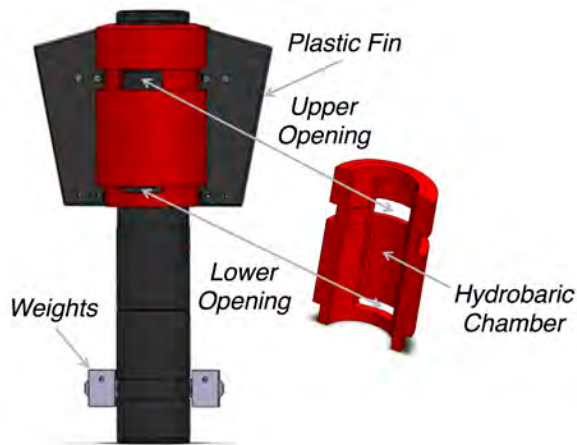


Fig. 57. The completed design of the production BSI C-SLOWS accessory. The (hollowed out) inside of the hydrobaric chamber for one half of the clamshell buoyant collar is shown to the right of the PRR-800 with C-SLOWS attached.

Nagoya University (Nagoya, Japan) deployed a legacy BioPRO without the C-SLOWS accessory, and the vertical resolution for the upper 5 m of the water column was approximately 4.3–8.0 cm. When the same instrument was deployed with the C-SLOWS prototype (Fig. 58), the vertical resolution for the upper 5 m of the water column improved significantly to approximately 1.2–1.7 cm. Similarly, Hokkaido University (Hakodate, Japan) has deployed a legacy PRR-800 without C-SLOWS, and the vertical resolution for the upper 5 m of the water column was 13–15 cm. When the same instrument was deployed with the C-SLOWS prototype, the vertical resolution for the upper 5 m of the water column improved by a factor of 10–20 times.



Fig. 58. The Nagoya University legacy BioPRO fitted with the production C-SLOWS accessory being readied for deployment from the deck of the R/V *Hakuho Maru*.

A subsequent deployment of a production C-SLOWS accessory (Fig. 59) with a legacy PRR-800 by Hokkaido

University (Hakodate, Japan) obtained 459 data records in the upper 5 m of the water column, which equates to a nominal $V_r = 1.1$ cm. This does not include tilt filtering, which would remove some of the data. More impressively, for the first 2 m of the water column, 281 data records were obtained, which equates to $V_r = 0.7$ cm, a state-of-the-art accomplishment.

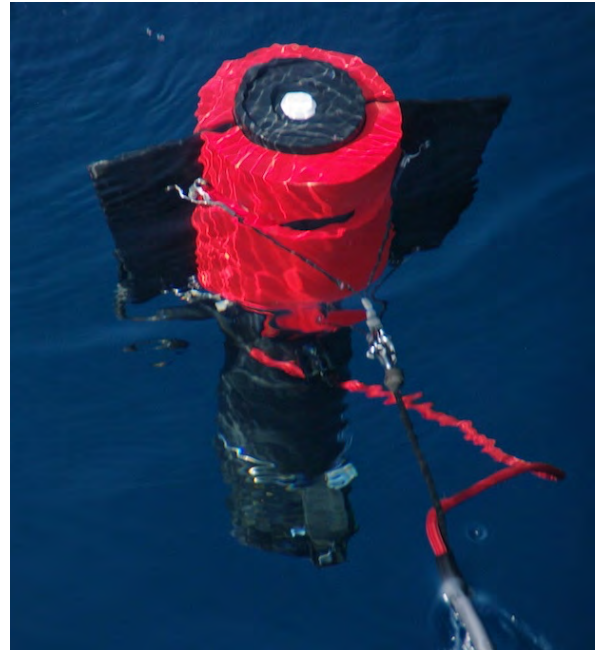


Fig. 59. A legacy BioPRO from the Hokkaido University (Hakodate) with the production C-SLOWS accessory being deployed into the clear waters of the western Pacific Ocean. Wave focusing effects are visible on the top of the profiler, which are a confounding influence of the wave field that requires high-resolution data to adequately resolve and mitigate correctly in a data processing scheme.


Based on the experiences obtained by the scientists who have deployed a legacy PRR-800 in the BioPRO configuration with and without the C-SLOWS accessory, the two most important advantages that C-SLOWS provides are as follows:

1. The PRR-800 is now able to obtain a significant amount of data near the sea surface, and the increase in descent speed due to the compressing of the hydrobaric bladders allows the entire euphotic zone to be sampled; and
2. The extrapolation of the near-surface light field to $z = 0^-$ at UV and NIR wavelengths was almost unrealistic with a PRR-800 deployed without the C-SLOWS accessory in coastal waters, because of the high attenuation of these data close to the sea surface.

These two advantages mean that the PRR-800 with the C-SLOWS accessory is useful not only for satellite and

airborne remote sensing, but also for primary production studies. Furthermore, any residual vertical resolution problems, perhaps caused by a high sea state, can be overcome with repeated data sampling using the C-SLOWS accessory.

There is nuance in reproducing these results, however, so some caution is required. The BSI cable used with BioPRO, as well as SuBOPS and C-OPS, is purposely designed to be almost neutrally buoyant and have a low coefficient of drag, so the profiler naturally falls freely through the water column.

 *An important aspect for collecting high quality data with a free-fall profiler is to prevent the telemetry cable from ever coming under tension*, because even brief periods of tension can adversely affect the vertical orientation (two-axis tilt), descent velocity, and, thus, vertical resolution of the data.

To ensure this does not occur, the operator should leave a few coils of cable at the surface, while ensuring a tangle-free and continuous feed of cable into the water. At terminal velocity, the profiler should descend at approximately $15\text{--}20\text{ cm s}^{-1}$ for shallow coastal ocean waters. For the deeper open ocean, higher descent rates (e.g., $50\text{--}60\text{ cm s}^{-1}$) are frequently used, so the depth of the chlorophyll maximum can be observed without losing available cable to the inevitable drift between the profiler and the deployment platform. In either shallow or deep waters, the amount of weight used should allow sampling to at least the depth of the 10% light level and typically to the depth of the 1% light level (water depth permitting). To ensure high quality data products in clear waters, descent speeds near the surface should be as low as possible. For this reason, the hydrobaric chambers used with BSI profilers allow for the use of multiple compressible bladders.

Chapter 6

The C-PUMPS Accessory

STANFORD B. HOOKER
*NASA Goddard Space Flight Center
Greenbelt, Maryland*

JOHN H. MORROW
*Biospherical Instruments, Inc.
San Diego, California*

HENRY F. HOUSKEEPER
*University of California Santa Cruz
Santa Cruz, California*

ABSTRACT

The C-PUMPS accessory allows seawater sample collection and optical profiling in circumstances wherein it is not possible to launch a small boat, so optical profiles are obtained by using the C-PrOPS accessory to launch the C-OPS backplane from a dock, offshore structure, or shoreline. In these circumstances, it is likely the water sample that would be collected where the profiler operator is located is likely not representative of the likely deeper water column where optical profiles are obtained (e.g., the dock or structure might be a source of contaminants, shoreline waters might be more turbulent and subjected to bottom resuspension, etc.). The equipment consists of 100 ft (30.5 m) of tubing with the distal end attached to the C-OPS backplane. The proximal end of the tubing is connected to a peristaltic pump in near proximity to the profiler operator. The profiler is kept at the surface in the same location where profiling occurs, and the pump is powered on. After the tubing has been flushed three times, which takes about 3 min, a 100 ml sample bottle can be filled in about 5 s, so a 1 l container can be filled in less than 1 min, plus the time to rinse the container and cap three times.

6.1 Introduction

The Compact-Profiler Underway Measurement Pumping System (C-PUMPS) is an accessory for the C-OPS backplane, but it is most effective when used in combination with the C-PrOPS accessory. The C-PrOPS accessory allows a C-OPS backplane to be launched from a shoreline or dock wherein it is impractical to launch a vessel. To ensure a representative water sample is obtained without having to disturb the water mass, for example by wading out to where profiling occurs, the C-PUMPS accessory allows water to be pumped from the profiling location back to the operator for storage in a suitable container (e.g., a plastic bottle, amber glass vial, etc.).

Because C-PUMPS is designed to be deployed in shallow waters, turbidity is expected to be elevated, so a relatively small volume of water is likely necessary for laboratory analysis. This means the pumping mechanism does not have to be particularly powerful. To ensure timeliness, however, a relatively short lag time between the distal and proximal ends of the hose is beneficial to reduce variance caused by water mass heterogeneity, which is also likely.

Because the C-PrOPS accessory uses digital thrusters to move the C-OPS backplane out to the sampling site, while maintaining it at the surface, it is relatively simple to acquire a surface sample once the pumping mechanism is activated. All that is required is for the operator to hold on to the C-OPS sea cable with the thrusters powered once the sampling site is reached, turn on the pump, wait for the water to move from the distal end to the proximal end of the hose, allow some time for the water to flush out the hose, and then fill a container with the sample water.

It is also straightforward to obtain a bottom water sample, by turning off the thrusters, letting the profiler sink and rest on the bottom, turn on the pump, allow for flushing, and then fill a container with the sample water. Intermediate water column water samples are more difficult to obtain, but with a bit of practice it is possible in many circumstances. Although the C-PrOPS thrusters do not autonomously allow the backplane to hover, a small amount of thrust can be used to resist the sinking rate and maintain the backplane at a relatively constant depth.

6.2 Background

The water sample obtained contemporaneously with optical profiling can be used for many laboratory analyses. Two recurring analyses are phytoplankton pigment concentration using high performance liquid chromatography (HPLC) and absorption coefficient due to colored dissolved organic matter (CDOM), a_{CDOM} . The former poses pumping concerns, because the pigments to be measured are contained within cells and it is desirable that the cells are preserved and not disrupted during pumping. For both measurements it is also desirable that the pump not be a contamination source.

A peristaltic pump uses flexible tubing or hose which is routed through rollers in the pump head. As the rollers are rotated, packets of fluid are formed between the rollers, and as the rollers advance, fluid is transported through the pump head; at one end a packet of fluid is captured and at the other end a packet of fluid is ejected. The flow rate is determined by the size of the packets and the speed of the rotating rollers.

A peristaltic pump confines the fluid to be pumped to within the tubing used to transfer the fluid. This means a peristaltic pump cannot contaminate the fluid and the fluid cannot contaminate the pump. The pumping action has low shear and does not damage the content of the fluid, e.g., cells and large proteins. Gentle, contamination-free pumping is the principal reason a peristaltic pump is used with C-PUMPS. The other reasons a peristaltic pump is used with C-PUMPS are as follows:

- The fluid is confined to the tubing, which makes maintenance easy and reduces downtime compared with other pumping technologies;
- The pump is self-priming and can draw fluid into the tubing when starting dry (some pumps require the operator to fill the pump and suction line with fluid before use, which can be inconvenient); and
- The pump is non-siphoning, which means back flow into the system is automatically prevented when the pump is turned off.

The principal disadvantage of a peristaltic pump is the flexible tubing is stressed by the compressive forces imparted by the rollers and requires periodic replacement. Because of this inevitable failure mode, the tubing used in the pump head is usually the most flexible possible, which means it is usually costly. Consequently, only a short piece of tubing is used, which is connected to the inlet and outlet hoses with hose barb fittings. The short periods of use to support C-OPS profiling ensures multiple field campaigns can be executed before the tubing inside the pump head must be replaced.

The flow from a peristaltic pump is necessarily pulsed, particularly at low rotation speeds, which can be a disadvantage for some applications. This is not a factor for C-PUMPS water collection, wherein exact metering is not

a requirement. Furthermore, the pump is run at maximum speed to ensure time-efficient sample collection, so there is little pulsing of the discharged water.

6.3 Design

The C-PUMPS accessory uses a 100 ft (30.5 m) length of plastic hose with an OD of 3/8 in (0.95 cm), although alternative dimensions are possible. The hose is a flexible, but abrasion-resistant polyurethane (Tygothane C-210A No. AEM02013) manufactured by the Saint-Gobain Corp. (Akron, Ohio). The hose is attached to a C-OPS backplane equipped with the C-PrOPS accessory using a 22 in (0.56 m) length of reinforced Tygon tubing, also made by Saint-Gobain Corp., fitted with 3/8 in (0.95 cm) plastic hose barbs at each end. The inlet hose barb is positioned to obtain samples from undisturbed water anterior to the profiler (Fig. 60). The depth offset of the orifice is 12 cm below the depth transducer. The hose is attached to the profiler sea cable with cable ties at approximately 2 m intervals for the first 15 m (Fig. 61) and then every 5 m thereafter.



Fig. 60. The C-OPS radiometers (left and right) with the C-PrOPS and C-PUMPS accessories fitted to the backplane. The clear hose for the latter is attached to the light green sea cable and then strung right to left across the middle of the backplane.



Fig. 61. The C-PUMPS tubing attached to the light green C-OPS sea cable with black cable ties.

The free end of the hose is attached to a MasterFlex 7553-20 peristaltic pump manufactured by Cole-Parmer (Barrington, Illinois). The pump is fitted with a 7015-20 pump head and a short piece of 3/8 in (0.95 cm) OD silicon tubing is attached to the hose and routed through the pump head rollers. The hose attached to the sea cable increases the overall bulkiness, but the buoyancy of the combined hose plus sea cable is rather similar to the sea cable alone, so the drag the two place on the profiler is not appreciably different. The profiles are usually to shallow depths, so any negative effects do not have a sufficient time period to influence profiling operations.

6.4 Results

A picture of the peristaltic pump in operation on a dock is presented in Fig. 62, wherein the characteristic pulsed discharge can be seen. When the collection tubing is attached to the C-OPS backplane, all water samples are taken at the maximum rated speed of the pump, which is 600 rpm. Volumetric sampling rates were determined by measuring the time required to obtain 100 ml aliquots of seawater. The latency time of the hose was determined using repeated samples of seawater differentiated using 25 ml of a red juice as a marker fluid between samples.



Fig. 62. The peristaltic pump, used to obtain water samples as part of the C-PUMPS accessory, in operation on a dock.

Three latency times to pump water from the inlet on the C-OPS backplane to the pump outlet were determined, as follows: a) 64 s for an empty dry hose; b) 64 s for an empty wet hose; and 56 s for a wet hose already full of water. This suggests the minimum time to flush the hose of a prior sample is about 3 min, because that allows the water to pass through the hose three times. This follows the same best practice used to flush a sample bottle of contamination from prior use, i.e., three sequential rinses of the container and cap. The flow rate is approximately 20 ml s^{-1} , which means it takes about 5 s to fill a 100 ml sample bottle (not including bottle and cap rinsing). This means a liter of water is obtained in less than a minute.

6.5 Conclusions

A picture of the C-PUMPS accessory being used at Little Lake Washoe (Nevada), which was overfilled during the anomalously wet 2016–2017 west coast winter, is shown in Fig. 63. As a result of the resulting near-shore flooding, the boat ramp was unserviceable. Consequently, the boat was backed up to the water's edge, the profiler was placed in the water at a depth allowing the backplane to be above the bottom, and the C-PrOPS thrusters were used to position the profiler far from shore wherein the high turbidity of the water resulted in a 1% light level that was less than the bottom depth.



Fig. 63. The C-PUMPS accessory in use as part of small-boat operations on the shore of Little Lake Washoe showing the following: **a)** the peristaltic pump; **b)** the tubing attached to a C-OPS with C-PrOPS sea cable; **c)** the profiler at the surface far from shore; **d)** the discharge from the pump; and **e)** the collapsible sample container.

The inability to launch a boat into a water mass is not restricted to the unexpected loss of facilities due to flooding. For the types of vessels usually used for scientific work, there are many reasons why boat access can be denied. Some of the most reasons are as follows:


1. The water level is reduced to below the minimum level for using the boat ramp, e.g., due to severe drought, agricultural diversion, etc.;
2. The absence of launch facilities coupled with a near-shore topography that prevents a shore launch, e.g., the water depth remains too shallow or the bottom type requires four-wheel drive and the tow vehicle is not so equipped;
3. Restrictions or prohibitions on the use of internal combustion propulsion, e.g., to limit environmental or drinking water contamination; and
4. Controls or inspections to prevent the introduction of invasive species in freshwater lakes and reservoirs.

The within-state and state-to-state variability in stopping the spread of invasive species places unique restrictions on small-boat operations. The use of enforcement procedures are usually identified by the signage shown in Fig. 64. Many of the programs are based on voluntary compliance by the boat operator, especially in remote areas or areas with low vehicular traffic. Most states include additional annual boat registration costs to pay for invasive species protection programs and a valid sticker must be affixed to the boat hull close to the registration number.



Fig. 64. Enforcement procedures to prevent the spread of invasive species are usually identified by a “STOP AQUATIC HITCHHIKERS!” sign.

The most recurring inspection requirement is that a trailer and boat—including the bilges, motor cooling system, storage spaces, drain holes, bait well(s), and all exterior and interior surfaces—must be completely dry before launching.

 *If a wet surface is present anywhere on the boat or trailer, the boat shall not be launched, because the larval or juvenile stage of many invasive species can survive as long as moisture is present.*

Facilities with enforcement personnel usually require additional per-use daily, weekly, or monthly fees in addition to specified registration fees. The per-use fees support the inspection process, which might include decontamination of the vessel before or after the boat is authorized to enter or leave the inspection facility. The majority of decontamination procedures rely on water that is heated to a temperature that kills any invasive larvae or juveniles. The hot water is sprayed on all accessible surfaces and pumped through the motor cooling system (Fig. 65). The hot water is recovered within a purpose-built decontamination area for proper disposal.



Fig. 65. Decontamination of the outboard motor cooling system after recovery of the R/V *Hobson’s Choice* at Lake Mead (Nevada).

A water mass that is not contaminated with an invasive species usually results in decontamination before boat launching, and a contaminated water mass usually results in decontamination after recovery (Fig. 65). In some cases, a decontaminated boat and trailer are *tagged*, so the vessel can be launched without additional decontamination procedures and costs. Tags, however, are not always accepted between lake districts, counties, or states. In such cases, lake sampling is restricted to the time period required to pass the boat and trailer test.

It is faster and easier to dry a C-OPS instrument suite rather than a boat and trailer. As long as a shore launch of the backplane is feasible, freshwater lakes and reservoirs can be visited one after the other in a rather short period of time. In this scenario, the screws holding the top on the hydrobaric chamber must be removed so the inside plus the compressible bladders can be dried; all other surfaces dry rather quickly.

ACKNOWLEDGMENTS

The high level of success achieved in the field work for the activities presented herein was the direct consequence of many individuals who contributed unselfishly. Their dedication is gratefully acknowledged. The captains and crew of the research vessels and aircraft who helped make the research a success are thanked for their professional contributions.

GLOSSARY

- 6F Six Female (sockets)
6M Six Male (pins)
- AC Alternating Current
ACE Aerosol, Clouds, and ocean Ecosystem
ADC Analog-to-Digital Converter
AHRS Attitude and Heading Reference System
AOD Aerosol Optical Depth
AOPs Apparent Optical Properties
APD Absolute Percent Difference
ARC Ames Research Center
ASCII American Standard Code for Information Interchange
AUV Autonomous Underwater Vehicle
AWG American Wire Gauge
- BH Bulkhead
BioGPS Biospherical Global Positioning System
BioGyro Biospherical Gyro
BioPRO Biospherical Profiler
BioSHADE Biospherical Shadow band Accessory for Diffuse Irradiance
BSI Biospherical Instruments Incorporated
- C-AERO Compact-Airborne Environmental Radiometers for Oceanography
C-AIR Coastal Airborne Instrument Radiometers
C-CAPS Compact-Conductivity Accessory for Profiling Systems
C-HARRIER Coastal High Acquisition Rate Radiometers for Innovative Environmental Research
C-HORSE Coastal High-resolution Observations and Remote Sensing of Ecosystems
C-HyR Compact-Hybridspectral Radiometer
C-OPS Compact-Optical Profiling System
C-PrOPS Compact-Propulsion Option for Profiling Systems
C-PUMPS Compact-Profiler Underway Measurement Pumping System
C-SAW Compact-Submersible Autonomous Winch
C-SLOWS Compact-Surface Loitering Option for Water Samplers
C-TRAC Compact-Thruster Remote Accessory
Cat 5 Category 5 (cable)
Cat 6 Category 6 (cable)
CCD Charge-Coupled Device
CDOM Colored Dissolved Organic Matter
CGS Compact Grating Spectrometer
CIRPAS Center for Interdisciplinary Remotely-Piloted Aircraft Studies
COTS Commercial-Off-The-Shelf
CT Conductivity and Temperature
CTD Conductivity, Temperature, and Depth
CVR Calibration, Validation, and Research
- DAC Digital-to-Analog Converter
DACPRO Data Acquisition and Control for Photometric and Radiometric Observations
DC Direct Current
DCM Deep Chlorophyll Maximum
DE-9S D-subminiature E-size (nine-socket)
EOS Earth Observing System
EPIC Enhanced Performance Instrument Class
FG Female Grooves (locking sleeve)
FOV Field of View
FVA Full View Angle
- GmbH *Gesellschaft mit beschränkter Haftung*, which designates a private company with limited liability in Germany.
GND Ground
GPS Global Positioning System
GSFC Goddard Space Flight Center
GUI Graphical User Interface
- HARPOONS Hybridspectral Alternative for Remote Profiling of Optical Observations for NASA Satellites
HPLC High Performance Liquid Chromatography
HV High Voltage
HyPower Hybridspectral Power (box)
HySEAS3D Hybrid System for Environmental AOP Sampling of the Sea Surface Demonstration
- ID Inner Diameter
IL (SubConn) In-Line
InGaAs Indium Gallium Arsenide
IR Infrared
JP Jumper
LCD Liquid Crystal Display
LED Light-Emitting Diode
LSA Lowest Safe Altitude
MC (SubConn) Micro
MML-100 Monochromatic Microradiometer Radiance (model) 100
MODIS Moderate Resolution Imaging Spectroradiometer
MR Male Ridges (locking sleeve)
NASA National Aeronautics and Space Administration
NIR Near-Infrared
OCULLAR Ocean Color Underwater Low Light Advanced Radiometer
OD Outer Diameter
OSPRey Optical Sensors for Planetary Radiant Energy
PACE Plankton, Aerosol, Cloud, ocean Ecosystem
PCA Printed Circuit Assembly
PMT Photomultiplier Tube
PP Polypropylene
PROP Propulsion
ProPower Propulsion Power
PROSIT Processing of Radiometric Observations of Seawater using Information Technologies
PRR Profiling Reflectance Radiometer
PRR-800 PRR series 800
PTU Pan-Tilt Unit
PTU-D300 PTU model D300
PU Polyurethane
PVC Polyvinyl Chloride
PWR Power

RCA	Radiance Collector Assembly
RMSE	Root Mean Square Error
ROV	Remotely Operated Vehicle
RPD	Relative Percent Difference
RS-232	Recommended Standard 232
RS-485	Recommended Standard 485
SeaWiFS	Sea-viewing Wide Field-of-view Sensor
SiP	Silicon Photodetector
SMA	Subminiature (Version) A
SNR	Signal-to-Noise Ratio
SPI	Serial Peripheral Interface
SS	Stainless Steel
SubBOPS	Submersible Biospherical Optical Profiling System
SWIR	Short-Wave Infrared
TRL	Technology Readiness Level
Tx+	Transmission positive (voltage)
Tx-	Transmission negative (voltage)
UM	Ultra-Miniature
uRAD	Microradiometer
USB	Universal Serial Bus
USV	Unmanned Surface Vessel
UV	Ultraviolet
VAC	Voltage Alternating Current
VI	Virtual Instrument
VIS	Visible
XTRA	Expandable Technologies for Radiometric Applications

SYMBOLS

0^-	The null depth immediately below the water surface.
0^+	The height immediately above the water surface.
a_{CDOM}	The absorption coefficient due to CDOM.
$E(\lambda)$	The above-water spectral direct solar irradiance.
$E_d(\lambda)$	The in-water spectral downward irradiance.
$E_d(0^+, \lambda)$	The above-water spectral global solar irradiance.
$E_i(\lambda)$	The above-water spectral indirect (sky) irradiance.
$E_s(\lambda)$	The above-water spectral global solar irradiance.
$K_d(\lambda)$	The in-water E_d spectral diffuse attenuation coefficient.
$L_a(\lambda)$	The radiance from multiple scattering by aerosols in the absence of air.
L_{atm}	The radiance contribution from atmospheric interactions, $L_r(\lambda) + L_a(\lambda) + L_{ra}(\lambda)$.
$L_i(\lambda)$	The above-water spectral indirect (sky) radiance.
$L_r(\lambda)$	The radiance contribution from multiple scattering by air molecules (Rayleigh scattering).
$L_{ra}(\lambda)$	The radiance contribution from the interactions between air molecules and aerosols.
$L_{\text{sat}}(\lambda)$	The total radiance observed by the remote sensor (the top of the atmosphere for a spaceborne instrument).
L_{sfc}	The radiance contribution from reflections at the sea surface, $TL_g(\lambda) + tL_f(\lambda)$.
L_{sub}	The radiance contribution from subsurface interactions, $tL_W(\lambda)$.

$L_T(\lambda)$	The above-water spectral total radiance from the sea surface.
$L_u(\lambda)$	The in-water spectral upwelling radiance.
$L_W(\lambda)$	The spectral water-leaving radiance.
$\tilde{L}_W(\lambda)$	The spectral water-leaving radiance derived from an above-water method.
$\tilde{\tilde{L}}_W(\lambda)$	The spectral water-leaving radiance derived from an in-water method.
$[L_W(\lambda)]_N$	The spectral normalized water-leaving radiance; also designated $L_{WN}(\lambda)$, depending on the citation.
$N_s(z)$	The number of samples obtained within the water column above depth z .
R_{rs}	The remote sensing reflectance.
$tL_f(\lambda)$	The radiance contributions from foam reflections and the diffuse atmospheric transmittance (t).
$tL_W(\lambda)$	The radiance contributions from backscattering out of the water due to subsurface interactions.
$TL_g(\lambda)$	The radiance contributions from glint reflections and the direct solar transmittance (T).
V_r	The vertical resolution obtained within the water column above depth z .
X	An arbitrary variable in the RPD calculation.
X^{21}	An arbitrary variable in the RPD calculation for profiling system 21.
X^{34}	An arbitrary variable in the RPD calculation for profiling system 34.
z	The water depth.
θ	The zenith angle.
θ_s	The solar zenith angle.
λ	The wavelength.
λ_{19}	The 19 spectral fixed-wavelength channels of a radiometer.
$\lambda_{2,048}$	The spectral 2,048 pixels of the CGS.
ϕ	The azimuth angle with respect to the Sun direction ($\phi = 0$ for the solar azimuth).
φ	The vertical tilt.
φ_1	The pitch tilt.
φ_2	The roll tilt.
ψ	The relative percent difference.
$\bar{\psi}$	The average ψ value.
$ \psi $	The absolute percent difference.
Ω_{FOV}	The solid angle of a detector centered on the direction (θ, ϕ) .

REFERENCES

Ahmad, Z., B.A. Franz, C.R. McClain, E.J. Kwiatkowska, J. Werdell, E.P. Shettle, and B.N. Holben, 2010: New aerosol models for the retrieval of aerosol optical thickness and normalized water-leaving radiances from the SeaWiFS and MODIS sensors over coastal regions and open oceans. *Appl. Opt.*, **49**, 5,545–5,560.

Antoine, D., F. d’Ortenzio, S.B. Hooker, G. Bécu, B. Gentili, D. Tailliez, and A.J. Scott, 2008: Assessment of uncertainty in the ocean reflectance determined by three satellite ocean color sensors (MERIS, SeaWiFS and MODIS-A) at an offshore site in the Mediterranean Sea (BOUSSOLE project). *J. Geophys. Res.*, **113**, C07013, doi:10.1029/2007JC004472, 2008.

- Asrar, G., and R. Greenstone, 1995: *1995 MTPE/EOS Reference Handbook*, G. Asrar and R. Greenstone, Eds., NASA Goddard Space Flight Center, Greenbelt, Maryland, 277 pp.
- Bailey, S.W., S.B. Hooker, D. Antoine, B.A. Franz, P.J. Werdell, 2008: Sources and assumptions for the vicarious calibration of ocean color satellite observations. *Appl. Opt.*, **47**, 2,035–2,045.
- Bernhard, G., C.R. Booth, J.H. Morrow, R.N. Lind, and S.B. Hooker, 2010: “Biospherical Shadowband Accessory for Diffuse Irradiance (BioSHADE): A Marine Shadowband and GPS Accessory.” In: Morrow, J.H., S.B. Hooker, C.R. Booth, G. Bernhard, R.N. Lind, and J.W. Brown, *Advances in Measuring the Apparent Optical Properties (AOPs) of Optically Complex Waters. NASA Tech. Memo. 2010–215856*, NASA Goddard Space Flight Center, Greenbelt, Maryland, 51–59.
- Booth, C.R., J.H. Morrow, and S.B. Hooker, 2010: “Development of the Microradiometer.” In: Morrow, J.H., S.B. Hooker, C.R. Booth, G. Bernhard, R.N. Lind, and J.W. Brown, *Advances in Measuring the Apparent Optical Properties (AOPs) of Optically Complex Waters. NASA Tech. Memo. 2010–215856*, NASA Goddard Space Flight Center, Greenbelt, Maryland, 27–41.
- Ferris, C.D., W.F. Hammett, J.C. Whitaker, and W.E. DeWitt, 2005: “Safety.” In: *The Electronics Handbook, Second Edition*, J.C. Whitaker, Ed., CRC Press, Boca Raton, 2,317–2,324.
- Gordon, H.R., and K. Ding, 1992: Self shading of in-water optical instruments. *Limnol. Oceanogr.*, **37**, 491–500.
- Hooker, S.B., 2014: Mobilization Protocols for Hybrid Sensors for Environmental AOP Sampling (HySEAS) Observations. *NASA Tech. Pub. 2014–217518*, NASA Goddard Space Flight Center, Greenbelt, Maryland, 105 pp.
- , W.E. Esaias, G.C. Feldman, W.W. Gregg, and C.R. McClain, 1992: An Overview of SeaWiFS and Ocean Color. *NASA Tech. Memo. 104566, Vol. 1*, S.B. Hooker and E.R. Firestone, Eds., NASA Goddard Space Flight Center, Greenbelt, Maryland, 24 pp., plus color plates.
- , and S. Maritorena, 2000: An evaluation of oceanographic radiometers and deployment methodologies. *J. Atmos. Oceanic Technol.*, **17**, 811–830.
- , G. Lazin, G. Zibordi, and S. McLean, 2002: An evaluation of above- and in-water methods for determining water-leaving radiances. *J. Atmos. Oceanic Technol.*, **19**, 486–515.
- , G. Zibordi, J-F. Berthon, and J.W. Brown, 2004: Above-water radiometry in shallow, coastal waters. *Appl. Opt.*, **43**, 4,254–4,268.
- , C.R. McClain, and A. Mannino, 2007: NASA Strategic Planning Document: A Comprehensive Plan for the Long-Term Calibration and Validation of Oceanic Biogeochemical Satellite Data. *NASA Special Pub. 2007–214152*, NASA Goddard Space Flight Center, Greenbelt, Maryland, 31 pp.
- , R.N. Lind, J.H. Morrow, and J.W. Brown, 2010: “The Submersible Biospherical Optical Profiling System (SuB-OPS).” In: Morrow, J.H., S.B. Hooker, C.R. Booth, G. Bernhard, R.N. Lind, and J.W. Brown, *Advances in Measuring the Apparent Optical Properties (AOPs) of Optically Complex Waters. NASA Tech. Memo. 2010–215856*, NASA Goddard Space Flight Center, Greenbelt, Maryland, 17–26.
- , G. Bernhard, J.H. Morrow, C.R. Booth, T. Comer, R.N. Lind, and V. Quang, 2012: Optical Sensors for Planetary Radiant Energy (OSPREy): Calibration and Validation of Current and Next-Generation NASA Missions. *NASA Tech. Memo. 2012–215872*, NASA Goddard Space Flight Center, Greenbelt, Maryland, 117 pp.
- , J.H. Morrow, and A. Matsuoka, 2013: Apparent optical properties of the Canadian Beaufort Sea, part II: The 1% and 1 cm perspective in deriving and validating AOP data products. *Biogeosci.*, **10**, 4,511–4,527.
- , and J.W. Brown, 2018: Processing of Radiometric Observations of Seawater using Information Technologies (PRO-SIT): In-Water User Manual. *NASA Tech. Memo.*, (in prep.)
- Lind, R.N., C.R. Booth, G. Bernhard, J.H. Morrow, and S.B. Hooker, 2012: “Application of Microradiometers to EMR and OXR Sensors.” In: Hooker, S.B., G. Bernhard, J.H. Morrow, C.R. Booth, T. Comer, R.N. Lind, and V. Quang, *Optical Sensors for Planetary Radiant Energy (OSPREy): Calibration and Validation of Current and Next-Generation NASA Missions. NASA Tech. Memo. 2012–215872*, NASA Goddard Space Flight Center, Greenbelt, Maryland, 18–22.
- Mobley, C.D., 1999: Estimation of the remote-sensing reflectance from above-surface measurements. *Appl. Opt.*, **38**, 7,442–7,455.
- Morel, A., and B. Gentili, 1991: Diffuse reflectance of oceanic waters: its dependence on sun angle as influenced by the molecular scattering contribution. *Appl. Opt.* **30**, 4,427–4,438.
- Morrow, J.H., C.R. Booth, R.N. Lind, and S.B. Hooker, 2010: “The Compact-Optical Profiling System (C-OPS).” In: Morrow, J.H., S.B. Hooker, C.R. Booth, G. Bernhard, R.N. Lind, and J.W. Brown, *Advances in Measuring the Apparent Optical Properties (AOPs) of Optically Complex Waters. NASA Tech. Memo. 2010–215856*, NASA Goddard Space Flight Center, Greenbelt, Maryland, 42–50.
- Mueller, J.L., and R.W. Austin, 1992: Ocean Optics Protocols for SeaWiFS Validation. *NASA Tech. Memo. 104566, Vol. 5*, S.B. Hooker and E.R. Firestone, Eds., NASA Goddard Space Flight Center, Greenbelt, Maryland, 43 pp.
- , and R.W. Austin, 1995: Ocean Optics Protocols for SeaWiFS Validation, Revision 1. *NASA Tech. Memo. 104566, Vol. 25*, S.B. Hooker, E.R. Firestone, and J.G. Acker, Eds., NASA Goddard Space Flight Center, Greenbelt, Maryland, 66 pp.

- , 2000: “Overview of Measurement and Data Analysis Protocols.” In: Fargion, G.S., and J.L. Mueller, Ocean Optics Protocols for Satellite Ocean Color Sensor Validation, Revision 2. *NASA Tech. Memo. 2000–209966*, NASA Goddard Space Flight Center, Greenbelt, Maryland, 87–97.
- , 2002: “Overview of Measurement and Data Analysis Protocols.” In: Mueller, J.L., and G.S. Fargion, Ocean Optics Protocols for Satellite Ocean Color Sensor Validation, Revision 3, Volume 1. *NASA Tech. Memo. 2002–21004/Rev3–Vol1*, NASA Goddard Space Flight Center, Greenbelt, Maryland, 123–137.
- , 2003: “Overview of Measurement and Data Analysis Methods.” In: Mueller, J.L., and 17 Coauthors, Ocean Optics Protocols for Satellite Ocean Color Sensor Validation, Revision 4, Volume III: Radiometric Measurements and Data Analysis Protocols. *NASA Tech. Memo. 2003–211621/Rev4–Vol.III*, NASA Goddard Space Flight Center, Greenbelt, Maryland, 1–20.
- NEC, 2011: *National Electrical Code Handbook, Twelfth Edition*. M.W. Earley and J.S. Sargent, Eds., and C.D. Coache and R.J. Roux, Contribs., National Fire Protection Association, Quincy, 1,497 pp.
- Parker, C.D., 2009: In: *Encyclopedia of Electrochemical Power Sources*, Garce, J., C. Dyer, P. Moseley, Z. Ogumi, D. Rand, and B. Scrosati ,Eds., Elsevier, Amsterdam, 225–232 pp.
- Zibordi, G., B. Holben, S.B. Hooker, F. Mélin, J-F. Berthon, I. Slutsker, D. Giles, D. Vandemark, H. Feng, K. Rutledge, G. Schuster, and A. Al Mandoos, 2006: A Network for Standardized Ocean Color Validation Measurements. *Eos, Trans. Amer. Geophys. Union*, **84**, 293, 297.

